

THESIS

COLLAPSE SIMULATIONS OF STEEL BUILDINGS UNDER FIRE

Submitted by

Chao Qin

Department of Civil and Environmental Engineering

In partial fulfillment of the requirements

For the Degree of Master of Science

Colorado State University

Fort Collins, Colorado

Summer 2016

Master's Committee:

Advisor: Hussam Mahmoud

Rebecca Atadero

Allan Kirkpatrick

Copyright by Chao Qin 2016

All Rights Reserved

## ABSTRACT

### COLLAPSE SIMULATIONS OF STEEL BUILDINGS UNDER FIRE

Collapse analysis of steel structures under extreme hazards has been placed on the forefront of research in recent decades. This was primarily motivated by the September 11, 2001, terrorist attacks, which caused the complete collapse of the World Trade Centers (WTCs) including WTC-7. The collapse, attributed mainly to fires resulting from the attacks, raised concerns regarding the level of robustness in steel frames when subjected to fire loadings. While complete collapse of steel buildings under elevated temperature is considered a rare event, as no cases have been reported prior to 9/11, understanding collapse mechanisms of steel buildings under fire conditions can help in developing methods by which future failures can be avoided. One of the main limitations towards evaluating such collapse events is the experimental cost and complexity associated with conducting collapse tests. Numerical simulations, if properly employed, can yield significant dividends in understanding and quantifying structural response under extreme hazards.

With the worldwide move toward performance-based engineering, understanding, and quantifying system behavior through advanced numerical simulations, especially during the heating and cooling phases of realistic fire exposures, is essential for establishing proper performance-based provisions for fire engineering that ensure both safe and economical design. To that end, the primary objectives of this research are two folds - 1) to develop a numerical tool that would allow for the evaluation of steel frames under fire

loading, or any extreme hazard for that matter, up to and including collapse and 2) to evaluate the demand on steel frames, employing moment frames, braced frames, and gravity frames, under different fire scenarios. These two overarching objectives were realized through the development of advanced numerical models of two 6-story steel-frame buildings with moment frames, gravity frames, and different center bracing systems (one model utilized a concentrically braced frame while the other utilized eccentrically braced frame). The building structures were subjected to two different time-temperature curves and two different fire scenarios. Specifically, the ASTM E119 standard fire curve and the Eurocode 3 parametric fire curve were selected to simulate the fire loadings and were applied independently to the building models under two different contained fire scenarios. The two scenarios included – 1) first floor corner compartment fire and 2) whole first floor fire. This allowed for the assessment of different global system response where collapse is triggered by twist of the entire structure accompanied by lateral deformation in the case of a corner compartment fire and progressive vertical displacement of the entire system in the case of the whole first floor fire. The simulation results of this study show that structural response of steel buildings including collapse mechanism and behavior of structural members and connections during fire events can be predicted with reasonable accuracy using advanced numerical finite element analysis. The results provide substantial insight on the behavior of steel building systems under elevated temperature including the potential for system collapse.

## ACKNOWLEDGEMENTS

Though only my name appears on the cover of this thesis, a great many people have contributed to its production. I owe my gratitude to all those people who have made this thesis possible and because of whom my graduate experience has been one that I will cherish forever.

First and foremost, I have to thank my parents for their love and support throughout my life. Thank you both for giving me strength to reach for stars and chase my dream.

I would like to express sincerest gratitude to my advisor, Dr. Hussam Mahmoud, for his support, guidance, collaboration, and the many great opportunities he continued to present since the day we first met. I would also like to thank and recognize my committee members, Dr. Rebecca Atadero and Dr. Allan Kirkpatrick, for their support, inputs, and participation; each of which provided invaluable advice on topics of their own respect whether towards research and my professional development.

To all my friends, thank you for your understanding, encouragement and help in my many moments of crisis. I cannot list all the names here, but you are always on my mind. Your friendship makes my life a wonderful experience.

## TABLE OF CONTENTS

Chapter 1 Introduction .....	1
1.1 Statement of Problem .....	1
1.2 Objectives of Research.....	3
1.3 Scope of Research .....	4
1.4 Organization of Thesis .....	5
Chapter 2 Background and Literature Review .....	6
2.1 Introduction .....	6
2.2 Effect of Fire on Steel Structure.....	6
2.2.1 Overview .....	6
2.2.2 Case Studies of Past Fire Events .....	7
2.2.3 Fire Simulation Methodologies .....	15
2.2.4 Heat Transfer Mechanics.....	19
2.2.5 Behavior of Steel Frames Exposed to Fire .....	21
2.3 Braced Steel Frames Collapse Behavior Study.....	24
2.3.1 Modeling Technique .....	25
2.3.2 Past Analysis Review .....	26
2.4 Steel Connections under Fire .....	29
2.4.1 Overview .....	29
2.4.2 Shear Tab Connection.....	29
2.4.3 Moment Connection .....	37
2.5 Summary .....	40
Chapter 3 Structure Framework .....	41
3.1 Introduction .....	41
3.2 Structure Description .....	41
3.2.1 Building Configuration and Member Sizes .....	41
3.2.2 Connection Design .....	44
3.3 Material Properties .....	45
3.3.1 Steel Overview .....	45
3.3.2 Temperature-Dependent Mechanical Properties for Steel.....	46
3.3.3 Temperature-Dependent Thermal Properties for Steel .....	48
3.3.4 Johnson-Cook Damage Model for Steel.....	51
3.3.5 Lightweight Concrete Properties.....	52
3.4 Summary .....	53
Chapter 4 Finite Element Models .....	54

4.1 Introduction.....	54
4.2 Structural Members, Slab, and Gusset Plate Model.....	55
4.2.1 Overview.....	55
4.2.2 Columns, Girders, Beams, and Braces Model.....	55
4.2.3 Slab and Gusset Plate Model.....	56
4.3 Connection Model.....	57
4.3.1 Moment Connection.....	57
4.3.2 Shear Connection.....	57
4.3.3 Other Connections.....	59
4.4 Shear Link Model.....	59
4.5 Imperfection Model.....	61
4.6 Thermal Analysis.....	61
4.6.1 Fire Time-Temperature Curve Selection.....	62
4.6.2 Heat Transfer Model.....	65
4.7 Fire Induced Collapse Analysis.....	66
4.7.1 Gravity Load.....	66
4.7.2 Thermal Load.....	66
4.8 Modeling Technique Validation.....	66
4.8.1 Overview.....	66
4.8.2 Line Element Model Validation.....	67
4.8.3 Mechanical Response Validation.....	69
4.9 Summary.....	70
Chapter 5 Simulation Results and Discussion.....	72
5.1 Overview.....	72
5.2 Naming Scheme.....	72
5.3 Fire Analysis Scenarios – 8 Cases.....	74
5.4 Global System Response.....	77
5.4.1 Case 1.....	77
5.4.2 Case 2.....	78
5.4.3 Case 3.....	79
5.4.4 Case 4.....	80
5.4.5 Case 5.....	81
5.4.6 Case 6.....	82
5.4.7 Case 7.....	83
5.4.8 Case 8.....	84
5.5 Discussion.....	85
5.6 Response of Individual Frames.....	86
5.6.1 Case 1.....	86
5.6.2 Case 2.....	89
5.6.3 Case 3.....	91
5.6.4 Case 4.....	93

5.6.5 Case 5 .....	95
5.6.6 Case 6 .....	97
5.6.7 Case 7 .....	99
5.6.8 Case 8 .....	100
5.6.9 Discussion .....	102
5.7 Critical Behavior of Structural Members .....	103
5.7.1 Column Vertical Displacement.....	103
5.7.2 Column Axial Force .....	110
5.7.3 Column End Moment Diagram .....	126
5.7.4 Interaction Diagram.....	143
5.7.5 Shear Connector Failure.....	154
5.7.6 Moment Connector Rotation .....	164
5.8 Comparison .....	165
5.8.1 Different Fire Scenarios – Case 1 VS. Case 2.....	165
5.8.2 Different Bracing System – Case 6 VS. Case 8.....	167
5.8.3 Different Fire Curves – Case 3 VS. Case 7 .....	168
5.8.4 Discussion .....	169
5.9 Summary .....	170
Chapter 6 Conclusion.....	171
6.1 General .....	171
6.2 Summary .....	172
6.3 Conclusions .....	173
6.4 Recommendations .....	174
6.4.1 Design Recommendations.....	174
6.4.2 Analytical Modeling Recommendation and Future Work .....	175

## LIST OF TABLES

Table 3.1 Column Configuration .....	44
Table 3.2 Girder Configuration .....	44
Table 3.3 Beam and Brace Configuration .....	44
Table 3.4 Constants for 4340 Steel .....	52
Table 4.1 Material Parameters of CDP Model for Concrete (Jankowiak and Lodygowski 2005).....	56
Table 4.2 Dynamic Properties of Structures .....	70
Table 5.1 Simulation Cases Summary .....	75
Table 5.2 Collapse Sequence for Case-1 .....	78
Table 5.3 Collapse Sequence for Case-2.....	79
Table 5.4 Collapse Sequence for Case-3.....	80
Table 5.5 Collapse Sequence for Case-4.....	81
Table 5.6 Collapse Sequence for Case-5.....	82
Table 5.7 Collapse Sequence for Case-6.....	83
Table 5.8 Collapse Sequence for Case-7.....	84
Table 5.9 Collapse Sequence for Case-8.....	85
Table 5.10 Case-1 CBF Frame B Collapse Sequence .....	87
Table 5.11 Case-1 Gravity Frame 2 Collapse Sequence .....	88
Table 5.12 Case-2 CBF Frame B Collapse Sequence .....	89
Table 5.13 Case-2 Gravity Frame 2 Collapse Sequence .....	90
Table 5.14 Case-3 EBF Frame B Collapse Sequence .....	91
Table 5.15 Case-3 Gravity Frame 2 Collapse Sequence .....	92
Table 5.16 Case-4 EBF Frame B Collapse Sequence .....	93
Table 5.17 Case-4 Gravity Frame 2 Collapse Sequence .....	94
Table 5.18 Case-5 CBF Frame B Collapse Sequence .....	95
Table 5.19 Case-5 Gravity Frame 2 Collapse Sequence .....	96
Table 5.20 Case-6 CBF Frame B Collapse Sequence .....	97
Table 5.21 Case-6 Gravity Frame 2 Collapse Sequence .....	98
Table 5.22 Case-7 EBF Frame B Collapse Sequence .....	99
Table 5.23 Case-7 Gravity Frame 2 Collapse Sequence .....	100
Table 5.24 Case-8 EBF Frame B Collapse Sequence .....	101
Table 5.25 Case-8 Gravity Frame 2 Collapse Sequence .....	102
Table 5.26 Case-1 Ratios of $P_u/\phi P_n$ at Elevated Temperatures.....	112
Table 5.27 Case-2 Ratios of $P_u/\phi P_n$ at Elevated Temperatures.....	114
Table 5.28 Case-3 Ratios of $P_u/\phi P_n$ at Elevated Temperatures.....	116
Table 5.29 Case-4 Ratios of $P_u/\phi P_n$ at Elevated Temperatures.....	118
Table 5.30 Case-5 Ratios of $P_u/\phi P_n$ at Elevated Temperatures.....	120
Table 5.31 Case-6 Ratios of $P_u/\phi P_n$ at Elevated Temperatures.....	122

Table 5.32 Case-7 Ratios of $Pu\phi Pn$ at Elevated Temperatures.....	123
Table 5.33 Case-8 Ratios of $Pu\phi Pn$ at Elevated Temperatures.....	125
Table 5.34 Case-1 Ratios of $Mux\phi Mnx$ at Elevated Temperature .....	128
Table 5.35 Case-1 Ratios of $Muy\phi Mny$ at Elevated Temperature.....	129
Table 5.36 Case-2 Ratios of $Mux\phi Mnx$ at Elevated Temperature .....	130
Table 5.37 Case-2 Ratios of $Muy\phi Mny$ at Elevated Temperature.....	131
Table 5.38 Case-3 Ratios of $Mux\phi Mnx$ at Elevated Temperature .....	132
Table 5.39 Case-3 Ratios of $Muy\phi Mny$ at Elevated Temperature.....	133
Table 5.40 Case-4 Ratios of $Mux\phi Mnx$ at Elevated Temperature .....	134
Table 5.41 Case-4 Ratios of $Muy\phi Mny$ at Elevated Temperature.....	135
Table 5.42 Case-5 Ratios of $Mux\phi Mnx$ at Elevated Temperature .....	136
Table 5.43 Case-5 Ratios of $Muy\phi Mny$ at Elevated Temperature.....	137
Table 5.44 Case-6 Ratios of $Mux\phi Mnx$ at Elevated Temperature .....	138
Table 5.45 Case-6 Ratios of $Muy\phi Mny$ at Elevated Temperature.....	139
Table 5.46 Case-7 Ratios of $Mux\phi Mnx$ at Elevated Temperature .....	140
Table 5.47 Case-7 Ratios of $Muy\phi Mny$ at Elevated Temperature.....	141
Table 5.48 Case-8 Ratios of $Mux\phi Mnx$ at Elevated Temperature .....	142
Table 5.49 Case-8 Ratios of $Muy\phi Mny$ at Elevated Temperature.....	143
Table 5.50 Case-1 Interaction Equation Value at Key Temperature Points .....	145
Table 5.51 Case-2 Interaction Equation Value at Key Temperature Points .....	146
Table 5.52 Case-3 Interaction Equation Value at Key Temperature Points .....	147
Table 5.53 Case-4 Interaction Equation Value at Key Temperature Points .....	149
Table 5.54 Case-5 Interaction Equation Value at Key Temperature Points .....	150
Table 5.55 Case-6 Interaction Equation Value at Key Temperature Points .....	151
Table 5.56 Case-7 Interaction Equation Value at Key Temperature Points .....	152
Table 5.57 Case-8 Interaction Equation Value at Key Temperature Points .....	153

## LIST OF FIGURES

Figure 1.1 Elevation View of Braced Frame Systems .....	2
Figure 1.2 Collapse of WTC-7.....	3
Figure 2.1 Local Buckling of Column (Newman, 2000) .....	9
Figure 2.2 Churchill Plaza Fire .....	10
Figure 2.3 Fires on Floors 7 and 12 on the North Face (NIST, 2004) .....	12
Figure 2.4 Horizontal Progression to the West Side of WTC-7 (NIST, 2004).....	13
Figure 2.5 Windsor Building Fire (NILIM, 2005) .....	15
Figure 2.6 Conduction, Convection, and Radiation.....	20
Figure 2.7 Shear Tab Connection.....	30
Figure 2.8 Floor Plan of Cardington Fire Test Steel Structures (British Steel, 1999).....	32
Figure 2.9 Shear Tab Connection Failure in Cardington Fire Test (British Steel, 1999) .....	32
Figure 2.10 Modes of Failure for Shear Tab Connection.....	35
Figure 2.11 Local buckling of bottom flange of beam-to-column Specimen at 650°C (Yang et al., 2009) 38	
Figure 3.1 Plan View of Test Structure .....	42
Figure 3.2 Elevation View of Exterior and Interior Frames.....	43
Figure 3.3 Typical Shear Tab Connection Details.....	45
Figure 3.4 Reduction Factors for the Stress-Strain Relationship of Carbon Steel at Elevated Temperature .....	47
Figure 3.5 Temperature Dependent Relative Thermal Elongation of Carbon Steel.....	48
Figure 3.6 Thermal Conductivity of Steel.....	49
Figure 3.7 Specific Heat of Steel .....	50
Figure 4.1 Component-based model for shear tab connection.....	58
Figure 4.2 Schematic of Shear Link Model .....	60
Figure 4.3 Details of Shear Link Model (Khandelwal, El-Tawil, and Sadek 2009) .....	61
Figure 4.4 ASTM E-119 versus EC Parametric Fire Curves .....	63
Figure 4.5 The EHR and ZSR steel frames (Memari and Mahmoud 2014) .....	67
Figure 4.6 EHR Frame Results .....	68
Figure 4.7 ZSR Frame Results.....	68
Figure 4.8 Mode shapes of CBF .....	69
Figure 4.9 Mode Shapes of EBF.....	69
Figure 5.1 Generalized Floor Plan of the two Buildings with the inner frames being CBF in one case and an EBF in the other case .....	73
Figure 5.2 Elevation View of (a) CBF frame and (b) EBF frame.....	73
Figure 5.3 CBF with Corner Compartment Fire (a) front view and (b) isometric view .....	75
Figure 5.4 CBF with Whole Floor Fire (a) front view and (b) isometric view .....	76
Figure 5.5 EBF with Corner Compartment Fire (a) front view and (b) isometric view .....	76
Figure 5.6 EBF with Whole Floor Fire (a) front view and (b) isometric view .....	76

Figure 5.7 Case-1 Vertical Displacements of First Floor Columns.....	103
Figure 5.8 Case-2 Vertical Displacements of First Floor Columns.....	104
Figure 5.9 Case-3 Vertical Displacements of First Floor Columns.....	105
Figure 5.10 Case-4 Vertical Displacements of First Floor Columns.....	106
Figure 5.11 Case-5 Vertical Displacements of First Floor Columns.....	107
Figure 5.12 Case-6 Vertical Displacements of First Floor Columns.....	108
Figure 5.13 Case-7 Vertical Displacements of First Floor Columns.....	109
Figure 5.14 Case-8 Vertical Displacements of First Floor Columns.....	110
Figure 5.15 Case-1 First Floor Column Axial Forces.....	112
Figure 5.16 Case-2 First Floor Column Axial Forces.....	114
Figure 5.17 Case-3 First Floor Column Axial Forces.....	116
Figure 5.18 Case-4 First Floor Column Axial Forces.....	118
Figure 5.19 Case-5 First Floor Column Axial Forces.....	120
Figure 5.20 Case-6 First Floor Column Axial Forces.....	121
Figure 5.21 Case-7 First Floor Column Axial Forces.....	123
Figure 5.22 Case-8 First Floor Column Axial Forces.....	125
Figure 5.23 Case-1 First Floor Column End Moment.....	128
Figure 5.24 Case-2 First Floor Column End Moment.....	130
Figure 5.25 Case-3 First Floor Column End Moment.....	132
Figure 5.26 Case-4 First Floor Column End Moment.....	134
Figure 5.27 Case-5 First Floor Column End Moment.....	136
Figure 5.28 Case-6 First Floor Column End Moment.....	138
Figure 5.29 Case-7 First Floor Column End Moment.....	140
Figure 5.30 Case-8 First Floor Column End Moment.....	142
Figure 5.31 Case-1 Interaction Equation Value.....	145
Figure 5.32 Case-2 Interaction Equation Value.....	146
Figure 5.33 Case-3 Interaction Equation Value.....	147
Figure 5.34 Case-4 Interaction Equation Value.....	148
Figure 5.35 Case-5 Interaction Equation Value.....	150
Figure 5.36 Case-6 Interaction Equation Value.....	151
Figure 5.37 Case-7 Interaction Equation Value.....	152
Figure 5.38 Case-8 Interaction Equation Value.....	153
Figure 5.39 Floor Plan of the Buildings showing the Selected Shear Connector.....	155
Figure 5.40 Case-1 First Floor Shear Connector Nodes Separation.....	156
Figure 5.41 Case-2 First Floor Shear Connector Nodes Separation.....	157
Figure 5.42 Case-3 First Floor Shear Connector Nodes Separation.....	158
Figure 5.43 Case-4 First Floor Shear Connector Nodes Separation.....	159
Figure 5.44 Case-5 First Floor Shear Connector Nodes Separation.....	160
Figure 5.45 Case-6 First Floor Shear Connector Nodes Separation.....	161
Figure 5.46 Case-7 First Floor Shear Connector Nodes Separation.....	162
Figure 5.47 Case-8 First Floor Shear Connector Nodes Separation.....	163

Figure 5.48 Selected Moment Connector .....	164
Figure 5.49 Moment Connector Rotation .....	165
Figure 5.50 Column Vertical Displacement – Case 1 VS. Case 2.....	166
Figure 5.51 Column Interaction Equation – Case 1 VS. Case 2 .....	166
Figure 5.52 Column Vertical Displacement – Case 6 VS. Case 8.....	167
Figure 5.53 Column Interaction Equation – Case 6 VS. Case 8 .....	167
Figure 5.54 Column Vertical Displacement – Case 3 VS. Case 7.....	168
Figure 5.55 Column Interaction Equation – Case 3 VS. Case 7 .....	169

# CHAPTER 1 INTRODUCTION

## 1.1 Statement of Problem

According to the National Fire Protection Association (NFPA) report, there were 1,298,000 fires reported in the United States in 2014 (NFPA, 2015). Of the reported cases, 494,000 were structural fires, causing 2,860 civilian deaths, 13,425 civilian injuries, and \$9.8 billion in property damage (NFPA, 2015). Due to recent structural collapse of the World Trade Centers on September 11, 2001, the response of steel structures subjected to fire loading has become an important design consideration. Consequently, significant increase in research on buildings under fire has been realized in the U.S. to develop a rational design methodology for steel structures subjected to elevated temperatures. While significant amount of research has been conducted in the past on steel members and subassemblies under fire, particularly in Europe, the response of steel buildings exposed to fire loadings has not received a similar level of attention. Furthermore, the 3D response of steel buildings with braced frames remains relatively unknown. In addition, only handful of previous studies encompassed the full response of the system all the way including collapse.

Steel braced frames are commonly used structural systems for mitigating lateral load demands such as winds and earthquakes. There are several types of bracing systems that can be employed in the construction of steel buildings. This study focuses on concentrically braced frames (CBFs) and eccentrically braced frames (EBFs), as shown in Figure 1.1 (a) and Figure 1.1(b), respectively. In CBFs, the steel braces provide lateral stiffness and strength to the structural system and contribute to seismic energy dissipation by yielding in tension and buckling in compression. In EBFs, the braces are designed to remain elastic during lateral

loading, so that energy dissipation is achieved by concentrating inelastic deformations in designated regions called “shear links”. The seismic behavior of CBFs and EBFs is fairly well understood as a result of extensive research conducted in the past. However, their behavior under fire loadings is yet to be fully investigated and therefore are the focus of this study.

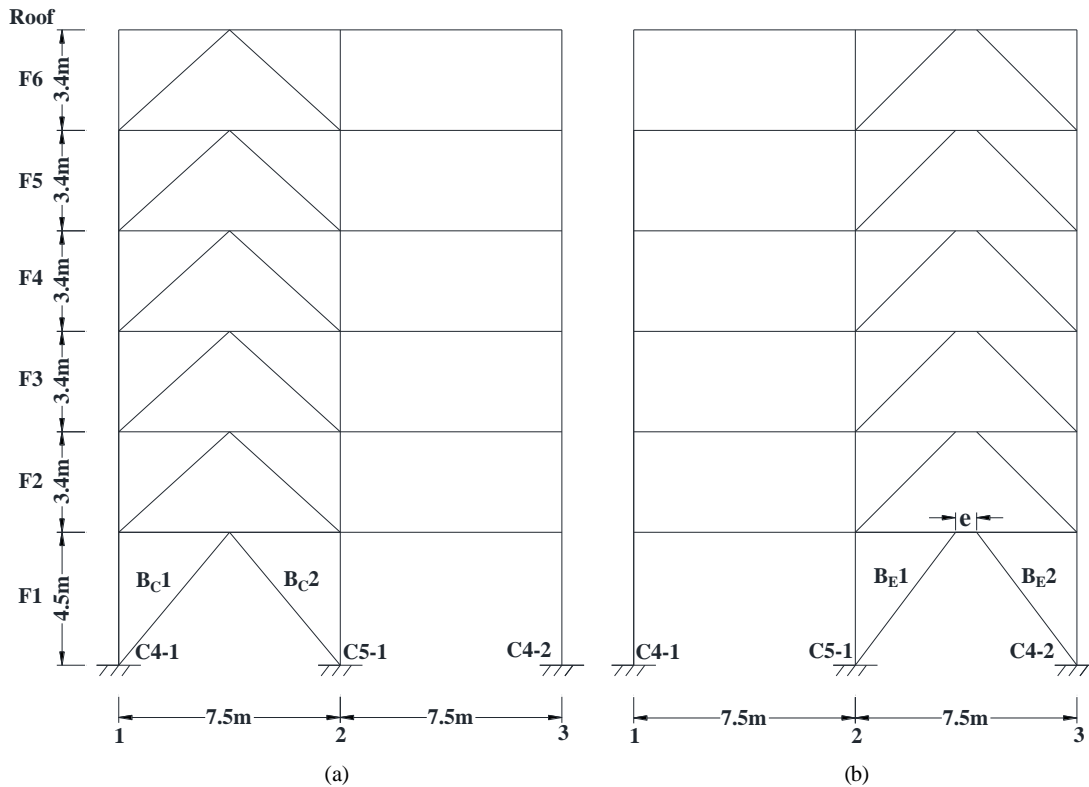


Figure 1.1 Elevation View of Braced Frame Systems

Progressive collapse is a complex dynamic process wherein a collapsing system seeks alternative load paths in order to survive loss of a critical structural member. The collapse of the old 7 World Trade Center (WTC-7), caused by failure of a northeast building column brought on by fire-induced damage to the adjacent flooring system and connections (Figure 1.2), has emphasized the need for a better understanding of the collapse behavior of steel structures during fire scenarios. The collapse made the old WTC-7 the first tall

building and skyscraper known to have completely collapsed primarily due to uncontrolled fires. Therefore, a better understanding of system response due to fire-induced progressive collapse can provide substantial insight that could potentially lead to advances towards developing performance-based design provision that can result in safe and economical design of steel buildings under fire loadings. In this study, a new simulation methodology for the collapse assessment of steel buildings with braced frames exposed to fire is devised. In addition, the developed simulation approach is utilized to evaluate the full response of 3D steel building, up to and including collapse, when subjected to different fire loading conditions.



Figure 1.2 Collapse of WTC-7 (Photo: CBS News)

## 1.2 Objectives of Research

The objective of this research is to understand the 3D fire-triggered progressive collapse mechanisms of steel buildings that employ different types of braced frames. The specific objectives of this research are summarized as follows:

- 1) Advance knowledge that would allow for systematic evaluation of collapse performance of steel framed buildings under fires or other hazards.
- 2) Evaluate force and displacement demands on steel building structures during different fire events.

- 3) Investigate failure of steel members under elevated temperature and evaluate possible alternative load carrying paths.
- 4) Assess performance of braced frames in a typical steel-framed building under localized fire, and explore improved design concepts and details.
- 5) Provide an analytical case study for evaluating the adequacy of current building code provisions, considering the potential failure modes during fire exposure.

The ultimate goal is to develop and apply analytical simulations for systematic evaluation of the collapse limit-state for steel buildings of various frame configurations under different fire scenarios.

### **1.3 Scope of Research**

The objectives described in the previous section are realized using various research tasks that encompass the scope of this study. Specifically, three-dimensional numerical models are developed and analyzed using the general-purpose finite element software ABAQUS (SIMULIA, 2014). Two six-story structures with different bracing systems (one with CBF and one with EBF) are evaluated using different time-temperature curves and under different fire scenarios. The steel properties at elevated temperature defined in *European code* (Eurocode 3 EN 1993-1-2, 2005) are utilized in the simulations. Proper failure criteria are added in the models to allow for element separation and fracture so that accurate simulation results can be obtained.

## **1.4 Organization of Thesis**

This thesis is divided into six chapters. Chapter 1 introduces the statement of problem, objectives, and scope of this research. Chapter 2 provides the relevant background material including past significant fire cases in steel buildings and review of related studies. Chapter 3 describes the tested structures and the material properties at elevated temperature used in the numerical models. Chapter 4 starts with description of the modeling approach followed by a validation analysis and focuses on extending previous simulation techniques to allow for capturing localized failures and system collapse. Chapter 5 presents the results of the numerical simulations. Chapter 6 provides a summary of this research as well as conclusions and recommendations based on the outcomes of the study.

## **CHAPTER 2 BACKGROUND AND LITERATURE REVIEW**

### **2.1 Introduction**

Relevant background materials related to this study are reviewed in this chapter, including a high-level overview of fire science, the effects of fire on steel frame buildings, and studies related to steel building collapse. Extensive analytical and experimental studies have been previously conducted to evaluate the performance of steel components under elevated temperature. However, studies pertaining to the collapse of steel buildings under ambient and elevated temperature are generally limited. Section 2.2 introduces fundamental knowledge on the response of steel structures to fire loading including review of past major steel building fire events. Section 2.3 follows with presenting state-of-the-art techniques for modeling progressive collapse of braced steel frames. Section 2.4 discusses damage models that have been developed for shear and moment connections under fire. The final section provides a brief summary of this chapter.

### **2.2 Effect of Fire on Steel Structure**

#### **2.2.1 Overview**

While steel structures are generally known to perform adequately under elevated temperature, the performance under such loading conditions is not well understood. The term “adequately” here refers to the ability of the structure to substantially deform and withstand the elevated temperatures without collapsing. Of course, the term “adequate” is subjective since one might desire to have minimal to no deformation as a performance objective. That being said, conducting life-cycle cost assessment could provide a more

quantifiable mean for assessing the adequacy under elevated temperature or any other extreme hazard for that matter. The reason for the limited understanding of the response of steel structures under fire loading is because of the substantial reduction in stiffness and strength of steel at elevated temperature, which requires specific testing and simulation capabilities. From a simulation perspective, the problem is multifaceted in nature and requires simulation of 1) fire behavior, 2) heat transfer to the structure and among the structural components and 3) structural response where substantial deformations are expected. For structural engineers, the primary effect is the degradation of stiffness and strength of steel at elevated temperatures and the consequential possibility of localized structural failures that could lead to global system collapse.

The following sections provide relevant background material for this study related to historical events pertaining to the response of steel structures exposed to fire. Case studies from past building fires are examined and relevant observations and implications are discussed. A brief overview of all components involved in the simulation of buildings exposed to fire is presented. These include simulation of fire, heat transfer mechanisms, and the response of braced steel frames under elevated temperature.

### **2.2.2 Case Studies of Past Fire Events**

Experimental testing and analytical simulations are very critical to evaluate the behavior of steel structures under fire. Substantial number of studies have been conducted on the material, single steel member, and connection levels; however very limited work has been conducted to evaluate global system response of steel structures under elevated temperature. The lack of system-level analysis is due to the technical

difficulties associated with testing or numerically simulating system response under elevated temperature. Due to the lack of enough studies on a system-level, assessment of past true fire events is therefore critical to understanding crucial behavioral issues.

#### **2.2.2.1 Broadgate Phase 8 Fire, London, UK (1990)**

In 1990, a fire ignited within a construction site on the first level of a partially completed 14-story steel-frame office building at the Broadgate development in London (British Steel, 1999). Flame temperatures during the fire were estimated to be over 1000°C. At the time of the fire, much of the steel framework was unprotected, and an approximate area of 40m by 20m was damaged beyond repair. However, investigators noted that the heat-affected framework responded in a ductile manner, and that the system remained stable by redirecting load along alternative paths. In addition, the integrity of the composite floor slab was maintained throughout the duration of exposure. Following the fire, a metallurgical investigation concluded that temperatures in the steel framework did not exceed 600°C (British Steel, 1999). A similar investigation on the bolts used in the steel connections also concluded that the peak temperature, which was either attained during the manufacturing process or as a consequence of the fire, was less than 540°C (British Steel, 1999).

Beams that had large permanent displacements showed evidence of local buckling in the bottom flange and web regions near the end supports. This behavior was thought to be predominately influenced by mechanical restraint against thermal expansion provided by the surrounding cooler structure (Newman, 2000). Unprotected steel columns that were fully exposed to fire also showed signs of local buckling, and

subsequent axial shortening. The column deformations were thought to have been the result of the rigid transfer beams in the upper level of the building restraining thermal expansion of the heat-affected column regions. Figure 2.1 shows the local buckling in a heat-affected column. It was noted that the heavier exposed column sections within the fire compartment showed no signs of permanent deformation, most likely attributed to the larger volume-to-surface area aspect ratios that resulted in lower steel temperatures (Newman, 2000).



Figure 2.1 Local Buckling of Column (Newman, 2000)

#### **2.2.2.2 Churchill Plaza Fire, Basingstoke, UK (1991)**

In 1991, a fire developed on the 8<sup>th</sup> floor of the 12-story steel-frame Mercantile Credit Insurance Building located at Churchill Plaza in Basingstoke in south central England (British Steel, 1999). Failure of the glazing (Figure 2.2) allowed the fire to spread rapidly to the 10<sup>th</sup> floor. It is believed that the glazing failure also produced relatively cool fire exposure conditions due to increased ventilation.

The building was constructed in 1988 and utilized a passive fire protection scheme designed to have 90min fire resistance. The composite steel floor beams were protected with spray-applied fire-resistive insulation, and the steel columns were protected with heat-resistant boards. Investigators found that the fire protection materials performed well and that there were no permanent deformations in the steel framework. The protected steel frame connections also showed no signs of distress.

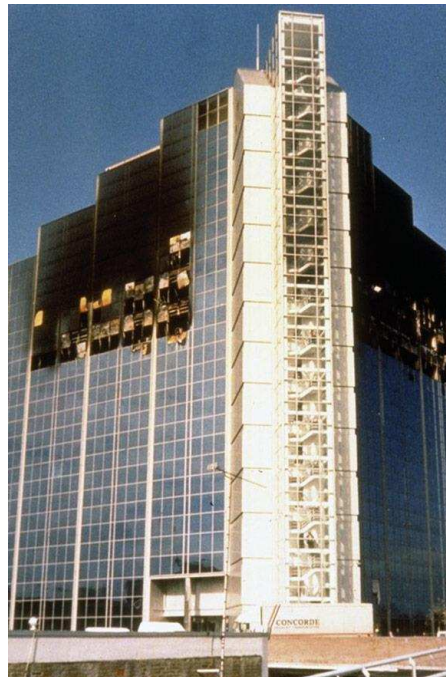


Figure 2.2 Churchill Plaza Fire (Photo: <http://www.newsteelconstruction.com/>)

### **2.2.2.3 World Trade Center building 7, New York, USA (2001)**

World Trade Center Building 7 (WTC-7) is one of the buildings in the World Trade Center complex that was 47-story tall. On September 11<sup>th</sup> 2001, this steel commercial building located in the north region of the complex, experienced a complete collapse at 5:21 p.m. (NIST, 2004). The collapse made the old WTC-7 the first tall building known to have collapsed primarily due to uncontrolled fires, and the first and only

steel skyscraper in the world to have collapsed due to fire. The overall dimensions of WTC building 7 were 100m long by 43m wide with approximate height of 190m (NIST, 2005). The final design for WTC7 was for a much larger building than originally planned when the substation was built (NIST, 2010). The structural design of WTC7 therefore included a system of gravity column transfer trusses and girders, located between floors 5 and 7, to transfer loads to the smaller foundation (NIST, 2008).

On the day of the collapse, heavy debris, from the failure of twin towers impacted the WTC-7, damaging the south face of the building and starting fires that continued to burn throughout the afternoon on at least 10 floors. However, only fires on floors 7-9 and 11-13 burned out of control as shown in Figure 2.3. While the building was equipped with a sprinkler system its vulnerability was rather elevated through various large potential of various single-point failures. For example, the sprinkler system required manual activation of the electrical fire pumps as opposed to being a fully automatic system. In addition, single connection to the sprinkler water riser were utilized at the floor-level control and power was required by the sprinkler system for the fire pump to deliver water (NIST, 2008). Moreover, the water pressure was low, with little or no water to feed sprinklers. The collapse initiation was at the eastern part of the building due to failure of a key column. The failure of the column was due to failure of a girder on floor 13 that lost its connection to the column, which essentially increased the effective length of the column and caused it buckle. The column buckling triggered progression of failure in the floor systems that reached the building's penthouse. It took about 8 seconds from first downward movement at the penthouse to initiation of the global collapse, which was a result of successive series of failures. It has been argued that the lack of a water supply for the automatic sprinkler system and the malfunctioning of the sprinkler system as a whole were responsible for

the WTC 7 collapse. While this might be true, the collapse of WTC 7 highlighted the importance of designing fire-resistant structures or at the very least understand the expected performance under fire conditions. Factors contributing to building failure included: thermal expansion occurring at temperatures hundreds of degrees below those typically considered in design practice for establishing structural fire resistance ratings; significant magnification of thermal expansion effects due to the long-span floors, which are common in office buildings in widespread use; connections that were designed to resist gravity loads, but not thermally induced lateral loads; and a structural system that was not designed to prevent fire-induced progressive collapse (NIST, 2008). The probable sequence of events leading to the collapse is illustrated in Figure 2.4.

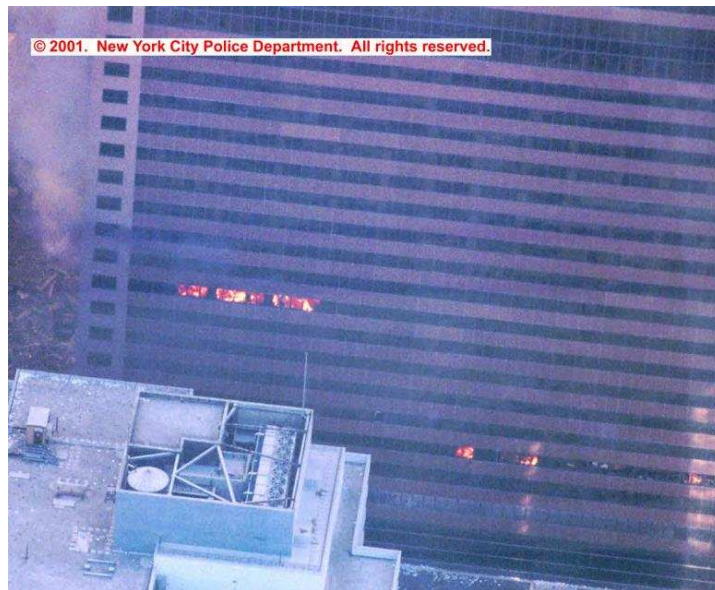


Figure 2.3 Fires on Floors 7 and 12 on the North Face (NIST, 2004)

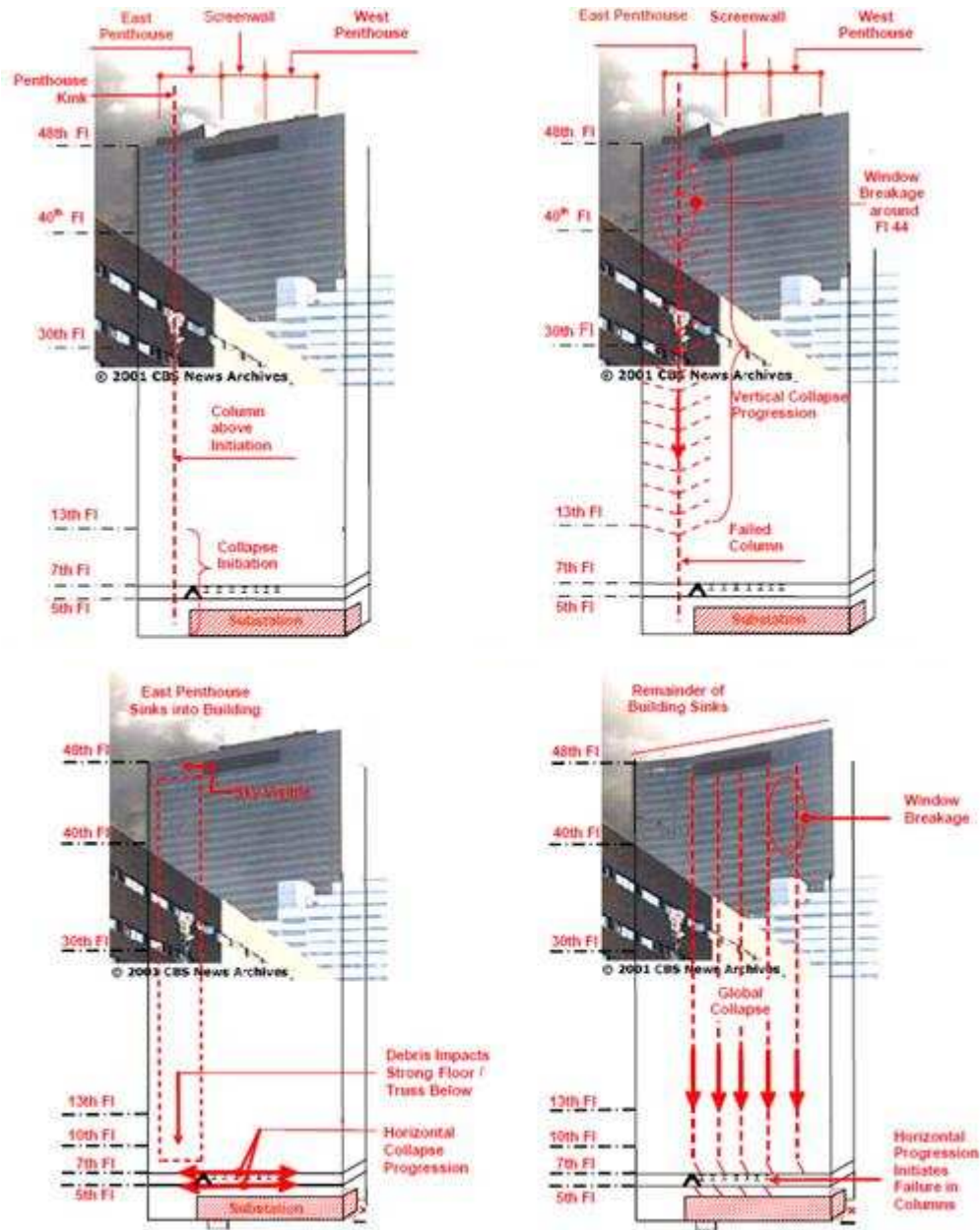


Figure 2.4 Horizontal Progression to the West Side of WTC-7 (NIST, 2004)

#### 2.2.2.4 Windsor Building, Madrid, Spain (2005)

On February 12<sup>th</sup>, 2005, fire ignited in the Windsor building in Madrid, Spain. The fire ignited at approximately 11:00 p.m. on the 21st floor of the 32-story (106m) office building and quickly progressed

to the top floor by 1am the next day. The top ten floors were eventually totally consumed in flames, which gradually spread to the lower floors ultimately reaching downward to the 4<sup>th</sup> floor by 9:00 a.m. The fire was not under control until almost 2:00 p.m., giving the fire a total duration between 18 and 20 hours.

The floor plan is approximately 40m x 25m. The building was a composite steel and reinforced concrete structure. The structure, completed in 1979, was constructed based on the 1970's Spanish design codes, which had minimal specifications regarding fire protection. The building was under renovation when the fire occurred, which included installation of sprinklers as well as fire protection on structural members. The renovations had been implemented on the ground floors all the way to the 17<sup>th</sup> floor but no protection had been installed on the 18<sup>th</sup> floor or higher up.

Structural damage was significant on the top 11 stories due to the lack of fire protection. Perimeter steel columns including exterior bays of waffle slabs almost completely collapsed. However, the reinforced concrete core maintained its strength and prevented total collapse of the structure. The partial collapse mechanisms reported in NILIM (2005) was described in the following manner: (1) the steel columns near the fire buckled due to material degradation at elevated temperatures; (2) the axial loads on the buckled columns were redistributed to adjacent structural members; (3) the number of deteriorated columns increased due to the developing fire; however the waffle slab worked as a cantilever and prevented structural collapse; (4) The fire spread and the waffle slabs reached their load capacity as a cantilever for the extended supporting area and ultimately collapsed; and (5) the floor collapse triggered failure of other floors and the waffle slabs were ripped off at the connections to the core. It was found that a mechanical floor between

the 16<sup>th</sup> and 17<sup>th</sup> floors provided enough redundancy to prevent progressive collapse. Figure 2.5 provides a before, during, and after the event images of the structure.



Figure 2.5 Windsor Building Fire (NILIM, 2005)

## 2.2.3 Fire Simulation Methodologies

### 2.2.3.1 Overview

The amount of fuel available, the flow of oxygen, and the temperature of the fire are key factors to the development of fires in building structures. Building fires are caused from a wide range of scenarios but the initial combustion reaction only occurs when a fuel temperature is raised above its combustion point in the presence of oxygen. Once the initial combustion of the fuel source begins, it releases heat thereby increasing the temperature of the surrounding environment. As the adjoining fuel sources reach their combustion point, the fire grows engulfing the surrounding environment until it becomes fully developed. The fire continues to burn at this extreme temperature until the fuel sources are exhausted and the fire begins to decay and eventually burn out.

A natural fire curve can be divided into three main phases: growth, full development, and decay. The flashover point is the transition point of the fire from growing to fully developed; this typically involves fire spreading from the area of localized burning to all combustible surfaces within the area. After flashover, the heat release rate remains at a maximum as long as fuel and oxygen supplies last. This is important because once a building fire reaches the flashover point it is almost impossible for firefighters to stop it and sprinklers are designed to only work at the growth phase of the fire. The sprayed-on fire proofing material is the only defense against a fully developed fire at this point.

Simulating the response of buildings and their members under fire loading is extremely complicated due to the intricate nature of building fires. Most countries around the world use simple fire resistance tests that utilize standardized fire curves to evaluate the behavior of building components and structural members during a fire. This methodology has several limitations and has been severely criticized by the structural engineering community because it does not take into account any of the physical parameters affecting fire growth and development. This has led researchers to start to use more realistic and complex methods for simulating the response of structures to fire loading. The following sections provide a brief overview of standard fire curves as well as parametric fire curves, which are considered more realistic since they include both a heating and cooling phase.

### **2.2.3.2 Standard Fire Curves**

The typical methodology for determining the performance of structural members and various nonstructural building components during a fire is based upon fire resistance testing. These tests utilize standard fire curves that have been established by the industry, most notably ASTM E-119 (ASTM, 2016), ISO 834 (ISO, 2014) and the Eurocode Standard Fire Curve model (EC1, 2002).

The standard fire curve used in the United States comes from the ASTM E119 - Standard Test Methods for Fire Tests of Building Construction and Materials (ASTM, 2016), which was one of the first published standardized tests that established a fire resistance rating for steel members through a prescribed method. This test also served as a basis for the determination of fire resistance ratings in other tests such as ISO 834 and various European codes. The basic principle behind standard fire resistance testing is to expose a single structural member or assembly to a standard fire curve with designated fuel load and intensity. Results are based on the highest temperature seen by the unexposed surface of the member being tested and if that member fails in a way that creates the release of hot gases. In addition to these requirements, the E119 standard test for wall systems also includes an assessment of the ability of the wall to withstand the pressure of fire hose following the fire. A fire resistance rating is then assigned to the specimen based on the time it took to fail.

These standard tests have numerous shortcomings that limit the amount of useful information that can be obtained from them. The standard fire curves were based on fuels that were commonly found in buildings at the time when the tests were first published in the early 1900s. This has proven rather non-conservative

since it has been shown that modern fuel sources can create fires with considerably faster rates of growth and higher radiative fractions, which can have an impact on the fire spread rates (NIST, 2005). Another consideration is the addition of automatic sprinkler systems, which can limit the growth phase of the fire and is not often considered during standard fire testing today. The physical limitations of standard furnaces are another major weakness of these tests. A typical furnace only allows for specimens to be tested individually and cannot accommodate and include the interaction of structural systems or the implementation of boundary loads (gravity, lateral, etc.). End restraints and loading conditions are very difficult to accurately replicate in a furnace making it difficult to test anything other than very basic structural elements. These tests are outdated and provide a prescriptive rating that reflects a time when prescriptive design was primarily used. However, recent shift towards performance-based design has created a need for other more realistic methods to be developed.

### **2.2.3.3 Parametric Fire Curves**

In addition to the previously discussed standard fire curves, various codes and standards now include parametric fire curves. These fire curves provide a simplified design procedure to estimate room temperature in post-flashover compartment fires. The ventilation conditions, compartment size, and thermal properties of compartment walls and ceilings, and the fuel load are considered in parametric fire curves. In addition, a parametric fire curve includes a cooling phase that are critical for evaluating the proper demand on structural elements since significant demand is thought to develop through this cooling phase particularly in the presence of member restraints.

In comparison to the previously discussed standard fire curves, parametric fires provide a more realistic estimate of the compartment temperature to be used in structural fire design. While this methodology provides a much more realistic fire scenario, it should be noted that there are several assumptions that form the basis for the development of these curves:

1. Complete combustion occurs and is contained within the boundaries of the compartment.
2. The temperature within the compartment is uniform.
3. Estimated values for thermal inertia are typically used.
4. The flow of heat through the compartment walls is assumed to occur only in one direction.

#### **2.2.4 Heat Transfer Mechanics**

Heat transfer during a fire event can be divided into three transport mechanisms: conduction, convection, and radiation, which are illustrated schematically in Figure 2.6. The following sections provide a brief discussion regarding each of these processes.

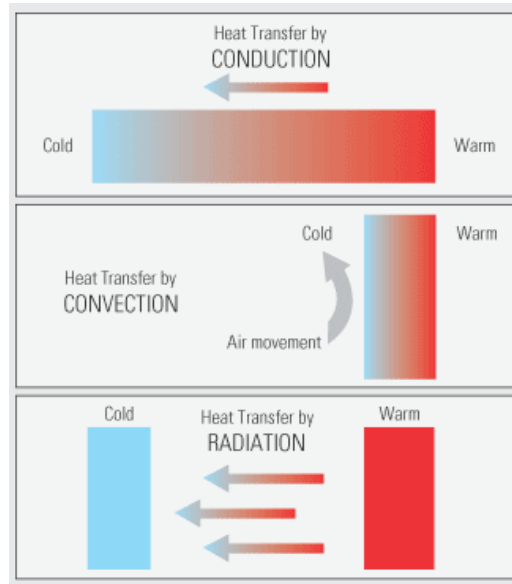


Figure 2.6 Conduction, Convection, and Radiation; (<http://www.metroglass.co.nz/catalogue/093.aspx>)

#### 2.2.4.1 Conduction

In solid materials, conduction is the mechanism for heat transfer. In materials that are good conductors, heat is transferred by interactions involving free electrons. As a result, materials that are good electrical conductors are usually good conductors of heat as well. In materials that are poor conductors, heat is conducted by mechanical vibrations of the molecular lattice. Conduction of heat is an important factor in the ignition of solid surfaces, and in the fire resistance of fire protections and structural members.

#### 2.2.4.2 Convection

Convection is heat transfer mechanism caused by the movement of fluids and is an important factor in flame spread throughout system as well as the upward transport of smoke and hot gas. The rate of heating or cooling for a solid body immersed in a fluid environment is highly dependent on the fluid velocity at the

boundary surface. In a building compartment fire, convective heat transfer is driven by buoyancy forces that arise from temperature gradients in the heated air. This process is referred to as natural convection.

#### **2.2.4.3 Radiation**

Radiation is the transfer of energy by electromagnetic waves, which can travel through a vacuum or through a transparent solid or liquid. Radiation is extremely important in fires because it is the main mechanism for heat transfer from flames to fuel surfaces, from hot smoke to building objects, and from a burning building to an adjacent building. Thermodynamic considerations show that an ideal thermal radiator, or blackbody, will emit energy at a rate proportional to the fourth power of the absolute temperature of the body and directly proportional to its surface area.

#### **2.2.5 Behavior of Steel Frames Exposed to Fire**

Understanding the behavior of braced steel frames exposed to fire is the focus in this study. Several subjects including properties of structural steel at elevated temperatures along with the expected response of steel connections and structural members exposed to thermal loading require thorough understanding. The following sub-sections provide a review of materials on steel frames under fire. The temperature dependent properties of steel are provided in detail in the next chapter.

### **2.2.5.1 Review of Experimental Work**

The performance of complete structural frames under the simultaneous action of fire, vertical, and horizontal loads was investigated by Rubert and Schaumann (1986). The study focused on evaluating the failure temperatures of heated systems in relation to design parameters at ambient temperature such as the load factor and the system slenderness. Several steel frames were tested in the study, two of which were selected for validation of the modeling technique as discussed in chapter 4.

Early experimental work on the behavior of steel structures under fire was usually conducted on simply supported specimens or on small size frames. However, two large-scale fire tests of steel buildings at elevated temperature have been conducted. In 1990, a series of large-scale fire tests were conducted at the Broken Hill Proprietary (BHP) Research Laboratories in Melbourne, Australia to evaluate the fire performance of an existing 41-story steel frame office building (British Steel, 1999). The tests were conducted using a purpose-built test structure that was representative of a 12m by 12m corner bay of the actual building. The test structure was furnished with a 4m by 4m compartment designed to resemble a typical office environment. A total of four fire tests were conducted. Two of the tests were concerned with evaluating the performance of the existing light hazard sprinkler system, and a third was designed to assess the fire resistance of the existing composite slab. In the fourth test, a simulated office fire was conducted to evaluate the fire resistance of unprotected steel beams, considering the influence of thermal shielding from a conventional suspended ceiling system. The office fire produced a peak atmospheric temperature of 1228°C and steel temperature of 632°C. Steel temperatures in the shielded beams reached 632°C. The peak beam displacement, measured at mid-span, was recorded as 120mm, and it was noted that most of this

deflection was recovered after the test. The study concluded that the thermal shielding from a conventional suspended ceiling system could significantly enhance the fire resistance of a steel frame floor system during fire exposure.

In the mid-1990s, one of the most significant experimental programs investigating fire behavior of steel buildings was the Cardington program as mentioned before, in which a full-scale eight-story steel framed structure was studied under fire exposure at the Cardington, UK research facility of the Building Research Establishment (Cardington, 1998). The steel building tested at Cardington was constructed with composite floors, and a number of steel beams in the composite floors were not fire protected and would not have satisfied the U.S. prescriptive fire protection requirements. Despite the absence of fire protection, the floor system and the entire structure was capable of sustaining severe fire exposure without collapse. The Cardington tests demonstrated the potential for significant cost savings in fire protection while still maintaining the safety of steel structures under fire exposure. One of the important outcomes of the Cardington research was the conclusion that the key behavioral factor that affects the ability of a floor system to survive a fire is the development of tensile catenary and membrane action resulting from the large vertical displacements, which normally occur in a fire.

#### **2.2.5.2 Review of Analytical Work**

Saab and Nethercot (1991) conducted analytical assessments of frames using nonlinear finite element simulations of two-dimensional steel frames under fire. The simulations included the effects of material inelasticity and geometric nonlinearity, and temperature variations along and across members. Comparisons

were made with fire test results on frames and columns that represented a wide range of problem parameters such as slenderness, end conditions, load levels, and temperature distributions. In all cases, the agreements between the analytical models and the test results were satisfactory.

Najjar and Burgess (1996) developed three-dimensional frame analysis of skeletal frames under fire conditions. The models included material inelasticity as a function of temperature and accounted for geometric nonlinearities. When non-uniform temperature distribution is present, differential thermal expansion will occur and give rise to the spread of a inelastic behavior across the section. The model has been validated against a range of previous analyses of large-deflection elastic, inelastic and fire problems. The former case is shown to correspond well with the current British design code's prediction of failure temperature. After 9-11 event, the focus of steel frame study has been shifted to fire-induced collapse which will be reviewed in the next section.

### **2.3 Braced Steel Frames Collapse Behavior Study**

Because braced frames can significantly increase the lateral strength of structures, at a lower cost in comparison to moment frames, and provide extra loading path to prevent collapse, braced frames are a common design alternative of steel structures. Extensive studies on the behavior of braced frames under different types of loading, including fire, as well as collapse behavior has been conducted by various researches.

### **2.3.1 Modeling Technique**

Two-dimensional finite element modeling is commonly used by practicing engineers due to its efficiency, reasonable results and ease of convergence. However, the limitations of 2-D models are also obvious since they dismiss key behavioral features including participation of gravity frames, including floor beams, and concrete slabs in the load carrying mechanisms.

In Quiel and Garlock's (2008), some modeling parameters that affect the use of FE models to predict the behavior and capacity of a high-rise steel moment frame under fire were evaluated. In particular, the study focused on perimeter columns and girders that frame into them perpendicular to the building's exterior. The parameters examined included 3-D frame models versus a 2-D plane frame models and representation of the slab in the 2-D plane-frame model. Results from a prototype building frame show that the 3-D and 2-D models experience similar structural behavior and reach the element limit states. The 3-D models, however, require significantly more run time and computational effort. The 2-D models can therefore be used to reasonably and efficiently model the fire-exposed performance of a plane frame. Results also indicate that in the 2-D models, the slab should be considered in the thermal analysis of the girder, but it can be neglected in the structural analysis since it has a negligible effect. It is important to note that while these assumptions are valid for the purpose of the conducted study, these conclusions will not hold true when evaluating a fire-induced progressive collapse, which is the focus of this present study. This studies did not consider complete collapse, or progressive collapse, of the subassembly because of numerical convergence issues.

### **2.3.2 Past Analysis Review**

The mechanism of collapse of steel structures under extreme loading such as blast or fire is not fully understood. Fire-induced collapse analysis has attracted much attention following the 911 events. Various studies on collapse of steel structures at ambient and elevated temperature. Various limitations however exist such as the ability to only model local failure or a portion of the collapse.

Khandelwal, El-Tawil, and Sadek's (2009) investigated the progressive-collapse resistance of seismically designed steel braced frames by using validated computational simulation models. Two types of braced systems are considered in their study: special concentrically braced frames (SCBF) and eccentrically braced frames (EBF). The study was conducted on previously designed 10-story prototype building by applying the alternate path method. In this methodology, critical columns and adjacent braces, if present, are instantaneously removed from an analysis model and the ability of the model to successfully absorb member loss is investigated. Member removal in this manner is intended to represent a situation where an extreme event or abnormal load destroys the member. The simulation results show that while both systems benefit from placement of the seismically-designed frames on the perimeter of the building, the EBF is less vulnerable to progressive collapse than the SCBF. Improvement in behavior is due to improved system and member layouts in the former compared to the latter rather than the use of more stringent seismic detailing.

Sun, Huang, and Burgess (2012) developed a robust static–dynamic procedure to capture progressive collapse mechanisms of braced two-dimensional steel-framed structures under fire. A total of twenty cases were analyzed to study the mechanisms of progressive collapse for these frames, with different bracing

systems under different fire conditions. It was shown that the pull-in of columns is one of the primary factors which generate progressive collapse. The study also highlighted the limited ability of horizontal “hat truss” bracing systems in avoiding pull-in of columns supporting the heated floor. However, these systems can redistribute the vertical load that was carried by a column before it buckled to adjacent columns. Vertical bracing systems were also evaluated and they were shown to be able to not only increase the lateral restraint of the frame, which reduces the pull-in of the columns, but also of preventing local failures from developing into a progressive collapse. The study showed that frames with combined hat and vertical bracing system can be designed to enhance the capability of the frame to prevent progressive collapse when a heated column buckles.

Agarwal and Varma (2013) presents a qualitative assessment of the importance of gravity columns on the stability of a typical mid-rise steel building subjected to corner compartment fires. the study included the analysis of wo ten-story steel buildings with composite floor systems. The lateral load resisting systems in the analyzed frames comprised of a perimeter moment resisting frames (MRFs) in one building and an interior core of RC shear walls in the other buildings. Numerical finite element models were utilized to assess the effects of gravity loads and fire conditions on system performance. The results indicated that gravity columns govern the overall stability of the buildings as they are most likely to reach their critical temperatures first. Once a gravity column fails, the load will shed to neighboring columns in an attempt for the system to maintain its own overall structural stability. Additional improvements to the flexural and tensile strengths of the composite floor system was provided by the additional steel reinforcements, which allowed for the development of catenary action in the slab and the preservation of structural stability after

failure of a gravity column. In their study, the researchers only showed the early stage of failure and total collapse was not simulated.

Jiang, Li, and Usmani (2014) used OpenSees to study the collapse mechanisms of steel frames exposed to single and multi-compartment fires. The influence of the lateral and vertical bracings on the resistance of structures against progressive collapse is studied. The conclusions made in the study can be summarized as follows:

1. The collapse of steel frames under fire is triggered by buckling of a heated columns followed by subsequent buckling of the columns at the same story of that of the heated column or below.
2. The collapse mechanism of frames is in the form of lateral drift of the frame above the heated floors and downward collapse of frames along the heated bay. The sway of frames is driven by the unbalanced demand resulting from the tensile force generated in the heated floor due to the catenary action of beams under large deflection.
3. The resistance of steel frames against progressive collapse can be enhanced by applying lateral and vertical restraints and the combination of these two restraints shows a better resistance than that of the application of one of them alone.

## **2.4 Steel Connections under Fire**

### **2.4.1 Overview**

Steel connections have always been considered as important parts of any structure steel building because they provide the strong links between the principal structure members. Various experimental tests and analytical studies have been done to study behaviors of different types steel connection under different load including fire. In this review, the performance of two types of connections was evaluated and included shear tab connections and moment connections. Past fire events and previous tests showed that proper modeling of connection behavior at elevated temperature is critical for obtaining accurate structural response to fire. In the numerical model of the structure, connection modeling including the corresponding damage and failure characteristic is adopted in this study as will be explained later in Chapter 4.

### **2.4.2 Shear Tab Connection**

The shear tab connection or single-plate connection is a common type of shear connection in structural steel buildings. It is considered a simply supported connection since only small end moments can develop in the beam with this type of connection. A standard shear tab connection consists of a single plate welded to a column flange with a distance between the vertical weld and the bolt line of the connection, typical configuration of this type of connection is shown in Figure 2.7. The popularity of this connection type is largely due to its relatively low cost associated with fabrication and installation.

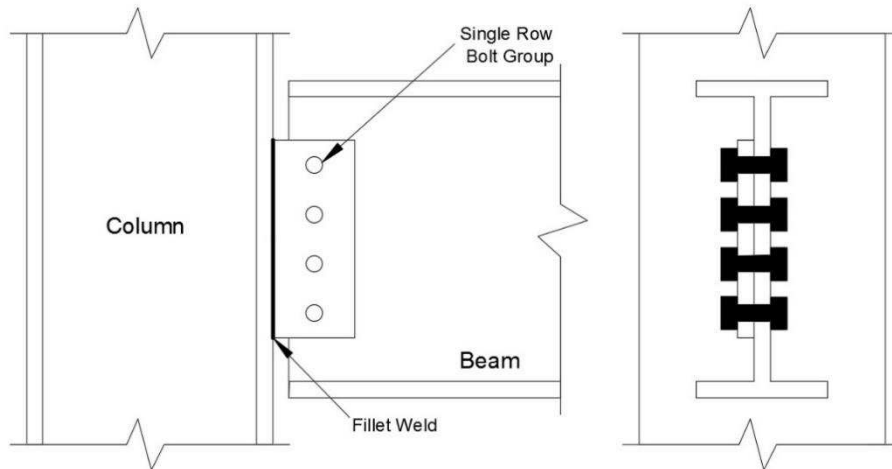


Figure 2.7 Shear Tab Connection

#### 2.4.2.1 Experimental Studies

The behavior and failure mode of shear tab connection under different loadings were well documented and predicted by several researchers. This review is only focused on tests of shear tab connections under fire condition. Experimental testing of shear tab connections subject to fire has been extensively investigated by various researchers.

Yu et al. (2009) investigated the robustness of common types of steel connections when subjected to fire. Test results on typical shear tab connections subjected to combination of shear and tying forces were presented. The test results showed that the resistances of shear tab connections are significantly affected by temperature. It was observed that, when weaker bolts were used, all shear tab connections failed by bolt shear fracture. The reduction in the resistance of the connection as a whole, relative to its resistance at ambient temperature, follows that of the bolts. Using stronger bolts caused the connections to fail by block shear of the beam web after high bearing deformation at ambient temperature. At elevated temperatures,

the failures were still controlled by bolt shear, but the maximum resistance was significantly enhanced. In general, the test results show bolt shear fracture tends to govern failure of shear tab connections at elevated temperatures. As a consequence, it was concluded that specifying shear tab connections seems inadvisable where large connection rotations are anticipated.

The Cardington Fire Test was a series of large-scale fire tests conducted of steel structures with composite concrete slab. This test identified the discrepancies between the behavior of an individual member and a member in a structural system at elevated temperature. The steel test structure was built in 1993 and comprised of steel framed construction using composite concrete slabs supported by steel decking in composite action with the steel beams. It has eight stories (33m height) and is five bays wide ( $5 \times 9 = 45\text{m}$ ) by three bays deep ( $6 + 9 + 6 = 21\text{m}$ ) in plan, see Figure 2.8. The main steel frame was designed for gravity loads, the connections consisting of flexible end plates for beam-to-column connections and shear tab for beam-to-beam connections were designed to transmit vertical shear load. Seven large-scale fire tests at various positions within the experimental building were conducted. The main objective of the compartment fire tests was to assess the behavior of structural elements with real restraint under a natural fire. The failures of shear tab connection were observed as shown in Figure 2.9 as the bolts sheared due to thermal contraction of the beam during cooling.

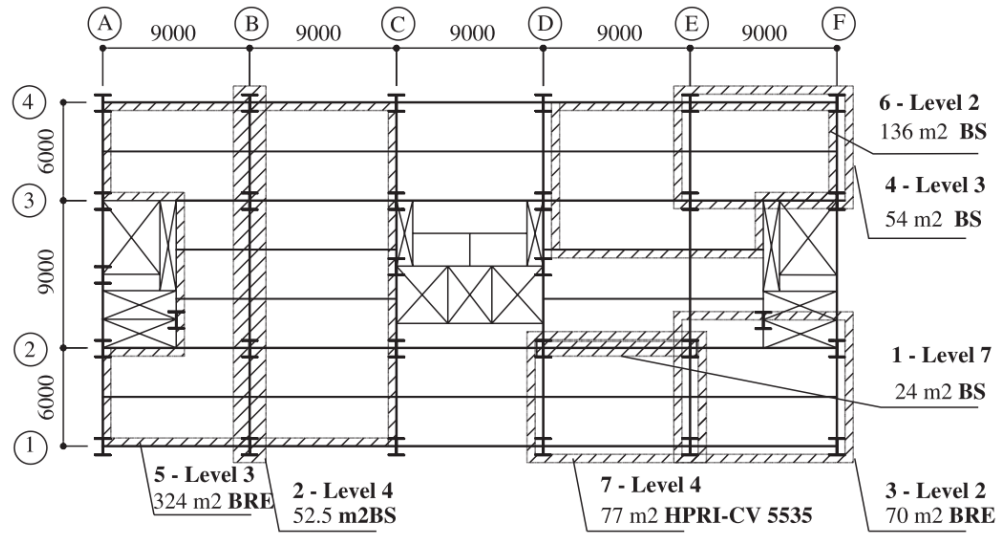


Figure 2.8 Floor Plan of Cardington Fire Test Steel Structures (British Steel, 1999)



Figure 2.9 Shear Tab Connection Failure in Cardington Fire Test (British Steel, 1999)

### 2.4.2.2 Analytical Studies

Most studies on the behavior of shear tab connections under fire were focused on predicting connection response to different loading such as shear, tying or combined forces. An extensive analytical study was

conducted by Selamet and Garlock (2010) on modeling shear tab connections under fire. It was found that large compressive and tensile forces could damage the connections and threaten the structural integrity of floors especially in multi-story buildings during a fire event. Shear tab connections should be robust enough to overcome fire-induced forces and secondary moments during both fire growth and fire decay in order to ensure the structural integrity of floor systems. The study investigated simple and cost-effective modifications of single plate connections to resist the forces and deformations induced by thermal loads during a real fire scenario. The results showed that significant improvements in behavior of such connections could be achieved by any of the following - 1) adding a double plate to the beam web; 2) matching the single plate thickness to the beam web thickness; 3) using a larger distance from the bolt-hole centerline to the beam end; and 4) increasing the gap distance between the end of the beam to the connected member. Using larger bolt holes can also improve the fire performance since the larger holes would provide less axial restraint as more freedom is given for the beam to move (expand, contract, rotate) with the fire-imposed thermal loads.

In Hu and Engelhardt's research (2010), the behavior of single plate connections was evaluated using finite element analysis during both the growth and decay phase of a fire. A refined three-dimensional finite element connection model was developed and used to study connection forces and deformations developed both during the heating and cooling phases of a fire event. Residual forces and deformations in the connection after completion of the cooling phase were also examined in the study. Design implications of the analyses were also discussed. Other than the parameters studied, the concrete slab was also believed to have significant effects on connection behavior in fire. Therefore, finite element modeling of the composite

action of a whole floor system including the concrete slab and shear studs is vital for proper quantification of the 3D response of the system. In addition, it was also noted that the finite element model captured the experimentally observed deformations quite well. However, the models were not able to accurately capture the final fracture modes of the connection, such as bolt shear fracture or bearing tear-out.

A component-based model for shear tab connections was developed by Sarraj (2007) and is adopted in this study. In the model, the whole connections are treated as a group of springs to represent each bolt row, plus bearing parts of two connected plates. A detail description of the connection model will give in the next chapter.

### **2.4.2.3 Shear Tab Connection Failure**

Six potential failure modes of shear tab connections are identified as follows: 1) yielding of the gross area of the plate, 2) bearing of the plate and beam web bolt holes, 3) fracture of the edge distance of bolts, 4) shear fracture of the net area of the plate, 5) fracture of bolts, and 6) fracture of welds. Consistent with the aim of providing a rational design procedure, the above failure modes were divided into two categories: ductile failure modes (Modes 1 and 2) involving yielding of steel and brittle failure modes (Modes 3 to 6) involving fracture of steel. For each failure mode, a design formula was suggested in the AISC Specifications (365-10). The design procedures were developed to ensure that the ductile failure mode will occur first, followed by the more brittle ones. The six failure modes for shear tab connections are summarized in Figure 2.10.

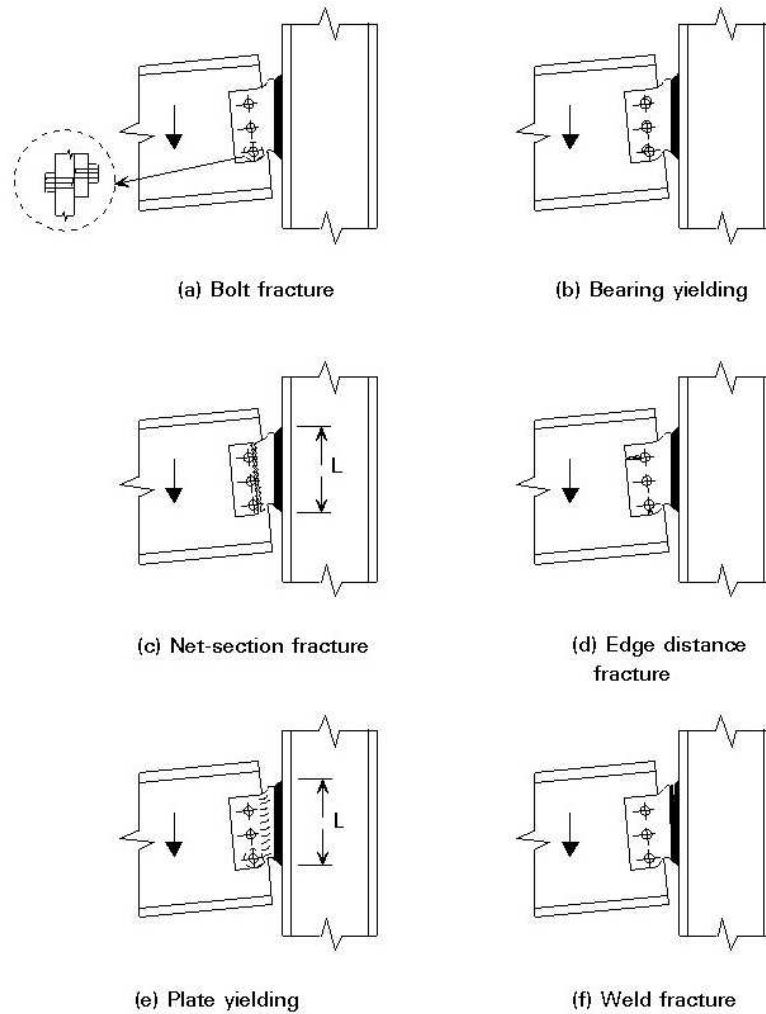


Figure 2.10 Modes of Failure for Shear Tab Connection (<http://www.fgg.uni-lj.si/~pmoze/esdep/master/wg11/10500.htm>)

Limit states of shear tab connections subjected to fire and design implication are given in Hu and Engelhardt (2010). Under fire conditions, structural deformations are less critical than at ambient temperature, and structural safety is a greater concern. Specifically, for beam end connections, fracture limit states are more critical than plate and web yielding or buckling in fire. While fracture in general is critical under fire loading, evidence from major fire events and high temperature tests suggest that weld fracture in fire is not typically

a controlling limit state, although further research is needed to confirm this issue. Therefore, based on the studies conducted to date, the critical limit states of shear tab beam end connections in fire can be identified as follows:

***In heating stage of fire event:***

- (1) Shear fracture or block shear fracture of the plate
- (2) Bolt shear fracture when the connection is under compression
- (3) Bolt shear fracture when the connection is under tension
- (4) Tear out fracture of the plate or beam web when the connection is under tension

***In cooling stage of fire event:***

- (1) Shear fracture or block shear fracture of the plate
- (2) Bolt shear fracture
- (3) Tear out fracture of the plate or beam web

The authors also suggested that when the connection is under compression in the initial stages of a fire, bolt shear fracture due to this large thermally-induced horizontal force combined with vertical gravity load is a key design concern. It was found that the thermally induced compression can cause local buckling in the beam web or single plate in previous studies and this phenomenon helps in reducing the compressive force. Therefore, a reasonably thin plate or beam web and strong bolts may be advantageous to ensure local buckling will occur before fracture of the bolts during beam expansion. When the connection is under

tension, no matter in the heating or cooling stage, bolt shear fracture, block shear fracture of the plate and tear out fracture are believed to be the critical failure modes. A combination of increased bolt hole edge distances with stronger bolts should be considered in design processes.

### **2.4.3 Moment Connection**

#### **2.4.3.1 Overview**

Moment connections are designed to carry a portion or the full moment capacity of the supported member as well as prevent any end-rotation of the member. Moment connections provide continuity between the supported and supporting members. The flanges of the supported member are attached either to a connection element or directly to the supporting member. Most tests and analyses have been focused on moment connections under cyclic loads, however in this review the main focus is moment connection behavior at elevated temperature.

#### **2.4.3.2 Effect of Elevated Temperature**

In the construction of steel buildings, prior to the 1994 Northridge earthquake, the welded flange-bolted web type moment connections are commonly used. The behavior of this type of connection under service load and seismic load has been studied extensively; however, the knowledge of its performance under fire load is limited. Experimental studies of welded flange-bolted web moment connections under fire loads were presented in Yang et al. (2009). Four full-size steel beam-to-column subassemblies, with and without fire-proofing materials, were selected to represent the moment connection commonly used in steel buildings.

From these studies, it was found that the beam-to-column connection was able to retain its design strength up to 650°C. However, the stiffness dropped to 25% of its value at ambient temperature. Ductile behaviors were observed with necking and tearing at the top flange and local buckling at the bottom flange. Local buckling at the bottom flange was observed in the study (Figure 2.11). The research also found that the stability and integrity of steel connections can be retained with proper fire-proofing materials.



Figure 2.11 Local buckling of bottom flange of beam-to-column Specimen at 650°C (Yang et al., 2009)

Mao et al. (2009) utilized the general purpose finite element software ANSYS to investigate the fire response of steel semi-rigid beam-to-column moment connections. The effect of bolts and weld was neglected in the study. The numerical model developed in their study was first verified by the full-scale fire tests implemented in Taiwan, and the results were found to be in good agreement with experimental results. The numerical results showed that the applied moments have significant effects on the stiffness of steel moment connections; however, the axial load of column, and shear and axial force of beam have less effect. For the cases of ambient temperature with increasing transverse load on beams, the connection stiffness is

constant when the connection is elastic, and it decreases with respect to the increase of transverse load on the beam when the plastic strain is reached. For the cases of constant load at elevated temperature, the stiffness of steel moment connections increases in the first stage before approximately 300°C, then a downturn occurs from the peak.

Following the failure of moment connections during the 1994 Northridge earthquake, a substantial experimental and numerical program was carried out to evaluate the behavior of reduced beam section connections under large inelastic demand. Memari and Mahmoud (2014) developed and analyzed a set of numerical models to assess the performance of low-, medium-, and high-rise moment resisting frames with RBS connection under single bay fire exposure including global system response and local behavior. Large axial force and deflection in the beams, yielding in the RBS connections, and buckling in the columns were observed in the simulations. Turbert (2013) and Mahmoud et al. (2015) investigated the behavior of steel RBS connections during a fire as well as during the combined events of fire following an earthquake (FFE).. In the study, 3D numerical finite element models were developed and employed the concept of adaptive boundary conditions in order to properly evaluate the performance of RBS connections under fire loading. The adaptive boundary conditions comprised of planar springs, with stiffness that varies with temperature, at the end of beam-column subassemblies, to represent the resistance that would be provided by the remainder of the frame. The presented methodology provided a practical analytical approach to perform accurate assessment of steel structures under fire and FFE and to investigate the characteristic behavior of critical connection details such as weld access holes, reduced portion of the beams, etc.

## 2.5 Summary

Relevant background materials for the study was presented in this chapter, the following list provides a summary of key points that were addressed:

- A review of past key fire events on steel structures were included in this chapter.
- A description of the various components that are needed for assessing the structural performance of steel buildings during a fire was presented. This included the different methodologies for simulating a fire and the heat transfer mechanisms.
- A brief comparison of standard fire curves and parametric fire curves were included in this part.
- A summary of previous experimental and analytical work that has been performed on steel buildings exposed to fire.
- The behavior of shear tab and moment connection under fire has been extensively investigated and is relatively well understood.
- A brief discussion of the progressive collapse studies that have been performed on braced steel structures. This sections includes a 3-D and 2-D modeling technic comparison.

## **CHAPTER 3 STRUCTURE FRAMEWORK**

### **3.1 Introduction**

In this study, two different six-story steel building structures were considered; namely a concentric braced frame (CBF) and an eccentrically braced frame (EBF). The two analyzed frames were previously experimentally tested at full-scale under seismic loading at the Ministry of Construction of Japan; as part of the U.S.-Japan Cooperative Earthquake Research Program (Roeder, Foutch, and Goel, 1988). The testing program comprised of various stages. Initially the building was constructed and tested as a concentric braced frame (CBF). The test building was then repaired, modified and tested as an eccentric braced frame (EBF). Following the EBF test, the building was further modified and tested as a moment frame without bracing system. Finally, cladding and other nonstructural elements were installed and further tests were conducted (Foutch, Roeder, and Goel, 1986). As previously indicated, in this present study the CBF and EBF frames are modeled and analyzed under different fire loadings and fire scenarios. Section 3.2 presents the detail descriptions of the model structure. The next section, Section 3.3, gives the material properties used in this study including damage model for materials. Finally, a brief summary of this chapter is provided in Section 3.4.

### **3.2 Structure Description**

#### **3.2.1 Building Configuration and Member Sizes**

The buildings are 15m square in floor plan with a height of 22.38m. The reference structure was designed as 2-bay by 2-bay six-story building that is 15m by 15m square (7.5m each bay) in both directions with slab

overhang girder line A and C by 0.5m. The general floor plan is shown in Figure 3.1. The structure includes three moment resisting frames A, B, and C in the direction of loading and three frames 1, 2, and 3 perpendicular to the loading direction. The girder-to-column connections in the frame lines A, B and C are fully welded moment connections. The pin connection between the girders and the columns and beams and girders at frame line 1, 2, and 3 are shear tab connections. The exterior frames 1 and 3, perpendicular to the direction of loading, contained X-braces in all bays to increase the building torsional stiffness. The elevation view of each frames is shown in Figure 3.2.

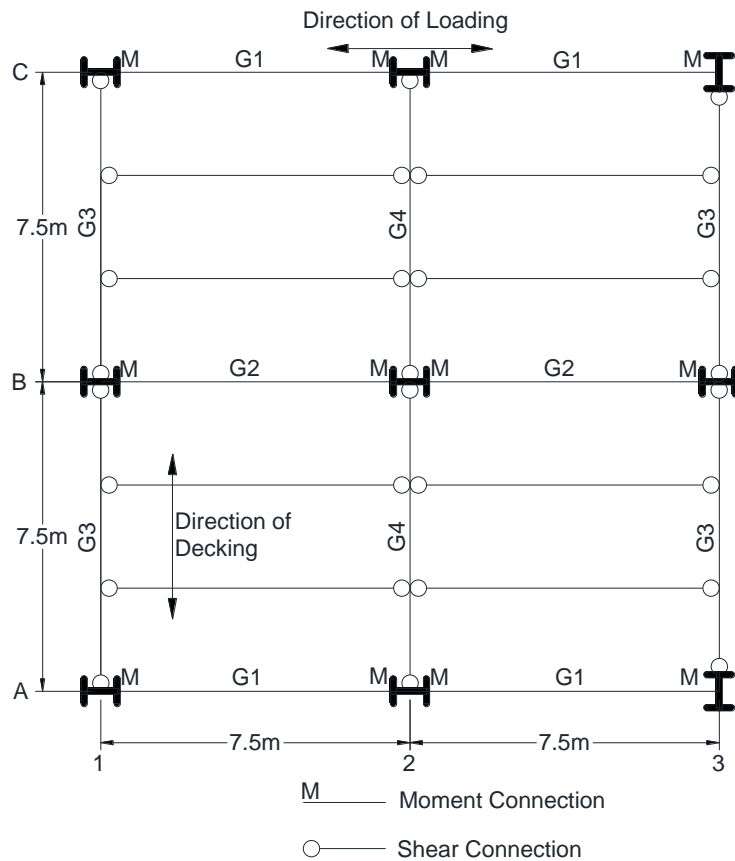


Figure 3.1 Plan View of Test Structure

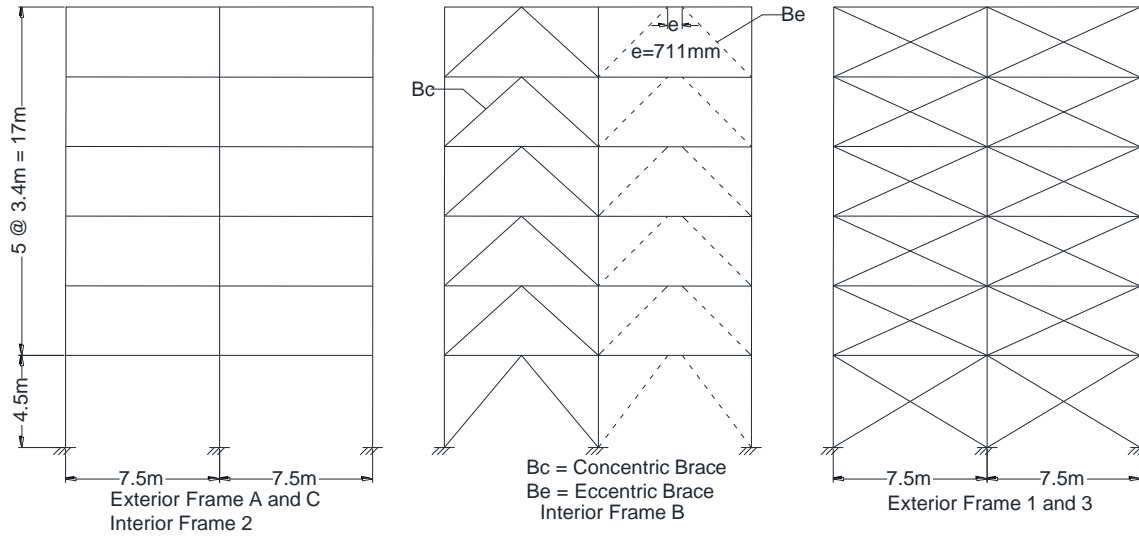


Figure 3.2 Elevation View of Exterior and Interior Frames

The columns, girders, and beams are wide-flange sections, sized as shown in Table 3.1, 3.2 and 3.3, respectively, and made with A36 steel material (Foutch, Roeder, and Goel 1986). The brace members are rectangular HSS made with A500 Grade B steel. Composite action between the beams and girders and the slabs was achieved using shear studs. The concrete slab was placed over a deep ribbed metal deck, and the ribs were parallel to the 1, 2, and 3 frames. The nominal slab thickness was 90mm and 165mm and was made of lightweight concrete. The concrete reinforcement bars were 6mm in diameter on a 100mm grid with a nominal minimum cover of 29mm. Shear studs were used to ensure composite action between the steel girders and the concrete slab.

Table 3.1 Column Configuration

Floor number	C1	C2	C3	C4	C5
6-5 F	W10x49	W10x33	W10x33	W10x33	W12x40
4-3 F	W12x65	W12x53	W10x39	W10x60	W12x72
2 F	W12x79	W12x65	W12x50	W12x79	W12x106
1 F	W12x87	W12x87	W12x65	W12x106	W12x136

Table 3.2 Girder Configuration

Floor number	G1	G2	G3	G4
R-6F	W16x31	W16x31	W18x35	W21x50
5F	W16x31	W18x35	W18x35	W21x50
4F	W18x35	W18x35	W18x35	W21x50
3F	W18x35	W18x40	W18x35	W21x50
2F	W18x40	W18x40	W18x35	W21x50

Table 3.3 Beam and Brace Configuration

Floor number	Floor Beam	X Brace	CBF Brace	EBF Brace
6-5 F	W16x31	ST 4x4x3/16	ST 4x4x3/16	ST 8x6x5/16
4 F	W16x31	ST 4x4x3/16	ST 5x5x1/4	ST 8x6x3/8
3-2 F	W16x31	ST 4x4x3/16	ST 6x6x1/4	ST 8x6x3/8
1 F	W16x31	ST 4x4x3/16	ST 6x6x1/4	ST 8x6x3/8

### 3.2.2 Connection Design

Different types of connections were utilized in this building as shown on the floor plan in Figure 3.1. Due to lack of details, in this present study all girder-to-column moment connections are assumed to be fully

weld. In addition, since no details for the shear connections were provided, the pin connection behavior is assumed to be introduced through the use of shear tabs and were designed using the 2010 AISC Specifications (AISC 365-10). The assumption made is that the number of bolts required for a shear tab connection would not change if an earlier version of an AISC Specification was used in the design. Figure 3.3 provides a detailed illustration of the typical shear tab connections assumed to have been used in this building.

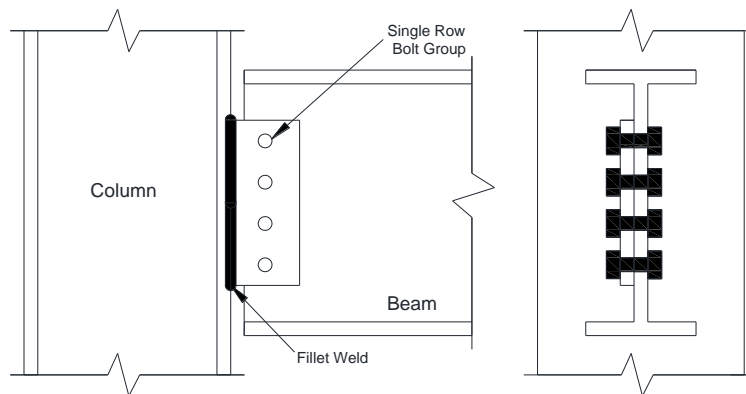


Figure 3.3 Typical Shear Tab Connection Details

### 3.3 Material Properties

#### 3.3.1 Steel Overview

The material specified for the W shapes was U.S. grade A36. The material properties required for the simulations comprised of density, damage, and temperature-dependent properties both for the thermal and mechanical analyses. The density of ASTM A36 steel was assumed as  $7800\text{kg/m}^3$ . The tensile strength of the A36 steel was assumed as 250 MPa with a Poisson's Ratio of 0.26. The brace members were cold formed square-shape tubes of ASTM A500 B steel with a specified yield stress of 315MPa. As most carbon steels the density of ASTM A500 B steel is around  $7850\text{kg/m}^3$ .

### 3.3.2 Temperature-Dependent Mechanical Properties for Steel

The temperature-dependent mechanical properties were adopted from *European code* (Eurocode 3 EN 1993-1-2, 2005). The mechanical properties of carbon steel included yield strength, Young's modulus, and thermal elongation.

Figure 3.4 shows the reduction factors for the stress-strain relationship for steel at elevated temperatures.

These reduction factors are defined as follows:

$k_{y,T} = f_{y,T}/f_y$  is the effective yield strength, relative to the yield strength at 20°C

$k_{p,T} = f_{p,T}/f_y$  is the proportional limit, relative to the yield strength at 20°C

$k_{E,T} = E_{a,T}/E_a$  is the slope of linear elastic range, relative to the slope at 20°C

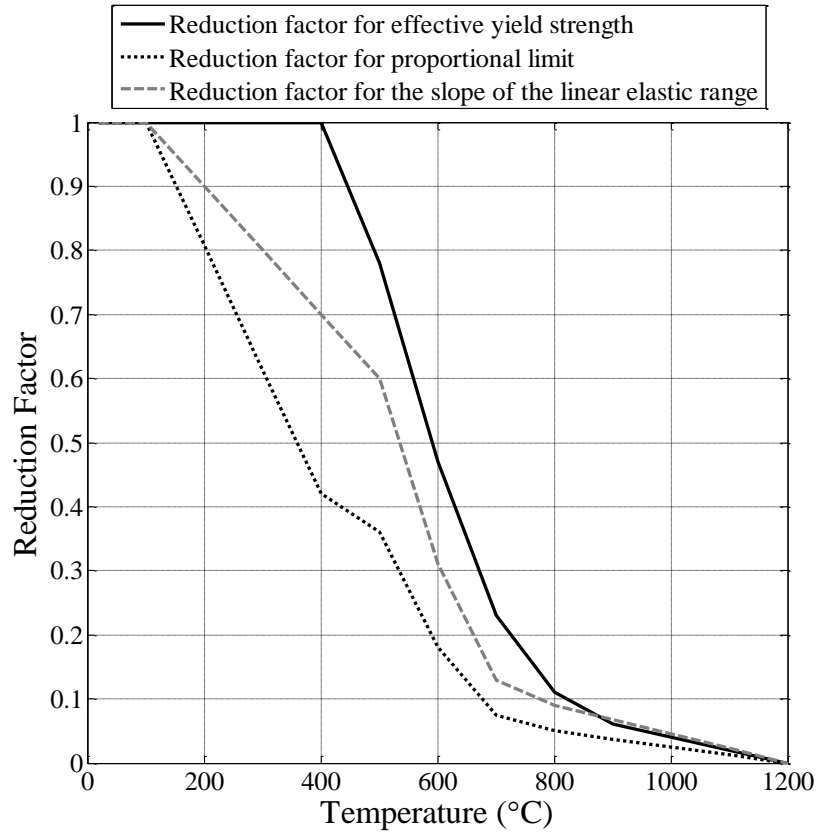


Figure 3.4 Reduction Factors for the Stress-Strain Relationship of Carbon Steel at Elevated Temperature

The relative thermal elongation of steel  $\Delta l/l$  is determined from the following equations in accordance with *European code* (Eurocode 3 EN 1993-1-8, 2005):

For  $20^{\circ}\text{C} \leq T < 750^{\circ}\text{C}$ ,

$$\Delta l/l = 1.2 \times 10^{-5}T + 0.4 \times 10^{-8}T^2 - 2.416 \times 10^{-4}$$

For  $750^{\circ}\text{C} \leq T \leq 860^{\circ}\text{C}$ ,

$$\Delta l/l = 1.1 \times 10^{-2}$$

For  $860^{\circ}\text{C} < T \leq 1200^{\circ}\text{C}$ ,

$$\Delta l/l = 2 \times 10^{-5}T - 6.2 \times 10^{-3}$$

Where:

$l$  is the length at 20°C;

$\Delta l$  is the temperature induced elongation;

$T$  is the steel temperature [°C].

The variation of the relative elongation with temperature according to *European code* (Eurocode 3 EN 1993-1-2, 2005) is illustrated in Figure 3.5.

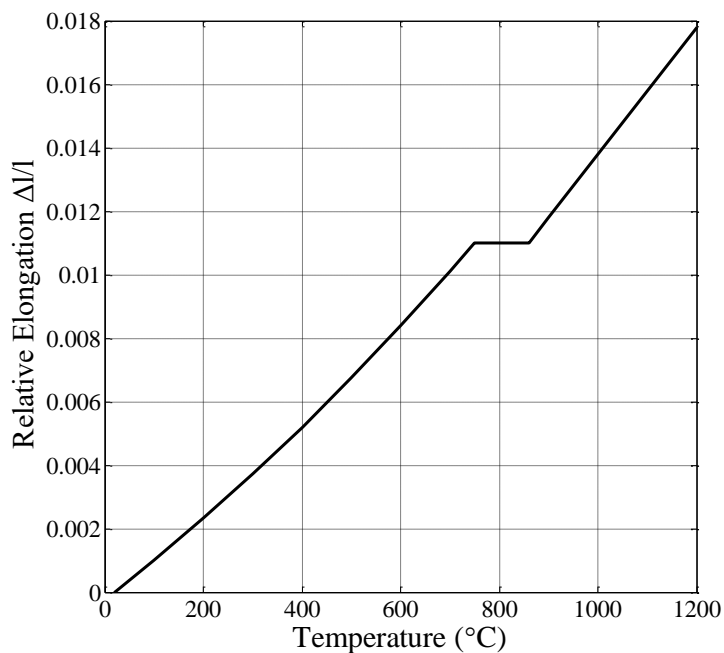


Figure 3.5 Temperature Dependent Relative Thermal Elongation of Carbon Steel

### 3.3.3 Temperature-Dependent Thermal Properties for Steel

The main thermal properties used in the heat transfer analysis in this study were thermal conductivity and specific heat. The relationships of these properties were also adopted from *European code* (Eurocode 3 EN 1993-1-2, 2005).

1) The thermal conductivity of steel  $\lambda_a$  (Figure 3.6) was determined from the following equations:

For  $20^\circ\text{C} \leq T < 800^\circ\text{C}$ ,

$$\lambda_a = 54 - 3.33 \times 10^{-2} T \text{ W/mK}$$

For  $800^\circ\text{C} \leq T \leq 1200^\circ\text{C}$ ,

$$\lambda_a = 27.3 \text{ W/mK}$$

Where:

T is the steel temperature ( $^\circ\text{C}$ ).

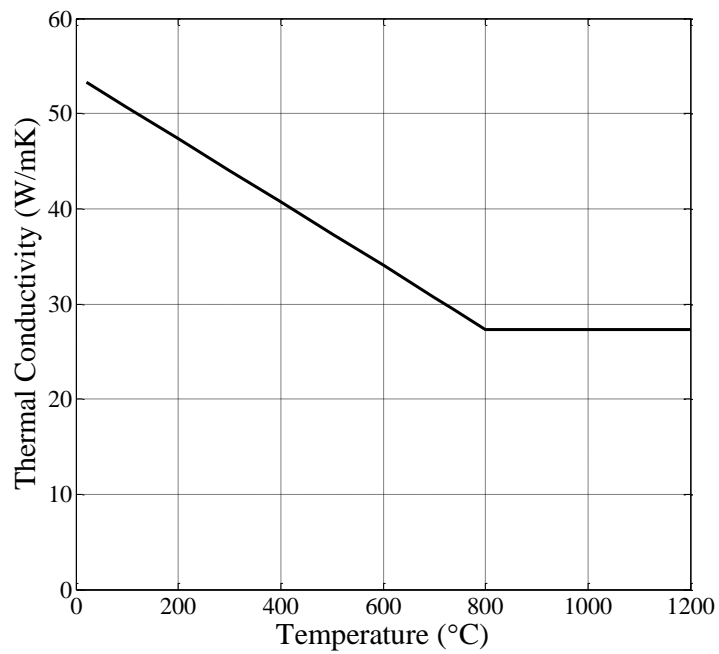


Figure 3.6 Thermal Conductivity of Steel

2) The specific heat,  $c_a$ , for steel (Figure 3.7) is determined from the following equations per *European code* (Eurocode 3 EN 1993-1-8, 2005):

For  $20^{\circ}\text{C} \leq T < 600^{\circ}\text{C}$ ,

$$c_a = 425 + 7.73 \times 10^{-1}T - 1.69 \times 10^{-3}T^2 + 2.22 \times 10^{-6}T^3 \text{ J/kgK}$$

For  $600^{\circ}\text{C} \leq T < 735^{\circ}\text{C}$ ,

$$c_a = 666 + \frac{13002}{738 - T} \text{ J/kgK}$$

For  $735^{\circ}\text{C} \leq T < 900^{\circ}\text{C}$ ,

$$c_a = 545 + \frac{17820}{T - 731} \text{ J/kgK}$$

For  $900^{\circ}\text{C} \leq T \leq 1200^{\circ}\text{C}$ ,

$$c_a = 650 \text{ J/kgK}$$

Where:

T is the steel temperature ( $^{\circ}\text{C}$ ).

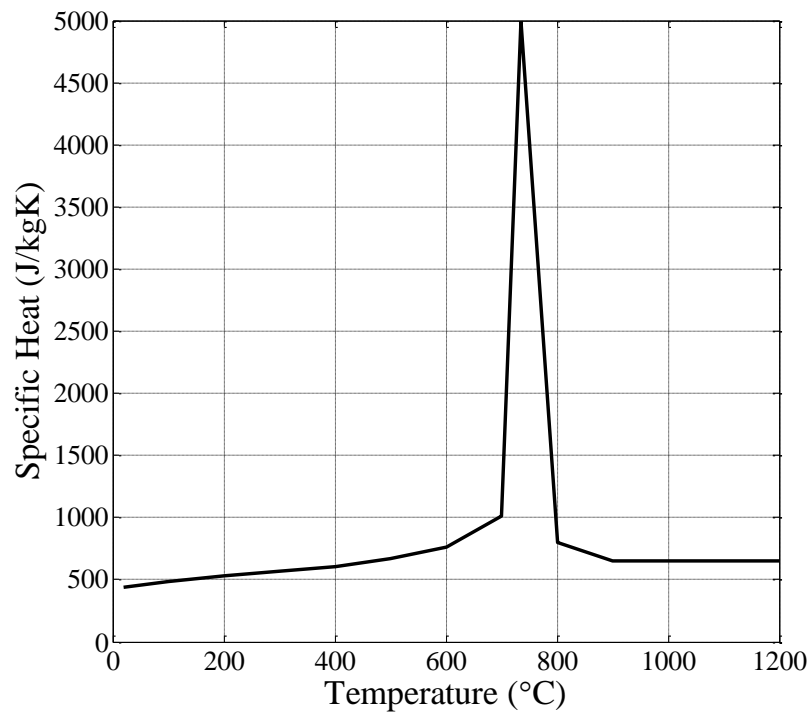


Figure 3.7 Specific Heat of Steel

### 3.3.4 Johnson-Cook Damage Model for Steel

The Johnson-Cook constitutive damage model was selected for inclusion of damage initiation in the material model (Johnson and Cook, 1983 & 1985). The three key material responses used in this model were strain hardening, strain-rate effects, and thermal softening. The Johnson-Cook constitutive model combines these three effects in a multiplicative manner as shown in the equation below:

$$\sigma = [A + B\varepsilon^n][1 + C \ln \dot{\varepsilon}^*][1 - T^{*m}]$$

Where,

$\varepsilon$  is the equivalent plastic strain

$\dot{\varepsilon}^* = \dot{\varepsilon}/\dot{\varepsilon}_0$  is the dimensionless plastic strain rate for  $\dot{\varepsilon}_0 = 1.0s^{-1}$

$T^*$  is the homologous temperature

$A, B, n, C, m$  are material constants

This model is expanded to include fracture based on cumulative damage. The equation below provides the cumulative damage fracture model:

$$\varepsilon^f = [D_1 + D_2 \exp D_3 \sigma^*][1 + D_4 \ln \dot{\varepsilon}^*][1 + D_5 T^*] \text{ Equation 2}$$

Where,

$\varepsilon^f$  is the equivalent strain to fracture

$\sigma^* = \sigma^m/\bar{\sigma}$  is the dimensionless pressure-stress ratio

$\dot{\varepsilon}^* = \dot{\varepsilon}/\dot{\varepsilon}_0$  is the dimensionless plastic strain rate for  $\dot{\varepsilon}_0 = 1.0s^{-1}$

$T^*$  is the homologous temperature

$D_1$  to  $D_5$  are five constants defined in the literature as follow Table 3.4

Table 3.4 Constants for 4340 Steel

	D <sub>1</sub>	D <sub>2</sub>	D <sub>3</sub>	D <sub>4</sub>	D <sub>5</sub>
4340 Steel	0.05	3.44	-2.12	0.002	0.61

Because insufficient data exists on damage modeling of A36 and A500 Grade B steel, the values for the damage model used in this study were representative of 4340 steel as presented in Johnson and Cook (Johnson and Cook 1985). While 4340 steel does slightly differ in composition from A36 and A500 Grade B steel, they are all classified as carbon steel where the differences in composition is thought to have negligible effect on the difference in cumulative damage between the different grade steel.

### 3.3.5 Lightweight Concrete Properties

Lightweight concrete slabs were used in the construction of the test building. The concrete strength was quantified through standard cylindrical tests. In the fire analysis in this study, the Young's modulus of concrete is set to be the average of the test results listed in Foutch, Roeder, and Goel (1986), which was determined to be 15GPa. Since it is lightweight concrete, the density was assumed to be 2400 kg/m<sup>3</sup>. The conductivity used for thermal analysis was 0.5 W/mK for concrete. The yield stress of the 6mm steel reinforcing bars used in the test was 398N/mm<sup>2</sup> from sample tests. Other properties of the reinforcement were set to be nominal steel properties because lack of information. Because concrete is a good thermal insulation material, the temperature-dependent mechanical properties of concrete and reinforcing steel were neglected in the study.

### 3.4 Summary

Descriptions of the analyzed structures are given in this chapter along with material properties. A summary of key information presented in this chapter are provided below:

- The two braced frames used in this study were tested at full scale by Foutch, Roeder and Goel (1986).
- ASTM A36 structural steel was selected for all beam and column members.
- ASTM A500 B was used for braced members.
- Properties of steel are adopted from *European code* (Eurocode 3 EN 1993-1-8, 2005).
- Lightweight concrete properties were used for the floor slab.

## CHAPTER 4 FINITE ELEMENT MODELS

### 4.1 Introduction

This chapter describes the nonlinear multi-resolution multi-degree-of-freedom (MDOF) finite element models developed to analyze the response the CBF and EBF frames under elevated temperature. All models used in this study were developed and analyzed using the general-purpose finite element (FE) program ABAQUS (SIMULIA 2014). In this study, 3D geometrical models are developed with line elements representing the beams and columns and shell elements representing the slabs. It is important to have the accurate material, damage, and mechanical models that can properly capture excessive yielding, member breakage, and connection failure in a progressive collapse analysis. The first section provides a description of the development and implementation of the line and shell elements in the models. The following two sections discuss the implemented modeling technique for connections and shear links. The initial imperfections used in the FE model are introduced in the next section. The fifth section provides a detailed description of building fire behavior and how it can be simulated in thermal analysis. The following section shows the fire-induced collapse analysis, which is an accumulation of the fire load from thermal analysis with the dead and live load. Description of the validation models used to partially confirm the finite element modeling techniques implemented in this study are discussed in Section 4.7. Finally, a brief summary of the chapter is provided in Section 4.8.

## **4.2 Structural Members, Slab, and Gusset Plate Model**

### **4.2.1 Overview**

The utilization of line and shell elements was required in order to determine nodal displacements used in the fire analysis as well as acquire the nodal temperature from thermal analysis while maintain computation efficiency. Line and shell element models were developed for both CBF and EBF structures discussed in the previous chapter. The models employ line elements for the entire frame, which incorporates variation in member sizes, mechanical properties, and thermal properties. Full length, from centerline-to-centerline of columns, was used in modeling the various members. Different element types were used to model the columns, girders, slab, connections, bracing member, and shear link. Each of these components is discussed in more detail in the proceeding sections followed by a description of the various simulations that were performed.

### **4.2.2 Columns, Girders, Beams, and Braces Model**

All structural members including columns, girders, beams, and braces were modeled using line elements to reduce the computational cost and improve the efficiency of the model. The line elements were featured with element separation to allow for the simulation of collapse. The Johnson-Cook damage model was selected to initiate damage in the elements. The onset of damage evolution, which allows for element breakage, was set when the fracture energy to be 500J to break the elements.

### 4.2.3 Slab and Gusset Plate Model

The concrete slabs and gusset plates in the EBF were modeled using shell elements. Reinforcement steel bars were modeled as rebar layer. The mesh size was determined so as to allow for the localized deformation at critical areas to be captured. For modeling the concrete slabs, the concrete damage plasticity (CDP) constitutive model was implemented to introduce softening. Table 4.1 summarizes the material parameters for the concrete including those for the CDP model as listed in Jankowiak and Lodygowski (2005).

Table 4.1 Material Parameters of CDP Model for Concrete (Jankowiak and Lodygowski 2005)

Material	B50 Concrete	The parameters of CDP model	
		$\beta$	38°
Concrete elasticity		m	1
E(Gpa)	19.7	$f = f_{b0}/f_c$	1.12
$\nu$	0.19	$\gamma$	0.666
Concrete compression hardening		Concrete compression damage	
Stress (MPa)	Crushing strain	Damage Comp.	Crushing strain
15.0	0.0	0.0	0.0
20.197804	0.0000747307	0.0	0.0000747307
30.000609	0.0000988479	0.0	0.0000988479
40.303781	0.000154123	0.0	0.000154123
50.007692	0.000761538	0.0	0.000761538
40.236090	0.002557559	0.195402	0.002557559
20.236090	0.005675431	0.596382	0.005675431
5.257557	0.011733119	0.894865	0.011733119
Concrete tension stiffening		Concrete tension damage	
Stress (MPa)	Cracking strain	Damage Tens.	Cracking Strain
1.99893	0.0	0.0	0.0
2.842	0.00003333	0.0	0.00003333
1.86981	0.000160427	0.406411	0.000160427
0.862723	0.000279763	0.696380	0.000279763
0.226254	0.000684593	0.920389	0.000684593
0.056576	0.00108673	0.980093	0.00108673

### 4.3 Connection Model

#### 4.3.1 Moment Connection

The rotational stiffness of the connectors can be determined from the stiffness matrix of a fixed-fixed beam where the stiffness coefficient is  $k = \frac{4E_T I}{L}$  where  $E_T$  is Young's Modulus as a function of temperature. The steel properties were adopted from Eurocode 3 (2005) as discussed in the previous chapter. A hinge-type connector was used in this study; with rotational restraints specified in all directions to mimic a fully welded connection. As noted before, in the test structures moment connections were employed using either a fully welded connection or a welded-flange bolted-web connection. Failure of the connection was specified when a rotation value of 0.06 radians was achieved. The use of 0.06 rad is based on the test results which showed that a well-behaved connection could sustain a rotation of 0.06 rad before failure at ambient temperature (Murray and Sumner, 1999). Undoubtedly, this value will likely increase, due to increase in ductility at elevated temperature. In fact, the tests by Yang et al. (2009) showed that, while the moment connection rotational capacity at elevated temperature will vary, an estimated value of approximately 0.1 rad can be assumed. Therefore, the use of 0.06 rad can be considered conservative.

$$k = \frac{4E_T I}{L}$$

#### 4.3.2 Shear Connection

Girder-to-column connections located in the frames perpendicular to the loading direction and all beam-to-girder connections are shear connections. Because of lack of information, all shear connections were assumed based on the connection layout presented in Figure 3.3 as shown in the previous chapter.

In this section, a component-based model for shear tab connection subjected to fire, developed by Sarraj (2007). In this model, the whole connection is treated as a group of springs representing each bolt row in addition to bearing springs representing the two connected plates, which are show in Figure 4.1.

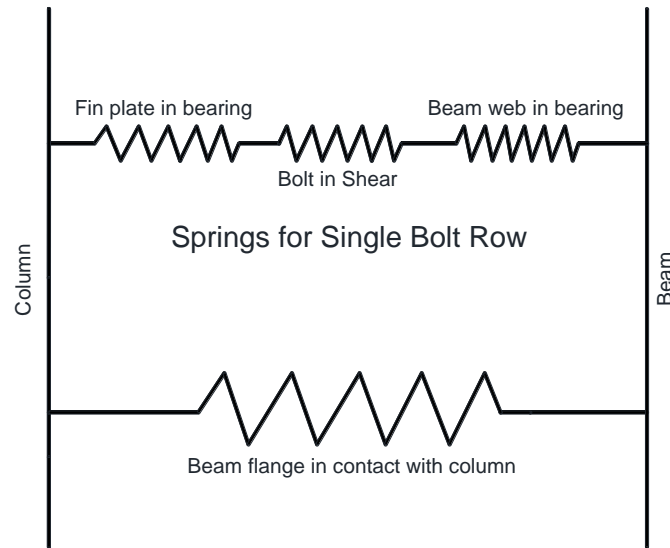


Figure 4.1 Component-based model for shear tab connection

### 1) *Plate in bearing*

The initial stiffness of a shear connection is denoted as,  $K_i$ , which is composed of three parts:

$$K_i = \frac{1}{\frac{1}{K_{br}} + \frac{1}{K_b} + \frac{1}{K_v}}$$

Bearing stiffness  $K_{br} = \Omega_t f_y (d_b / 25.4)^{0.8}$

Bending stiffness  $K_b = 32 E_t (e_2 / d_b - 0.5)^3$

Shear stiffness  $K_v = 6.67 G_t (e_2 / d_b - 0.5)$

Where,

$\Omega_t$  is parameter obtained by curve-fitting finite element analysis results and is presented directly in Table 4.2 as functions of temperature.

## 2) *Bolt in shear*

The bolt shear stiffness can be represented as the following proposed temperature dependent expression.

$$K_v = \frac{0.15G_T A_s}{d_b}$$

Where,

$G_T$  is the temperature dependent shear modulus

$A_s$  is the cross section area of the bolt

$d_b$  is bolt diameter

The length of the shear connector element is set to zero initially. The failure occurs when the length of the connector reaches certain number on x, y direction.

### 4.3.3 Other Connections

Bracing-to-gusset plate connection was welded according to the original structural design. In this study, this connection was assumed to have sufficient strength to transfer the load (i.e. brace failure would occur prior to brace-gusset connection failure); therefore no failure model was used in this kind of connection.

### 4.4 Shear Link Model

Shear links were represented as shown in Figure 4.2 and this model was adopted from previous progressive collapse study (Khandelwal, El-Tawil, and Sadek, 2009). The model employed a nonlinear spring AC, as

shown in Figure 4.3, with four bars pinned together at their ends to permit the desired shear-flexural deformation to occur. The elastic stiffness and strength of spring AC are given by the equations below. The failure rotation of the shear link spring is assumed 0.15 rad as recommended in the Federal Emergency Management Agency (2000).

$$k_{sl} = \frac{G(d_b - t_f)t_w}{L \cos^2(\theta)}$$

$$f_{sl} = \frac{0.6F_y(d_b - t_f)t_w}{\cos(\theta)} \left[ 1 + \frac{3b_f t_f^2}{L(d_b - t_f)t_w} \right]$$

Where,

$G$ : Shear modulus of steel,

$F_y$ : Yield strength of steel,

$L$ : Length of shear link,

$d_b$ : Depth of beam,

$t_w$ : Thickness of beam web,

$t_f$ : Thickness of beam flange,

$\theta$ : The angle between the spring AC and member AB,

$b_f$ : Width of beam flange.

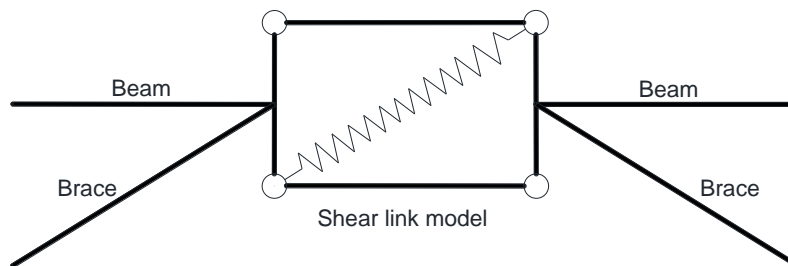


Figure 4.2 Schematic of Shear Link Model

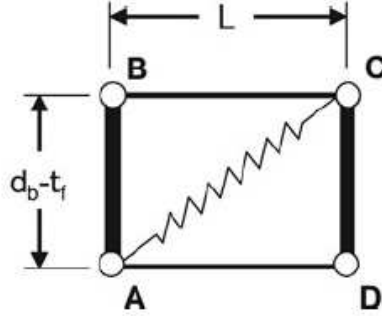


Figure 4.3 Details of Shear Link Model (Khandelwal, El-Tawil, and Sadek 2009)

#### 4.5 Imperfection Model

In order to capture buckling and post-buckling response in the simulations, initial imperfections were added to the model. Previous studies have shown that the magnitude of the imperfection controls member buckling strength but the post-buckling response is not dependent upon the level of imperfection. The initial imperfection introduced in the model was assumed as  $L_b/1000$  in this research study, where  $L_b$  is the length of the member. Based on Eurocode 3 (En, 2005), for the analysis of isolated vertical members a sinusoidal initial imperfection with a maximum value of  $L_b / 1000$  at mid-height should be used, when not specified by relevant product standards. The initial imperfections were scaled from eigenvectors according to the lowest eigenvalue from an ABAQUS buckling analysis.

#### 4.6 Thermal Analysis

Building fires are largely controlled by the amount of fuel, the flow of oxygen and the temperature of the fire. Fire starts when the temperature of fuel reaches its combustion point in the presence of oxygen. Once the initial combustion of the fuel source begins it releases heat, increasing the temperature of the

surrounding environment. More and more fuel starts to burn and the fire expands until it becomes fully developed. It continues to burn at this extreme temperature until the fuel sources are exhausted and the fire begins to decay and eventually burn out.

A fire curve can be divided into three main phases, growth, fully developed and decay. The flashover point is defined as the transition of the fire from growing to fully developed, which involves the fire spreading from the area of localized burning to all combustible surfaces within the compartment (L. Yu, 2006). After flashover, the heat release rate remains at a maximum as long as fuel and oxygen supplies last. Generally, once a building fire reaches the flashover point it is almost impossible for firefighters to stop it and sprinklers are designed to only work at the growth phase of the fire. This leaves sprayed-on fire proofing material as the only defense against a fully developed fire. Compartment fires in office buildings since they are the most common type of fires seen in buildings and has been focused in this study.

#### **4.6.1 Fire Time-Temperature Curve Selection**

Because of the intricate nature of building fires, simulating the response of buildings and their components under fire loading is extremely complicated. Most countries around the world use simple fire resistance tests that utilize standardized fire curves to evaluate the behavior of building components and structural members during a fire. These standard curves provide a simple means of assessing a specimen's response against a common set of performance criteria when subjected to closely-defined thermal and mechanical loading under prescribed support conditions. This methodology has several shortcomings and has been heavily criticized by the structural engineering community because it does not take into account any of the

physical parameters affecting fire growth and development. In addition, it cannot be used to analyze the response of a complete structure as it neglects the important interaction between components. This has lead researchers to start to use more realistic and complex methods for simulating the response of structures to fire loading.

Two different time-temperature curves were used in this study. First, the standard ASTM E-119 fire time-temperature curve (2000) is used which includes only a heating phase. In addition, a parametric fire curve, which includes a cooling phase is also used in this study. The parametric fire curve is determined by Eurocode 3 (2005). The realistic time-temperature curve used for this study can be seen in Figure 4.4 compared to the standard fire curve presented in ASTM E-119.

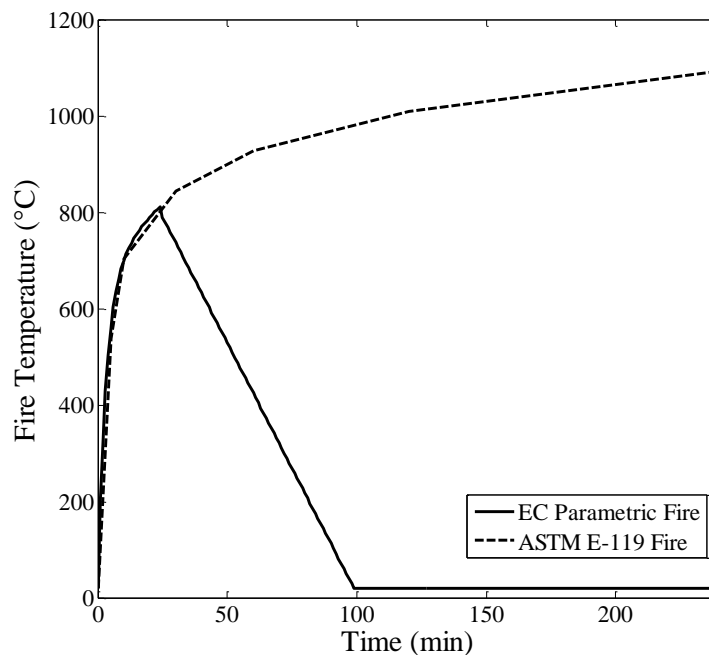


Figure 4.4 ASTM E-119 versus EC Parametric Fire Curves

#### 4.6.1.1 E119 Fire Curve

The standard fire curve used in the United States comes from the ASTM E119 - Standard Test Methods for Fire Tests of Building Construction and Materials (ASTM, 2016), which was one of the first published tests that established a fire resistance rating for steel members through a prescribed method.

#### 4.6.1.2 Eurocode Parametric Fire Curve

The realistic fire-temperature curve used in this research was adopted from EN 1991 Eurocode 1 Actions (EC1, 2004). Three phases are including in this curve, begin with a heating ramp then follow with a cooling ramp, finally reach a constant temperature.

1) The temperature-time curves in the heating phase are given by:

$$\theta_g = 20 + 1325(1 - 0.324e^{-0.2t^*} - 0.204e^{-1.7t^*} - 0.472e^{-19t^*})$$

Where;

$\theta_g$ : Gas temperature in the fire compartment,

$$t^* = t * \Gamma$$

$t$ : time

$$\Gamma = (O/b)^2 / (0.04/1160)^2$$

$$b = \sqrt{(\rho c \lambda)} \quad [J/m^2 s^{1/2} K]$$

$\rho$ : Density of boundary of enclosure

$c$ : Specific heat of boundary of enclosure

$\lambda$ : Thermal conductivity of boundary of enclosure

$O$ : Opening factor

$\Gamma$ : time factor function and is assume be 1.0 in this study.

2) The maximum temperature in the heating phase when  $t^* = t_{max}$

$$t_{max} = \max\{0.2 \times 10^{-3} \frac{q_{t,d}}{O}, t_{lim}\}$$

$t_{lim} = 20min$  for medium fire growth according to Eurocode

The testing building was assumed to be an open office building with fire parameter  $q_{t,d} = 100 MJ/m^2$ ,  $O = 0.05 m^{1/2}$ , and  $b = 2000 J/m^2 s^{1/2} K$ . According to these values, the maximum temperature of the heating phase is 811°C at 24 min.

3) The temperature-time curves in the cooling phase are given by:

$$\theta_g = \theta_{max} - 625(t^* - t_{max}^*) \text{ for } t_{max}^* \leq 0.5h$$

The cooling phase ending at ambient temperature in the 99 min. The ambient temperature is extended to 240 min to capture all residual stresses and permanent deformations and match the time of the ASTM E119 fire curve model.

#### 4.6.2 Heat Transfer Model

In order to run the dynamic collapse stress analysis, the temperature distribution in all elements of the structure had to be determined. Characterizing the temperature distribution was completed by conducting a transient heat transfer analysis step. At the conclusion of this analysis step, the temperature at each node was determined for the whole fire scenario. As previously indicated, in the thermal analysis, a selected fire-temperature curve was applied to the outmost compartment, which includes the braced frame, of first floor.

This assumes that no fire protection is present in the entire structure.

## **4.7 Fire Induced Collapse Analysis**

In this part of the simulation, the dead and live loads were combined with the fire load. The gravity loads were defined as summarized below with the load combination for the fire analysis.

### **4.7.1 Gravity Load**

The gravity loads were adopted from the Uniform Building Code (UBC, 1979) and 1981 Japanese building code. Total dead loads of 4.3 kN/m<sup>2</sup>, 3.6 kN/m<sup>2</sup>, and 1.4 kN/m<sup>2</sup> were used for the floor, roof, and exterior wall areas, respectively. The live load for the floor and roof areas were 2.8 kN/m<sup>2</sup> for slabs and beams and 1.8 kN/m<sup>2</sup> for girders.

### **4.7.2 Thermal Load**

Following the application of gravity loading, the selected CBF and EBF structures were subjected to the thermal load as a predefined field. A dynamic explicit step was used to run the collapse simulations. The floor dead and live load were the same as the design loads mentioned before. The load combination for the fire analysis was set to  $D + 0.5L + F$  (Ellingwood and Corotis, 1991).

## **4.8 Modeling Technique Validation**

### **4.8.1 Overview**

Experimental test data and analytical models were used to validate the modeling techniques employed in this study. In section 4.4.2, two previously tested and modeled frames were selected to verify the line element

model. An eigenvalue analysis was performed on both CBF and EBF structures and compared to results from the test (Foutch, Roeder, and Goel 1986) in the next section.

#### 4.8.2 Line Element Model Validation

To verify the numerical approach used in this study, a validation was conducted on two small frames that were previously tested (Rubert and Schaumann 1986) and modeled and are an L-shaped and two-span frame as shown in Figure 4.5. The L-shaped and two-span frame are commonly referred to as EHR and ZSR frames, respectively. IPE80 I-section was used for all member in these two frames. The structural members were uniformly heated using ISO-834 standard fire curve. The temperature-dependent steel properties were adopted from Eurocode 3 (2005) as discuss in the previous chapter. The loads were applied to the frames as show in the figure. The comparison between test and analytical models includes deflection at mid-span of column and beam in the HER frame and lateral displacement of ZSR frame. The displacement versus temperature plots of the validation models shows a good agreement to the test results and other analytical studies (Figure 4.6 and Figure 4.7).

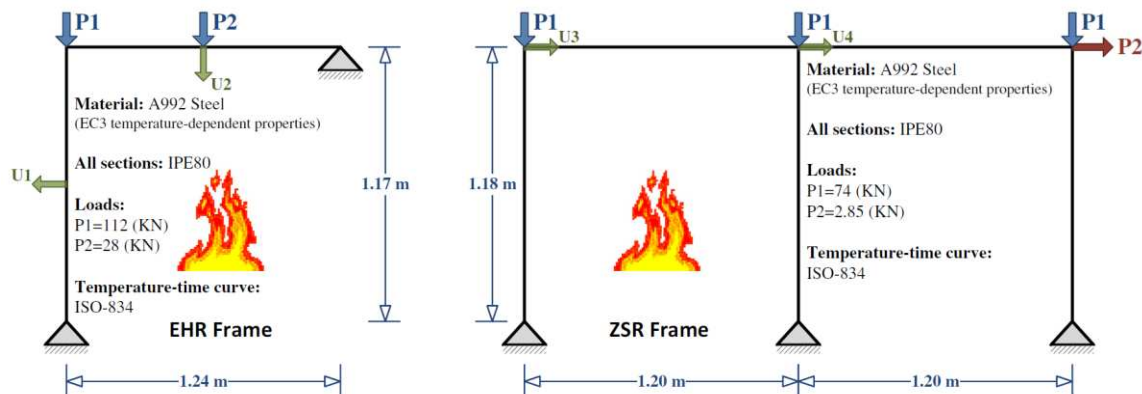


Figure 4.5 The EHR and ZSR steel frames (Memari and Mahmoud 2014)

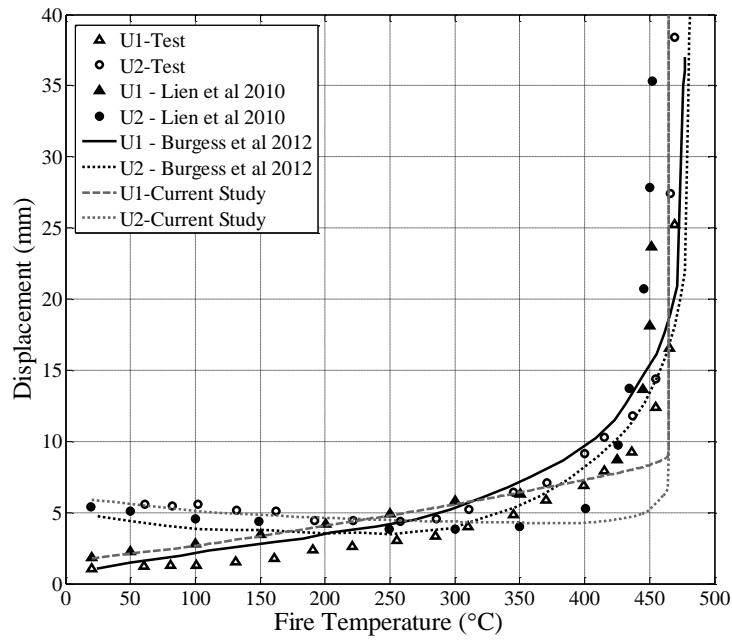


Figure 4.6 EHR Frame Results

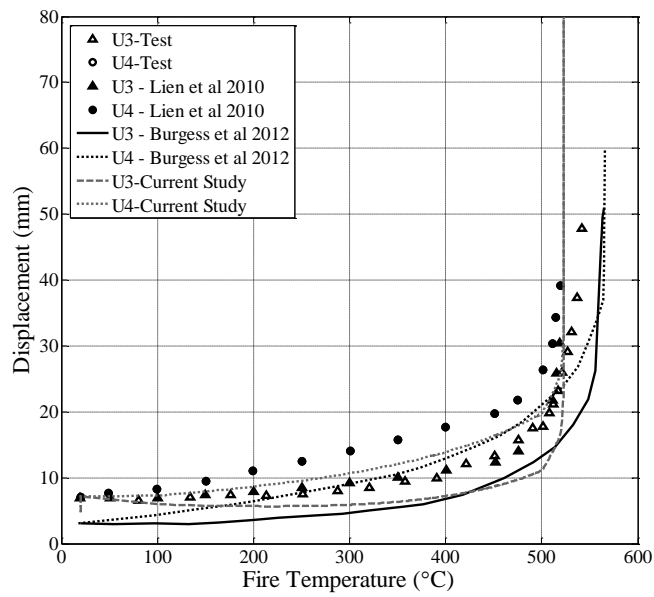


Figure 4.7 ZSR Frame Results

### 4.8.3 Mechanical Response Validation

For this section, an eigenvalue analysis was performed on both frame models and the natural period of vibration and mode shapes were compared to the test results. First three mode shapes for both the CBF and EBF structures were captured in Figure 4.8 and Figure 4.9. A comparison of the natural period of vibration values obtained in this study and the values presented by the preliminary test report (Foutch, Roeder, and Goel 1986) can be found in Table 4.2. The comparison between the analytical results and test results shows good agreement and serve as validation of the dynamic properties implemented in the model.

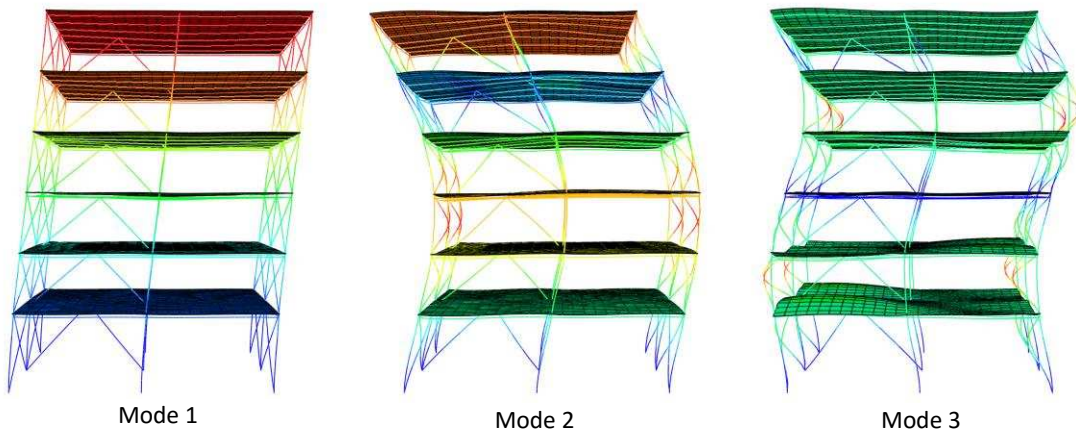


Figure 4.8 Mode shapes of CBF

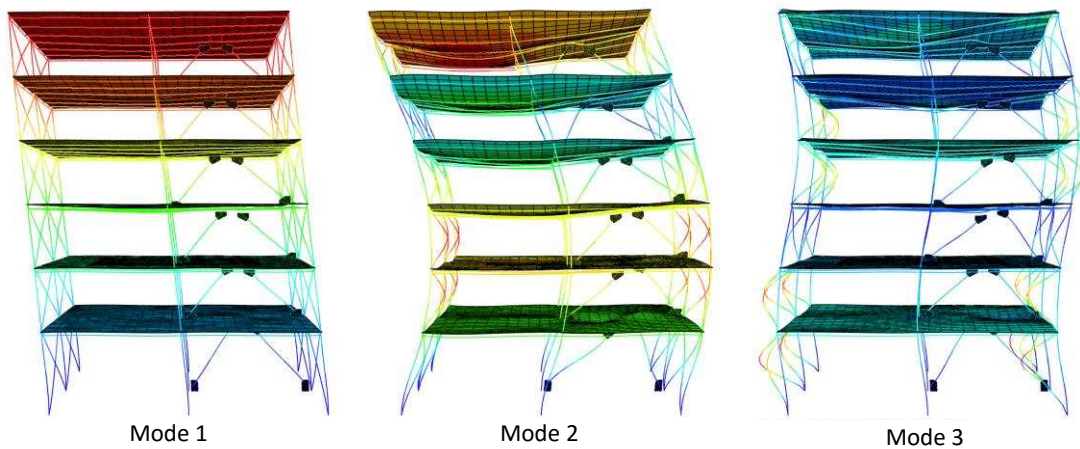


Figure 4.9 Mode Shapes of EBF

Table 4.2 Dynamic Properties of Structures

Mode	CBF			EBF		
	Test Result	Current Study	% Diff	Test Result	Current Study	% Diff
1	0.61	0.639	4.75	0.57	0.585	2.63
2	0.227	0.236	3.96	0.201	0.213	5.97
3	0.133	0.1399	5.19	-	0.124	-

#### 4.9 Summary

In this chapter, the finite element model technique implemented in this study were described in details. These included a full description of line, shell, connector elements, and springs used to represent the various structural components. The loading steps utilized were also discussed and were followed by the validation analysis for two previously tested frames under elevated temperature. Key points presented in this chapter were as follow.

- This analysis was performed using the commercial finite element software ABAQUS (Simulia 2014).
- Models of both CBF and EBF building were developed to analyze their global progressive collapse response under fire.
- Initial imperfections were added to the models in order to capture buckling.
- Two fire temperature curves were used in this study including ASTM E-119 Standard fire curve and EC parametric fire cure.
- Nodal temperature data used for the dynamic collapse analysis were imported from the heat transfer analyses.

- Validation models were used to ensure the modeling techniques employed in this study produced accurate results.
- These models used for validation included two small frame models and eigenvalue analysis models for CBF and EBF.

## CHAPTER 5 SIMULATION RESULTS AND DISCUSSION

### 5.1 Overview

This chapter presents the results from the collapse simulations of the full 3-D building system models discussed in Chapters 3 and 4. The presented results include global system response of the frames and the entire structures as well as the local behavior of members and connections. Section 5.2 introduces a naming scheme to facilitate representation and discussion of results. Section 5.3 provides a description of all eight fire scenarios used in the simulations. Section 5.4 and 5.5 include the results of system responses for the complete 3D systems as well as the moment and gravity frames, respectively. Section 5.6 summarizes results on the behavior of critical members and connections. Following these sections comparison of the results from all 8 fire cases is presented in section 5.7. Finally, a summary section is provided, highlighting the major findings in this chapter.

### 5.2 Naming Scheme

For the convenience of presenting the results and facilitating the discussion, a naming scheme is proposed in this section. As shown in Figure 5.1, the letters (C) and (G) are used to represent columns, girders, and beams, respectively, on each floor. The numbers adjacent to the letters correspond to specific sections as indicated in a combined table. The number following the dash line is an identifier for the specific member. The moment and gravity frames are highlighted in the plan view in Figure 5.1, the edge moment frames comprise of fully welded connections while the inner frames are the CBFs and EBFs. Figure 5.2 (a) and (b)

show the elevation view of the CBF and EBF, respectively. The floor number is also given in this figure as well as the brace designation for the first floor.

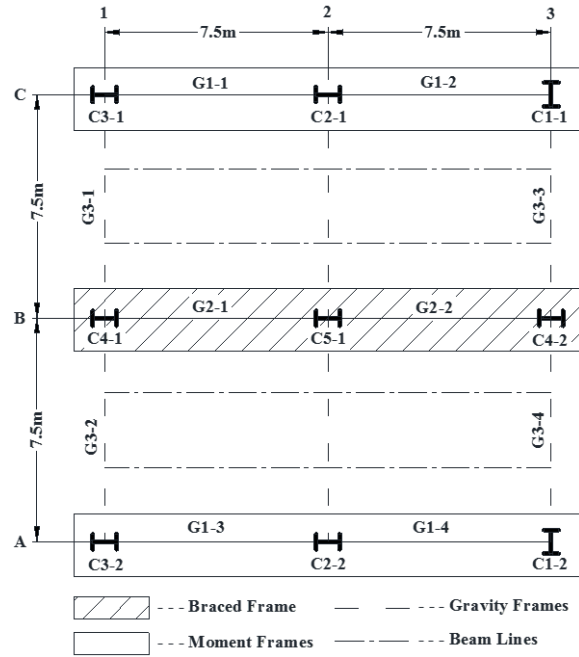


Figure 5.1 Generalized Floor Plan of the two Buildings with the inner frames being CBF in one case and an EBF in the other case

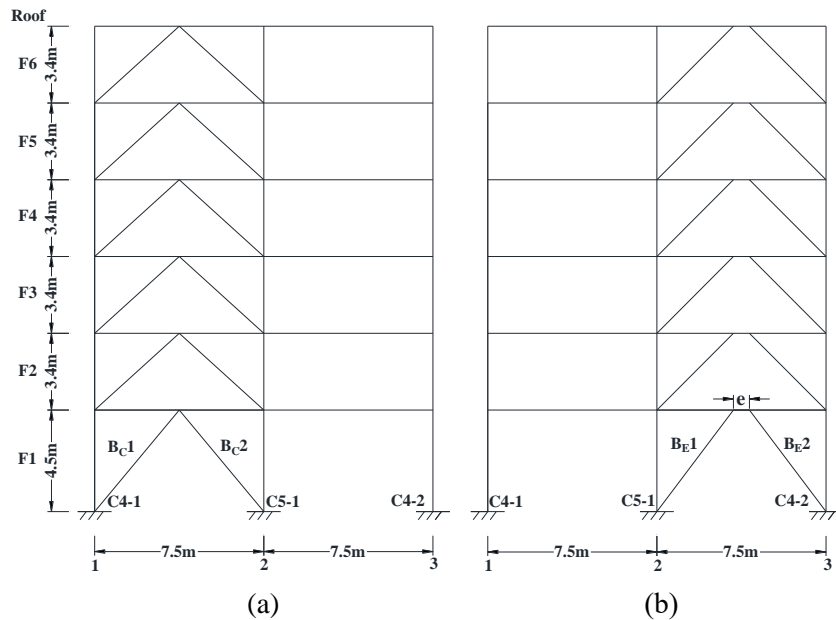


Figure 5.2 Elevation View of (a) CBF frame and (b) EBF frame

### 5.3 Fire Analysis Scenarios – 8 Cases

Two fire curves and two fire scenarios were selected for the study for the two 3D structures, for a total number of eight simulations. The fire curves utilized in the study included the ASTM E119 and the Eurocode 3 parametric fire curves. The reason for selecting these curves is to allow comparisons to be made between the results obtained from a standard fire and a realistic fire. The two fire scenarios selected included 1) a contained corner compartment fire on the first floor and 2) a whole first floor fire where all compartments are exposed to elevated temperature. A summary of all analyzed cases is listed in Table 5.1. Figure 5.3 to Figure 5.6 show render views of the ABAQUS models as well as the location of the fire applied. It is worth noting, as will be shown later, that it could be irrelevant to evaluate system response when subjecting to an only heating curve versus a heating-cooling curve if the collapse is initiated during the heating phase. In other words, if the system starts to lose its vertical load carrying capacity during the heating phase, then subjecting the system to a cooling phase become unnecessary since collapse has already initiated. While this was the case in this study, as will be discussed later, it was decided to keep all results since the cooling phase in the case of imposing a corner fire had an impact on overall collapse mechanism.

It is important to point out to the effect of loading ratio on the time in which collapse initiates and propagates. The loading ratio is defined as the loading intensity in fire as a proportion of ambient-temperature load capacity. Sun et al. (2012) conducted an extensive study on the effect of loading ratio on the failure temperature and progression of collapse. Specifically, it was noted that lower loading ratios would result in slower progression of collapse while higher loading ratios result in a much faster collapse rate. The study showed that a loading ratio of 0.75 resulted in collapse initiation at approximately 550°C and total collapse

at approximately 600°C. For a ratio of 0.5, collapse initiated at about 600°C and complete contact of the frame with the ground occurred at about 780°C. Finally, for a ratio of 0.3, collapse initiated at about 630°C and approximately 980°C. While the effect of the loading ratio on the failure of the columns is not explicitly investigated in this study, one can view the results presented in the following sections in light of approximate values listed by Sun et al. (2012).

Table 5.1 Simulation Cases Summary

Case Name	Frame Selected	*Fire Curve	Fire Location	Case Figure
Case-1	CBF	ASTM-E119	Corner Compartment	Figure 5.3
Case-2	CBF	ASTM-E119	Whole Floor	Figure 5.4
Case-3	EBF	ASTM-E119	Corner Compartment	Figure 5.5
Case-4	EBF	ASTM-E119	Whole Floor	Figure 5.6
Case-5	CBF	EC3-Parametric	Corner Compartment	Figure 5.3
Case-6	CBF	EC3-Parametric	Whole Floor	Figure 5.4
Case-7	EBF	EC3-Parametric	Corner Compartment	Figure 5.5
Case-8	EBF	EC3-Parametric	Whole Floor	Figure 5.6

Note: \*Fire curves are not shown in the figures.

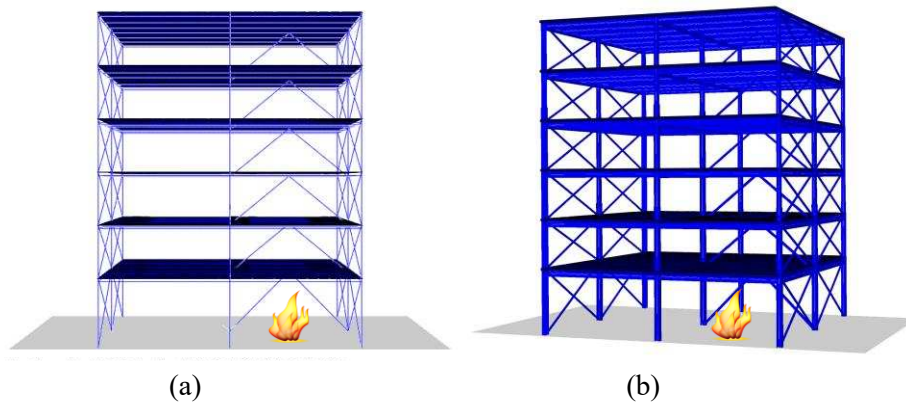
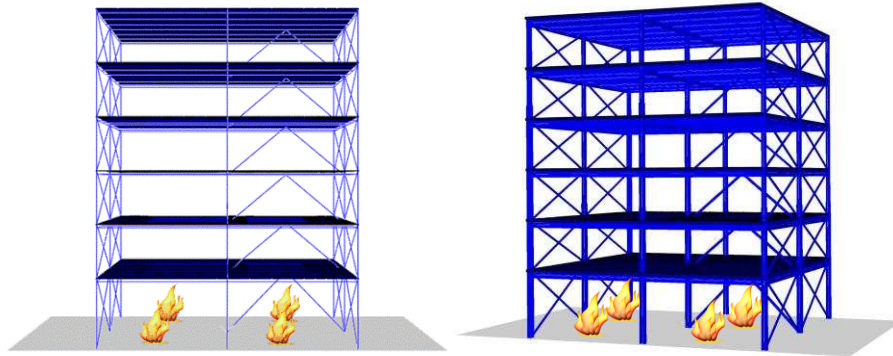


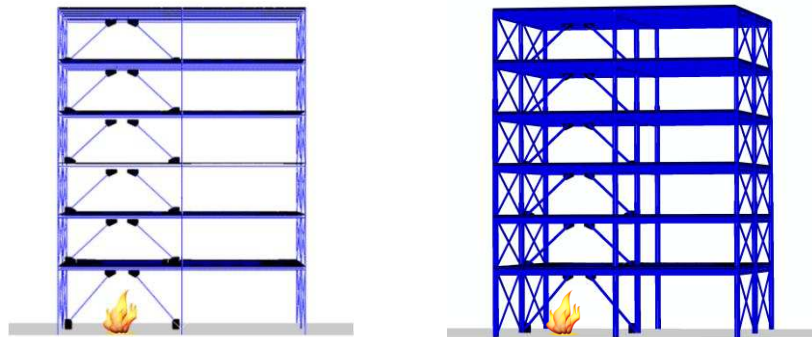
Figure 5.3 CBF with Corner Compartment Fire (a) front view and (b) isometric view



(a)

(b)

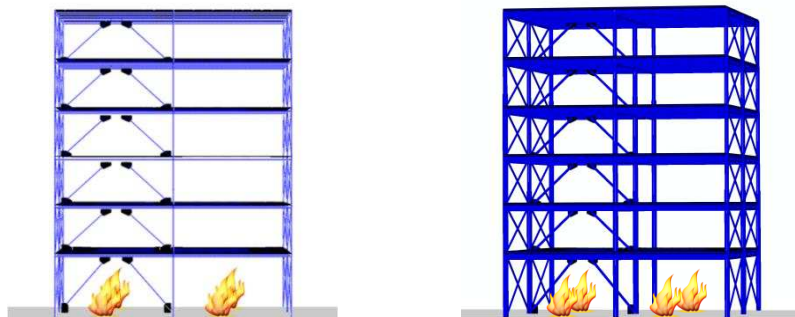
Figure 5.4 CBF with Whole Floor Fire (a) front view and (b) isometric view



(a)

(b)

Figure 5.5 EBF with Corner Compartment Fire (a) front view and (b) isometric view



(a)

(b)

Figure 5.6 EBF with Whole Floor Fire (a) front view and (b) isometric view

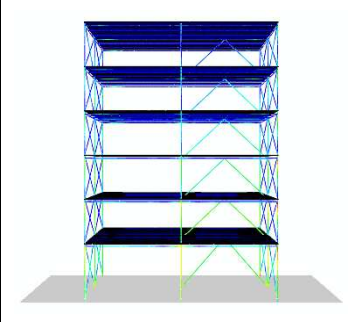
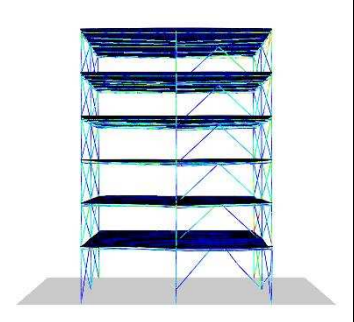
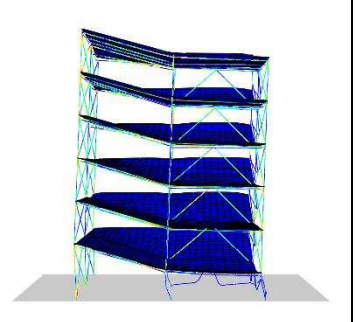
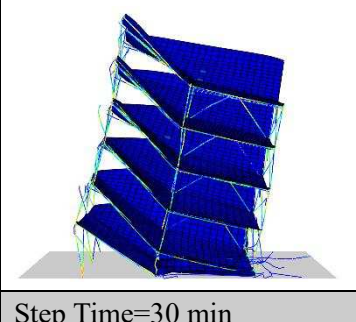
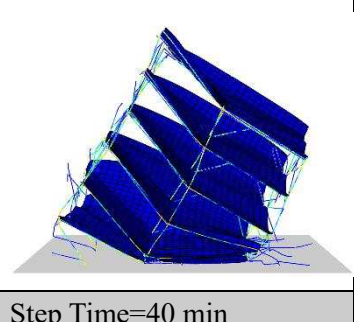
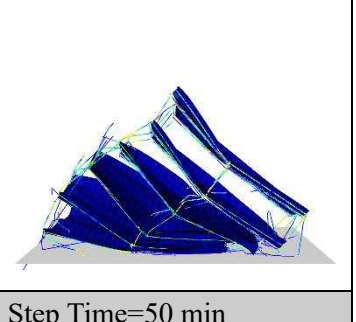
## 5.4 Global System Response

In this section, global system response is evaluated through assessment of collapse sequences. For each loading case, collapse sequences are presented in tables to provide a visual of the mechanisms leading to structural collapse under the different fire scenarios. The different fire scenarios were applied after the initial gravity loading stage where the dead and live loads were added in the model.

### 5.4.1 Case 1

For Case 1 (CBF and E119 in a single compartment), the collapse sequence is shown in Table 5.2 below. As shown in the table, when the step time is at 10 min, the temperature reached 704°C and the global response of the entire structure at this stage is marked by visible deformation in the concrete slab above the fire with bending in the braces in the bay where the fire is applied. At 20 min, the temperature reached 773.5°C, on the fire temperature curve, and substantial deformation of the concrete slab was observed. Significant deformations were also observed in the braces and columns in the fire-loaded bay. After half hour of heating the corner bay, where the temperature on the time-temperature curve was at 843°C, the entire corner bay collapsed and started to drag other floors with it, causing notable twist in the entire structure combined with lateral deformation. The substantial unbalanced forces resulted in several fractures of braces in the first two floors. At 40 min (860.6°C), the building lost its ability to sustain any loading as marked by the additional lateral and vertical downward deformation of the entire structure. Total collapse (i.e. structure brought to ground) occurred at 50 min (909.4°C) of the total time step of four hours.

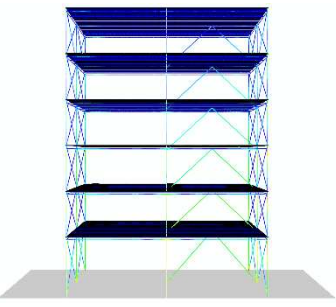
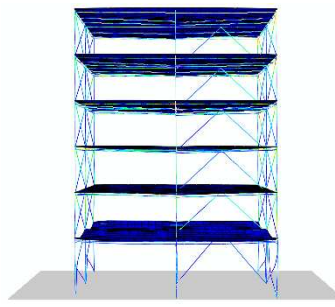
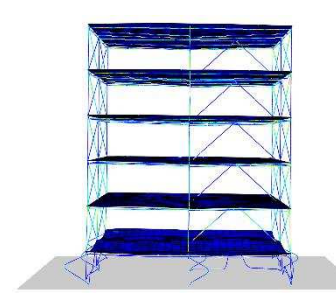
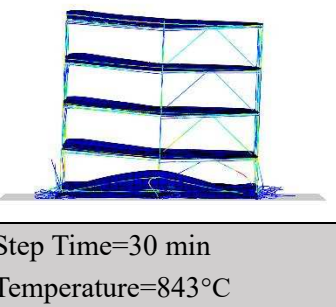
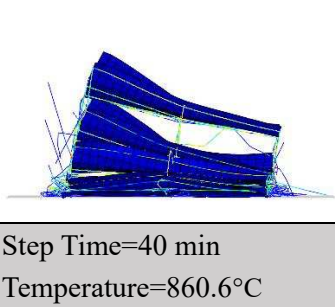
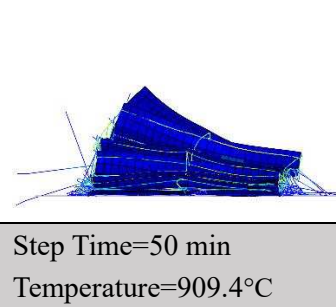
Table 5.2 Collapse Sequence for Case-1

		
Step Time=0 sec Temperature=20°C	Step Time=10 min Temperature=704°C	Step Time=20 min Temperature=773.5°C
		
Step Time=30 min Temperature=843°C	Step Time=40 min Temperature=860.6°C	Step Time=50 min Temperature=909.4°C

#### 5.4.2 Case 2

For Case 2, (CBF and E119 in the whole floor), the collapse sequence is shown in Table 5.3 below. At 704°C (10 min), membrane action of the first floor slab was observed between girder lines with visible deformation of the X braces in the first floor exterior frames. After 20 min of heating the corner bay, where the temperature on the time-temperature curve was at 773.5°C, large bending deformations were observed in all first floor members and the entire first floor starts to collapse. The impact of the first floor with the ground caused an amplification of demand on the second floor columns, and a subsequent failure of the second floor as shown at 30 min (843°C). The collapse progressed in a similar manner as shown at 40 min (860.6°C) and 50 min (909.4°C).

Table 5.3 Collapse Sequence for Case-2

		
Step Time=0 sec Temperature=20°C	Step Time=10 min Temperature=704°C	Step Time=20 min Temperature=773.5°C
		
Step Time=30 min Temperature=843°C	Step Time=40 min Temperature=860.6°C	Step Time=50 min Temperature=909.4°C

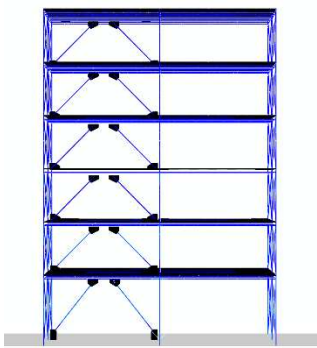
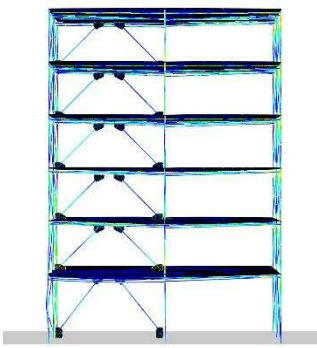
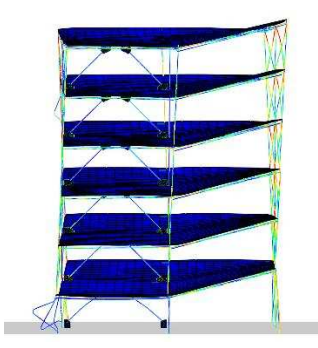
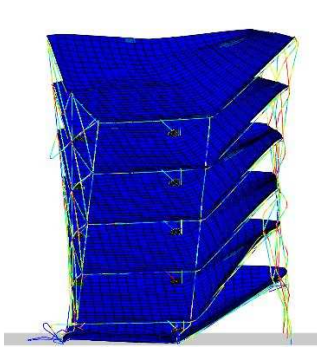
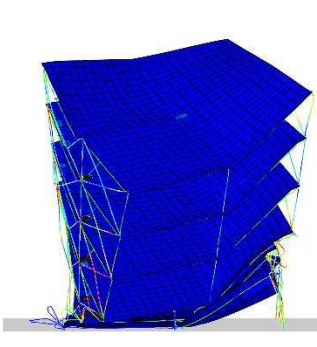
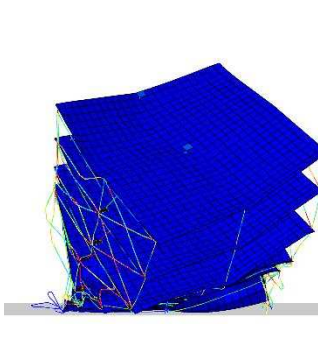
### 5.4.3 Case 3

For Case 3 (EBF and E119 in a single compartment), the collapse sequence is shown in Table 5.4 below.

As shown in the table, when the step time is at 10 min, the temperature reached 704°C, the X braces of the left side exterior frame in the compartment where the fire was initiated started to buckle. At 20 min, the temperature reached 773.5°C and the braces and columns in the heated compartment lost their strength, causing the corner bay of the first floor to drop. Once the drop of the first floor corner bay started, other floors were dragged with it, causing notable twist combined with lateral deformation for the entire structure. Membrane action can be seen in all floor slabs. At 30 min (843°C), the first two floors dropped and significant twist was observed. At 40 min (860.63°C), more floors dropped and more twisting of the entire

structure is noted. At 50 min (909.37°C), the collapse continued with a final total collapse of the first three floors.

Table 5.4 Collapse Sequence for Case-3

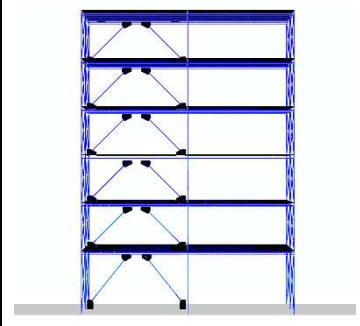
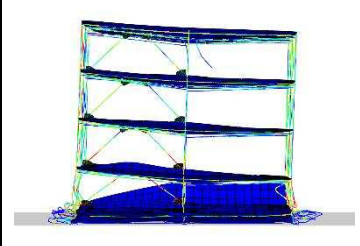
		
Step Time=0 sec Temperature=20°C	Step Time=10 min Temperature=704°C	Step Time=20 min Temperature=773.5°C
		
Step Time=30 min Temperature=843°C	Step Time=40 min Temperature=860.6°C	Step Time=50 min Temperature=909.4°C

#### 5.4.4 Case 4

For Case 4 (EBF and E119 in the whole first floor), the collapse sequence is shown in Table 5.5 below. As shown in the table, when the step time is at 10 min, the temperature reached 704°C. The first floor concrete slab started to membrane with visible deformation in the columns and braces including the exterior X braces. The first floor collapsed at 20 min (773.5°C) with large bending of first floor columns. At 30 min (843°C),

the lower two floors collapsed in a progressive manner due to increase in demand caused by the impact with the collapsed first floor. Total system collapse was observed at 50 min (909.37°C).

Table 5.5 Collapse Sequence for Case-4

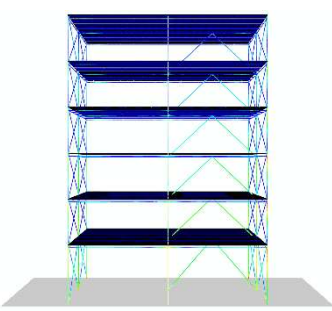
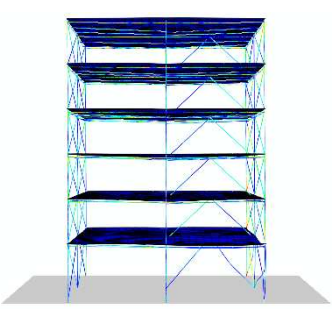
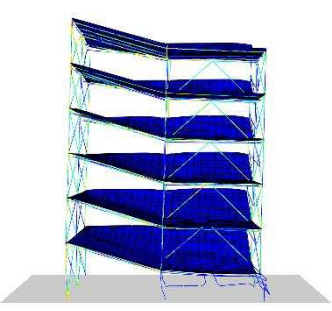
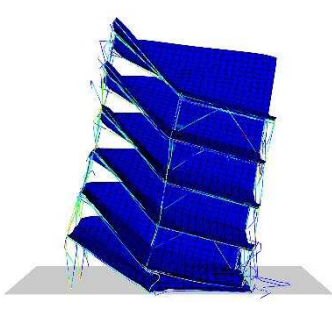
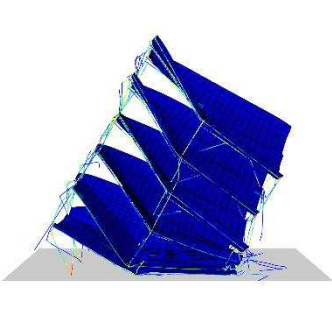
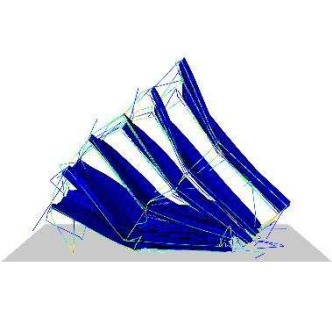
		
Step Time=0 sec Temperature=20°C	Step Time=10 min Temperature=704°C	Step Time=20 min Temperature=773.5°C
		
Step Time=30 min Temperature=843°C	Step Time=40 min Temperature=860.6°C	Step Time=50 min Temperature=909.4°C

#### 5.4.5 Case 5

For Case 5 (CBF and EC3 parametric fire curve in a single compartment), the collapse sequence is shown in Table 5.6 below. As shown in the collapse sequence, when the step time is at 10 min, the temperature reached 704°C and the floor slab of the heated compartment started to membrane with slight bending in the braces. The heated compartment collapsed at 20 min (789°C), and starts to drag other floors with it, which marked the onset of progressive collapse. *It is important to note here that while a parametric fire curve is used, collapse started at a temperature corresponding to the heating phase on the time-temperature curve.*

Therefore, the cooling phase will have no impact on preventing the collapse, although it does influence the response of some elements as will be highlighted later. After half hour with temperature was at 737.5°C, which corresponds to the cooling phase, the entire building continued to drop with notable twist in the entire structure combined with lateral deformation as can be observed. At 40 min (633.3°C) to 50 min (529°C), the building continued to laterally tilt and collapse with membrane action occurring in all floor slabs.

Table 5.6 Collapse Sequence for Case-5

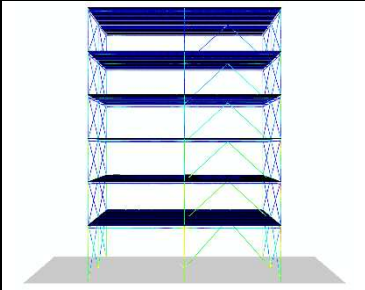
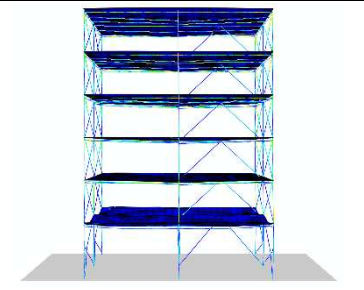
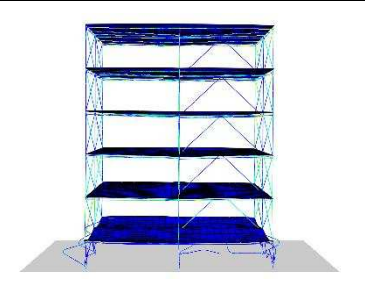
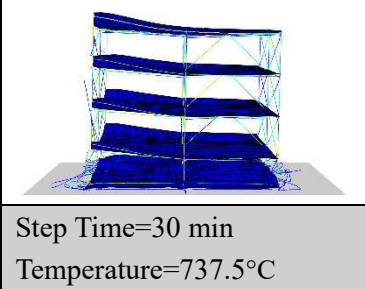
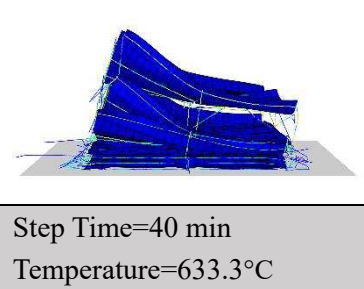
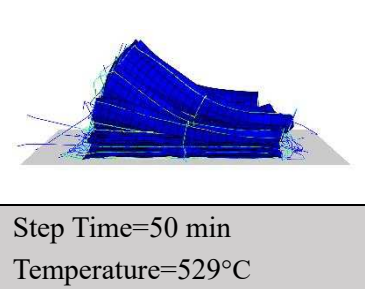
		
Step Time=0 sec Temperature=20°C	Step Time=10 min Temperature=700°C	Step Time=20 min Temperature=789°C
		
Step Time=30 min Temperature=737.5°C	Step Time=40 min Temperature=633.3°C	Step Time=50 min Temperature=529°C

#### 5.4.6 Case 6

In Case 6 (CBF and EC3 parametric fire curve in the whole first floor), the collapse sequence is shown in Table 5.7 below. As shown in the collapse sequence, when the step time is at 10 min, the temperature

reached 700°C. The first floor slab started to sag with small deformation of structural members observed. At 20 min (789°C), the first floor dropped vertically and substantial deformations in its columns is shown. After half hour of heating the first floor, where the temperature on the time-temperature curve is at 737.5°C, the lower two floors collapsed with several broken X braces observed. The building continues to drop straight down and total collapse is reached at 50 min (529°C).

Table 5.7 Collapse Sequence for Case-6

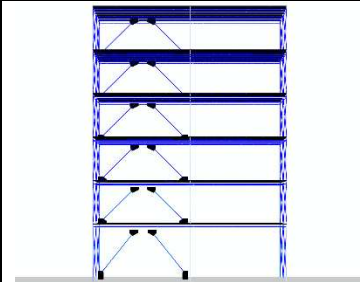
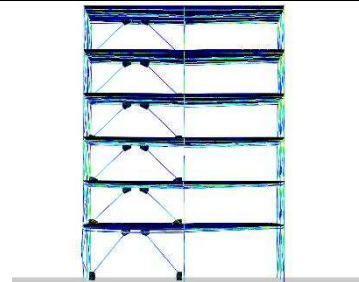
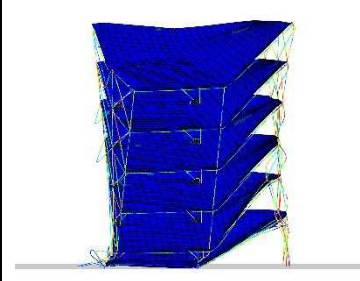
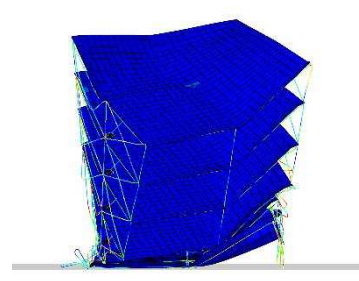
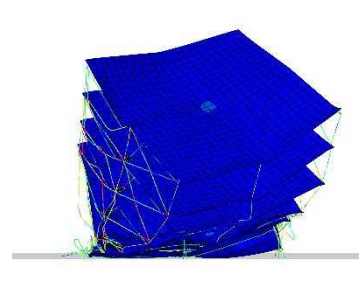
		
Step Time=0 sec Temperature=20°C	Step Time=10 min Temperature=700°C	Step Time=20 min Temperature=789°C
		
Step Time=30 min Temperature=737.5°C	Step Time=40 min Temperature=633.3°C	Step Time=50 min Temperature=529°C

#### 5.4.7 Case 7

In Case 7 (EBF and EC3 parametric fire curve in a single compartment), the collapse sequence is shown in Table 5.8 below. As shown in the collapse sequence table, when the step time is at 10 min, the temperature reached 700°C, membrane action of the floor slabs occurred with the rapidly increasing temperature. At 20 min (789°C), members in the heated compartment lost their load carrying capacity and the corner of the

first floor starts to drop with large deformation observed in the X braces. After half hour of heating the corner bay, where the temperature on the time-temperature curve is at 737.5°C, the first two floors dropped vertically with noticeable twisting of the entire structure. Substantial deformation is also observed in the braces and columns in fire-loaded bay. At 50 min (529°C), the failure continued with total collapse of the first three floors.

Table 5.8 Collapse Sequence for Case-7

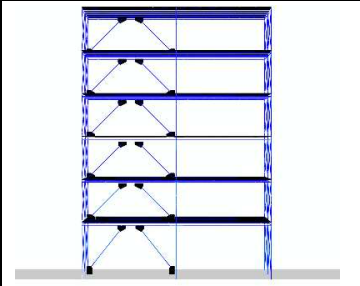
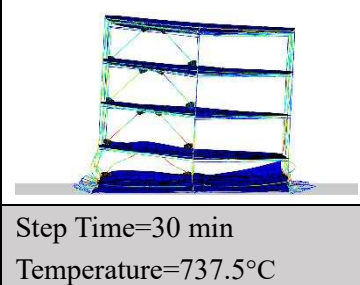
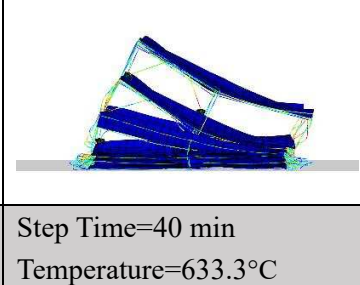
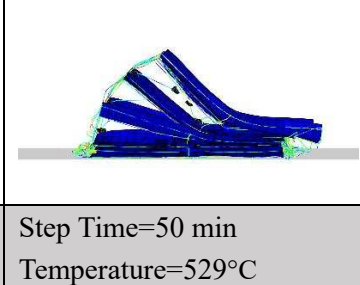
		
Step Time=0 sec Temperature=20°C	Step Time=10 min Temperature=700°C	Step Time=20 min Temperature=789°C
		
Step Time=30 min Temperature=737.5°C	Step Time=40 min Temperature=633.3°C	Step Time=50 min Temperature=529°C

#### 5.4.8 Case 8

In Case 8 (EBF and EC3 parametric fire curve in the whole first floor), the collapse sequence is shown in Table 5.9 below. Membrane action is observed in the first floor concrete slab with small visible deformation of the columns and braces at 10 min (700°C). The first floor collapsed at 20 min (789°C) with large bending

of first floor columns. At 30 min (737.5°C), the lower two floors collapsed in a progressive manner where the demand on second floor increased substantially once the first floor was totally collapsed and also substantial increase in demand on the third floor once the second floor was in contact with the ground. At 40 min (860.6°C) and 50 min (909.4°C), total system collapse was observed with slight tilt of the structure due to its unsymmetrical nature.

Table 5.9 Collapse Sequence for Case-8

		
Step Time=0 sec Temperature=20°C	Step Time=10 min Temperature=700°C	Step Time=20 min Temperature=789°C
		
Step Time=30 min Temperature=737.5°C	Step Time=40 min Temperature=633.3°C	Step Time=50 min Temperature=529°C

## 5.5 Discussion

Total eight simulations were done in this study with different fire curves and fire scenarios. Two types of collapse behavior were observed in the simulations. In the corner compartment fire cases of the first floor, the building models were shown to twist, lean towards the compartment in which the fire is applied, and laterally sway. On the other hand, in the full first floor fire cases, the building models collapsed straight

down and no visible twist was observed. During the vertical straight-down collapse, it was observed that collapse of a floor was accelerated once that floor became in contact with the floor below that was already collapsed and was in contact with the ground. It is also important to point out that this vertical collapse mechanism is not the same as what is typically referred to as pancaking. In pancaking events, collapse is typically triggered by failure of an upper floor that essentially fails and drops on the floor below it, causing the pancaking effect. In this study, since the progressive collapse event was triggered during the heating phase, the effect of using a parametric fire curve with a cooling phase did not make much difference in response. Some difference in the force demand was observed, however, on some of the columns during the cooling phase and the structure continued to collapse as will be discussed later.

## **5.6 Response of Individual Frames**

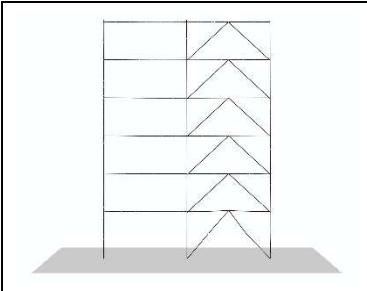
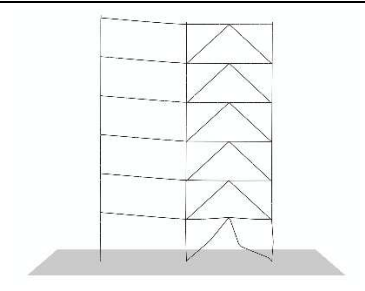
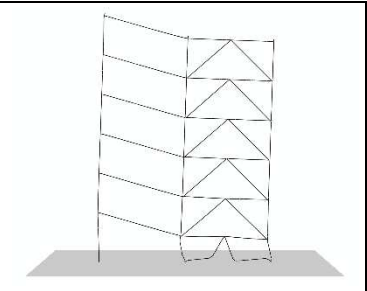
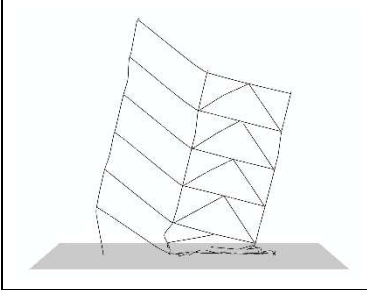
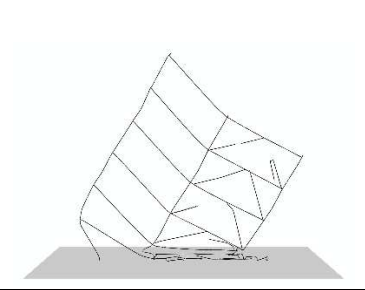
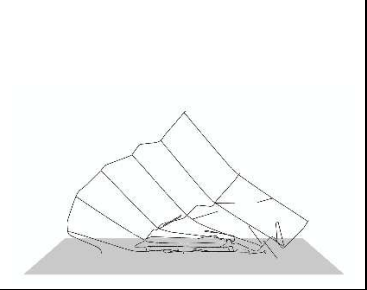
After focusing on the whole system response, this section attempts to assess the collapse mechanisms for the braced frames as well as the gravity frames. In the 3D model, the braced frames are marked by Frame B in Figure 5.1, which is either a CBF or an EBF. For the gravity frames, the focus is on the center frame (Frame 2 in Figure 5.1), which is perpendicular in direction to the moment frames and the braced frames. The collapse sequence tables below provide insight into the overall collapse mechanisms of the braced frames and the gravity frames under the eight different fire-loading cases.

### **5.6.1 Case 1**

The collapse mechanism of the CBF in Case 1 (CBF and E119 in a single compartment) is shown in Table 5.10. As shown in the table, when the step time is at 10 min with a corresponding temperature of 704°C, no

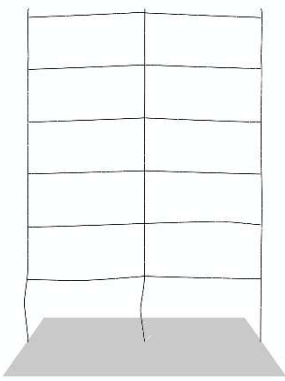
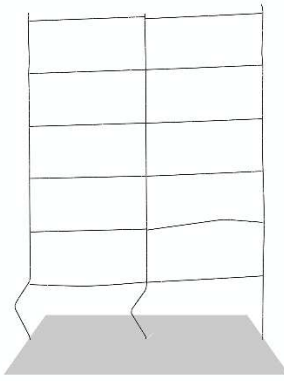
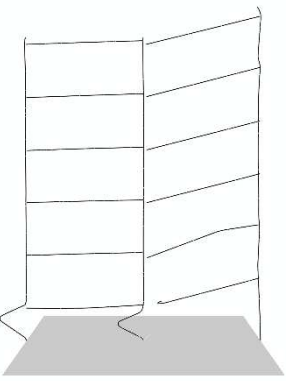
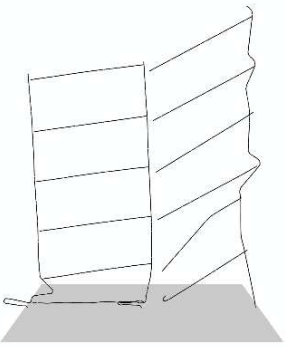
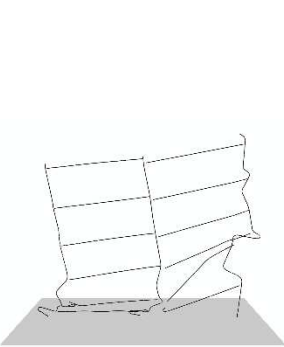
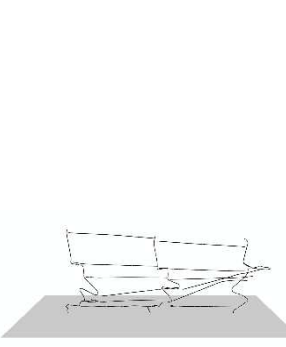
visible deformation was observed in the selected braced frame. Significant buckling was observed, however, in the first story brace at step time equal to 15 min (718.4°C). At 20 min (773.5°C), substantial deformations were observed in both braces and columns of the first floor compartment and the two braces were in contact with the ground at that point. With rapid increase in temperature at 30 min (843°C), the first two floors dropped to the ground and one side of the brace on the second floor fractured at its connection with the frame further tilting due to the overturning moment caused by the unbalanced forces. At 40 min (860.6°C), the third floor collapsed with several visible fractured braces at third, fourth and sixth floors. Around 50 min (909.4°C), total collapse of the frame occurred with more brace fracture and excessive tilting of the entire frame.

Table 5.10 Case-1 CBF Frame B Collapse Sequence

		
Step Time=10min Temperature=704°C	Step Time=15 min Temperature=718.4°C	Step Time=20 min Temperature=773.5°C
		
Step Time=30 min Temperature=843°C	Step Time=40 min Temperature=860.6°C	Step Time=50 min Temperature=909.4°C

For the gravity frame of Case 1 (CBF and E119 in a single compartment), shown in Table 5.11, columns of the first floor started to buckle at 10 min (704°C) and large deformation of the columns in the left bay was observed at 15 min (718.4°C). When temperature reached 773.5°C (20 min), the first floor shear connectors failed with collapse of the entire first floor. Visible separations of the right bay shear connectors of all floors can be seen at 30 min (843°C). The first two floors collapsed at 40 min (860.6°C) and a total collapse occurred around 50 min (909.4°C).

Table 5.11 Case-1 Gravity Frame 2 Collapse Sequence

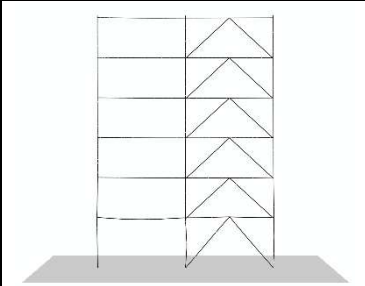
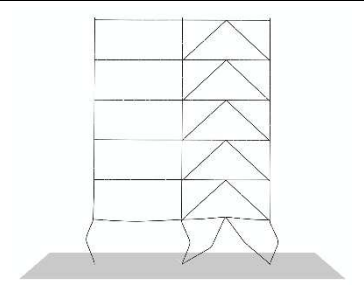
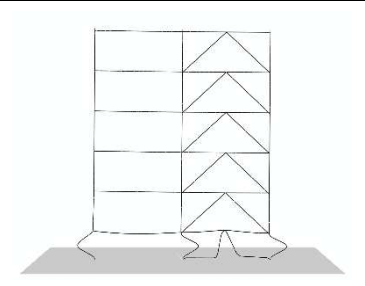
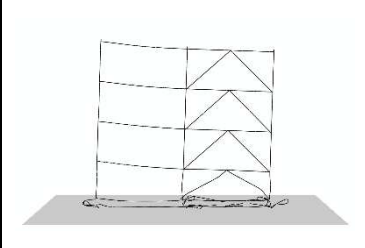
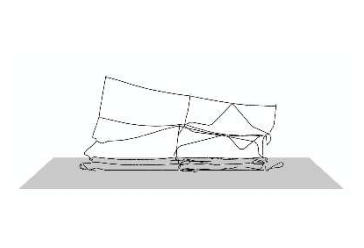
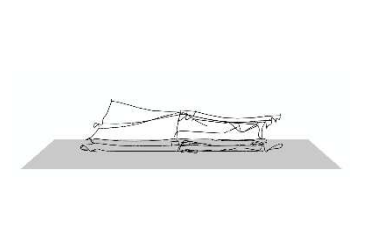
		
Step Time=10min Temperature=704°C	Step Time=15 min Temperature=718.4°C	Step Time=20 min Temperature=773.5°C
		
Step Time=30 min Temperature=843°C	Step Time=40 min Temperature=860.6°C	Step Time=50 min Temperature=909.4°C

### 5.6.2 Case 2

The collapse mechanism of the CBF in Case 2 (CBF and E119 in the whole floor) is shown in Table 5.12.

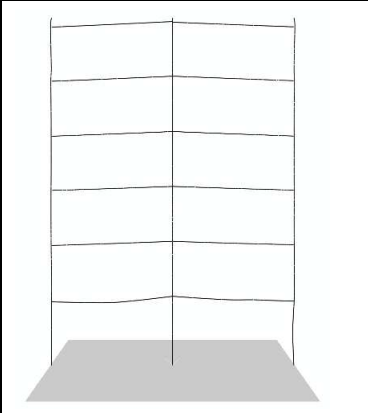
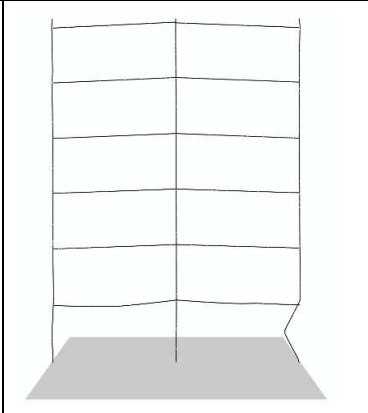
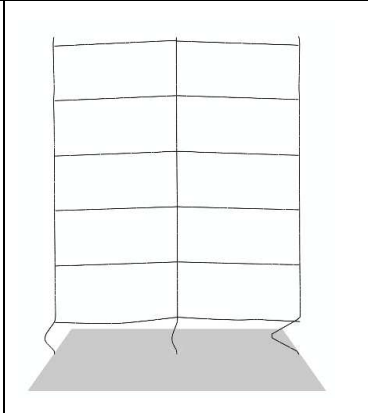
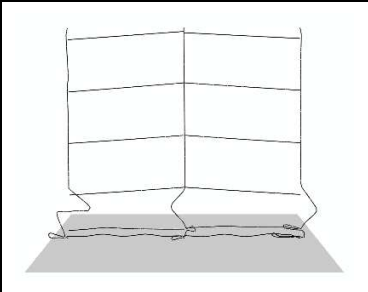
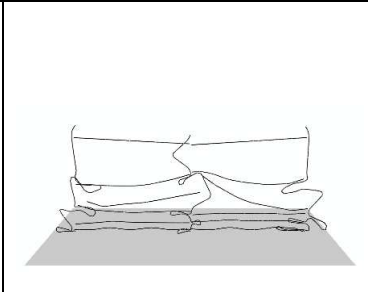
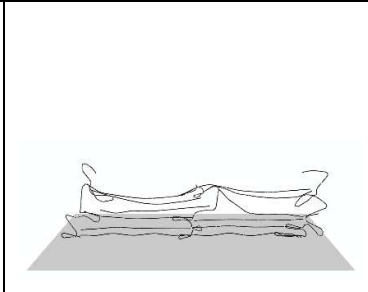
As shown in the table, when the step time was at 10 min, the temperature reached 704°C and the structure was still intact with no sign of deformation in the braced frame. Because of the fire was introduced to the whole first floor, plastic deformations were generated on all the columns and braces of first floor at 15 min (718.4°C). After 5 min of heating, the first floor dropped significantly with large deformation of columns and braces and both braces of the first floor were in contact with the ground. The first two floors vertically collapsed at 30 min (843°C) with no sign of element separation in the remaining floors as would be expected. The progression of collapsed continued at 40 min (860.6°C) with total collapse of the frame occurring around 50 min (909.4°C).

Table 5.12 Case-2 CBF Frame B Collapse Sequence

		
Step Time=10 min Temperature=704°C	Step Time=15 min Temperature=718.4°C	Step Time=20 min Temperature=773.5°C
		
Step Time=30 min Temperature=843°C	Step Time=40 min Temperature=860.6°C	Step Time=50 min Temperature=909.4°C

For the gravity frame of Case-2 (CBF and E119 in the whole floor), shown in Table 5.13, when the step time was at 10 min, the temperature reached 704°C and slight deformation was seen in the gravity frame. Large inelastic deformations occurred in the right columns of the right bay on the first floor at 15 min (718.4°C). After half hour of heating the corner bay, where the temperature on the time-temperature curve was at 843°C, the first two floors collapsed, and the entire third floor columns buckled with separation of the connector of the right column of the right bay. Several further separations can be seen at 40 min (860.6°C) with more buckled columns and total collapse occurring around 50 min (909.4°C).

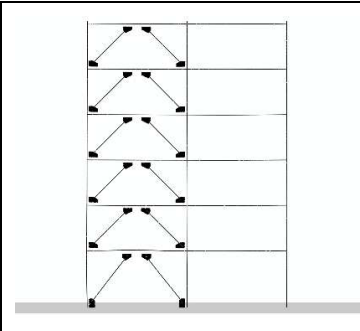
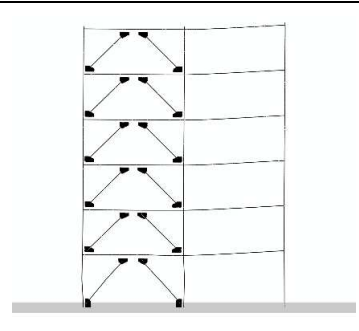
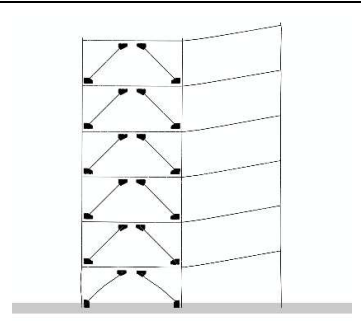
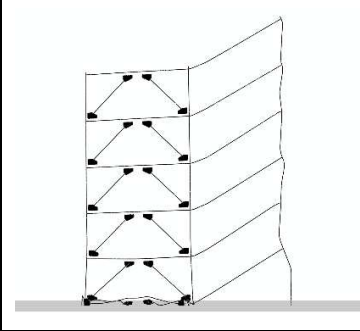
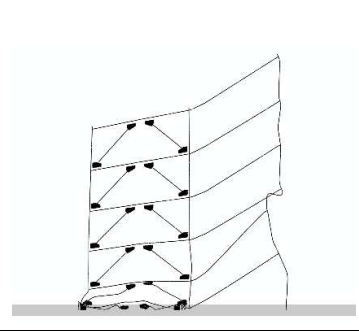
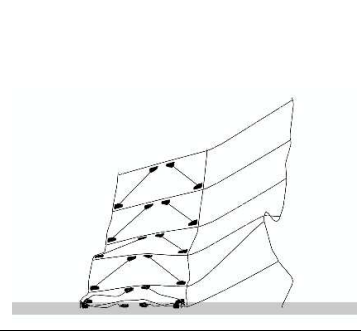
Table 5.13 Case-2 Gravity Frame 2 Collapse Sequence

		
Step Time=10min Temperature=704°C	Step Time=15 min Temperature=718.4°C	Step Time=20 min Temperature=773.5°C
		
Step Time=30 min Temperature=843°C	Step Time=40 min Temperature=860.6°C	Step Time=50 min Temperature=909.4°C

### 5.6.3 Case 3

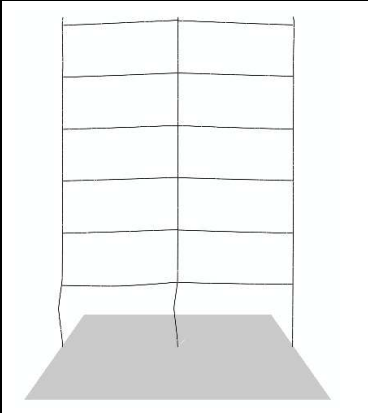
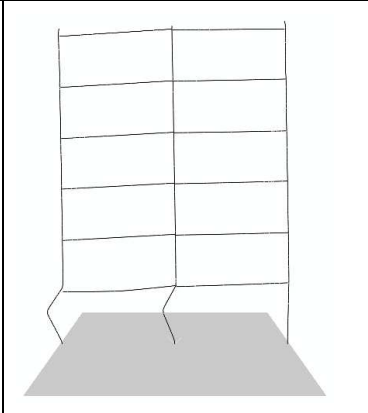
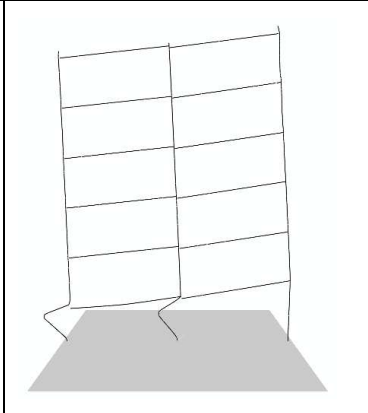
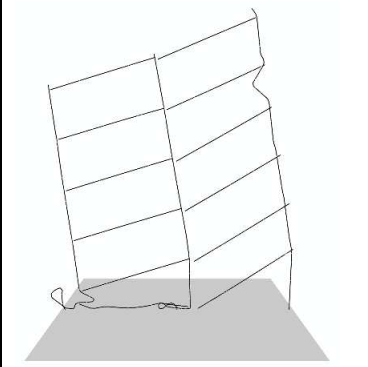
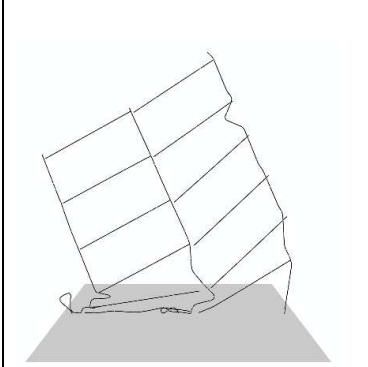
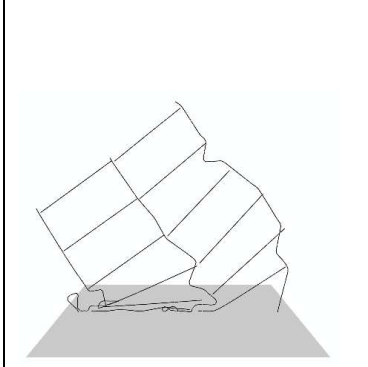
The collapse mechanism of the EBF in Case 3 (EBF and E119 in a single compartment) is shown in Table 5.14. As shown in the table, when the step time is at 10 min, the temperature reached 704°C with no sign of deformation in the braced frame. Visible downward displacement of the fire-loaded bay was observed at 15 min (718.4°C). Large deformations of the structural members of the left bay occurred around 20 min (773.5°C). After 10 min (843°C), the left bay of the braced frame continued to displace significantly and the floor slab was in contact with the ground. At 40 min (860.6°C), the third floor right column in the right bay substantially deformed because of the unbalanced forces caused by the collapse of the first two floors of the left bay. Some fold action was observed at 50 min (909.4°C) with the upper frame moving backward.

Table 5.14 Case-3 EBF Frame B Collapse Sequence

		
Step Time=10min Temperature=704°C	Step Time=15 min Temperature=718.4°C	Step Time=20 min Temperature=773.5°C
		
Step Time=30 min Temperature=843°C	Step Time=40 min Temperature=860.6°C	Step Time=50 min Temperature=909.4°C

For the gravity frame of Case 3 (EBF and E119 in a single compartment), shown in Table 5.15, some buckling can be observed in the first floor two left side columns. This was followed by significant deformations in same columns around 15 min (718.4°C) with visible separation of the left side shear connector, after additional 5 minutes of heating, substantial deformation of the first was noted with clear separation of the shear connector at left side. At 30 min (843°C), total collapse occurred in the first floor fire compartment. With collapse of the first two floors of the left bay, the frame tilts significantly to the left, which caused increase in separations in the connections at 40 min (860.6°C). The frame continued to substantially sway to the left at 50 min (909.4°C).

Table 5.15 Case-3 Gravity Frame 2 Collapse Sequence

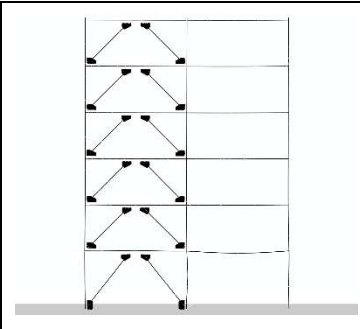
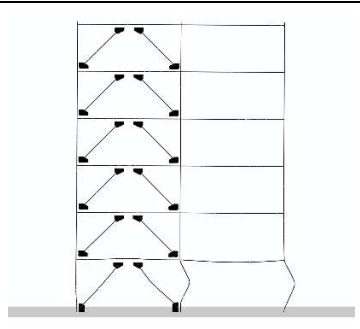
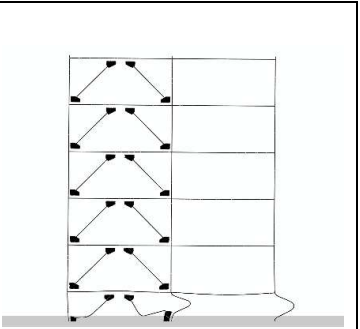
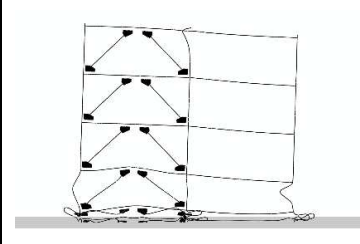
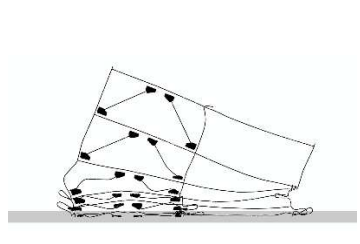
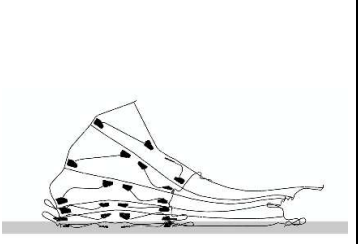
		
Step Time=10min Temperature=704°C	Step Time=15 min Temperature=718.4°C	Step Time=20 min Temperature=773.5°C
		
Step Time=30 min Temperature=843°C	Step Time=40 min Temperature=860.6°C	Step Time=50 min Temperature=909.4°C

### 5.6.4 Case 4

The collapse mechanism of the EBF in Case 4 (EBF and E119 in the whole floor) is shown in Table 5.16.

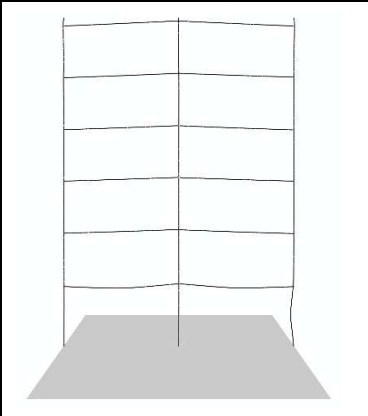
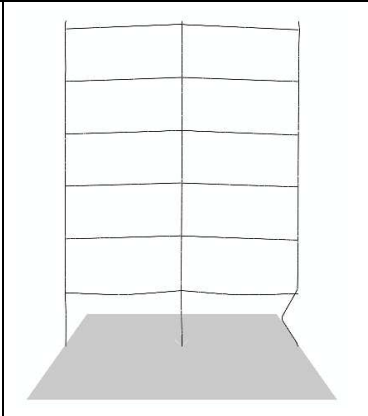
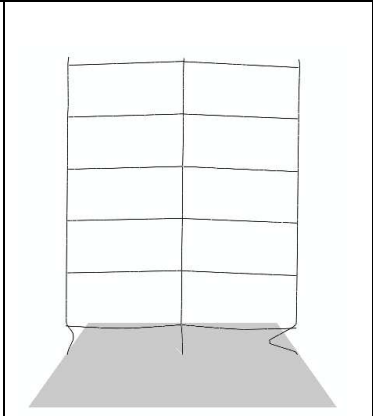
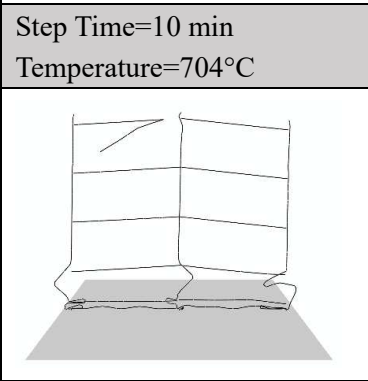
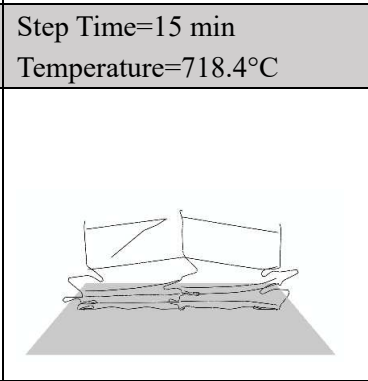
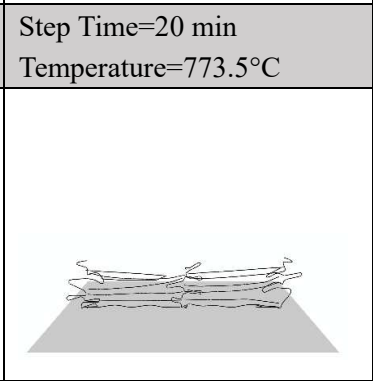
As shown in the collapse sequence when the step time was at 10 min, the temperature reached 704°C with no obvious deformation in the structural members except for only small deformation in the first floor girder of the right bay. At 15 min (718.4°C), the first floor columns of the right bay experienced large flexural deformations. At 20 min (773.5°C) the whole entire first floor displaced downward significantly due to buckling of braces of the first floor left bay. At 30 min (843°C), the first two floors experienced complete collapse and the collapse progressed until around 50 min (909.4°C) with some fold action, extreme bending and fracture in braces.

Table 5.16 Case-4 EBF Frame B Collapse Sequence

		
Step Time=10 min Temperature=704°C	Step Time=15 min Temperature=718.4°C	Step Time=20 min Temperature=773.5°C
		
Step Time=30 min Temperature=843°C	Step Time=40 min Temperature=860.6°C	Step Time=50 min Temperature=909.4°C

For the gravity frame of Case 4 (EBF and E119 in the whole floor), shown in Table 5.17, slight downward deformation of two exterior columns and girders can be observed at 10 min (704°C). A plastic hinge was at the bottom column around 15 minutes (718.4°C) of step time. The first floor had a significant drop after five minutes heating, all the first floor columns buckled at this point. At 30 minutes (843°C), lower two floors collapsed with large element distortion of the top girder cause by uneven collapse force. More floors collapsed with several connector separations found in the frame at 40 min (860.6°C). Total collapsed occurred around 50 minutes (909.4°C).

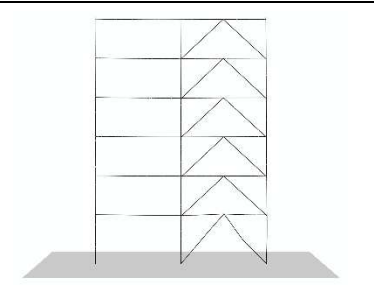
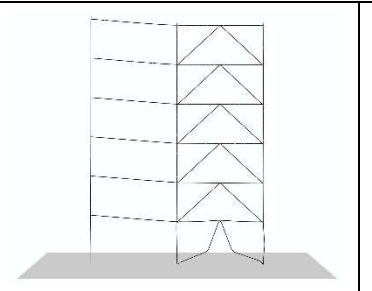
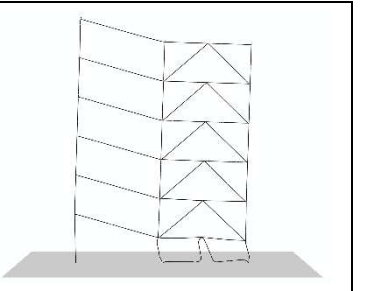
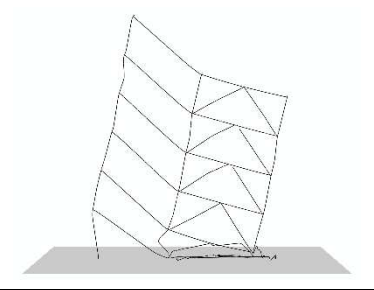
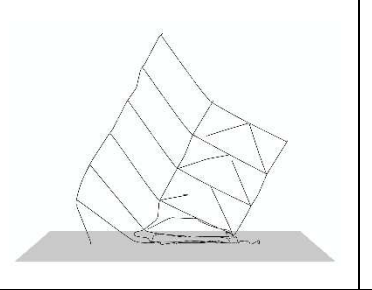
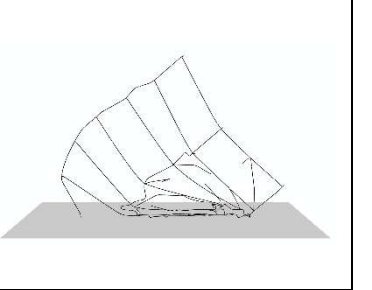
Table 5.17 Case-4 Gravity Frame 2 Collapse Sequence

		
Step Time=10 min Temperature=704°C	Step Time=15 min Temperature=718.4°C	Step Time=20 min Temperature=773.5°C
		
Step Time=30 min Temperature=843°C	Step Time=40 min Temperature=860.6°C	Step Time=50 min Temperature=909.4°C

### 5.6.5 Case 5

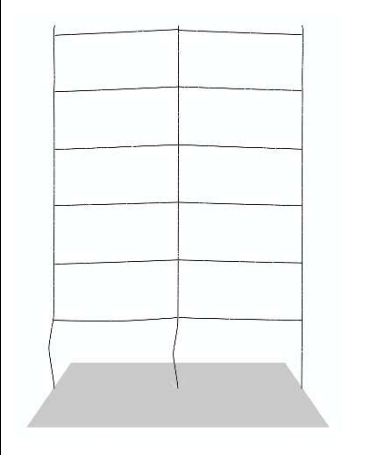
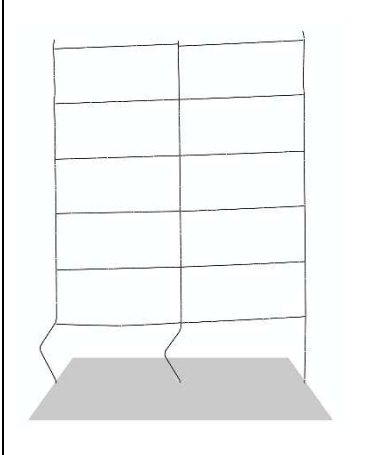
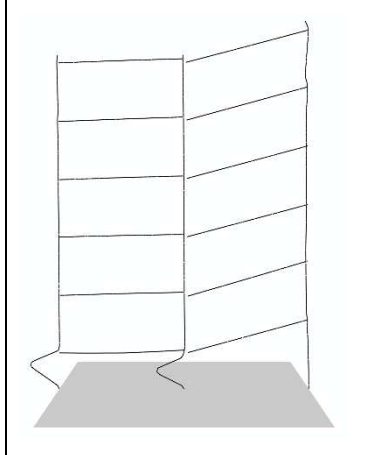
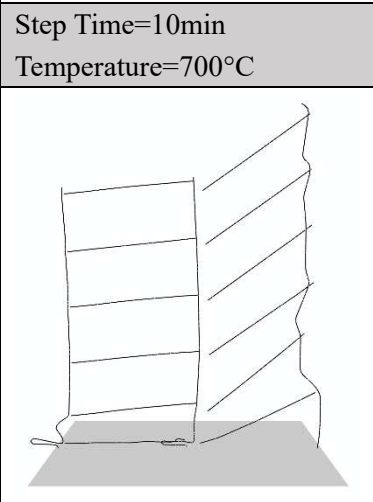
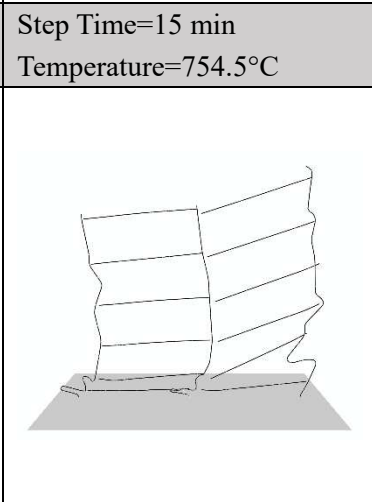
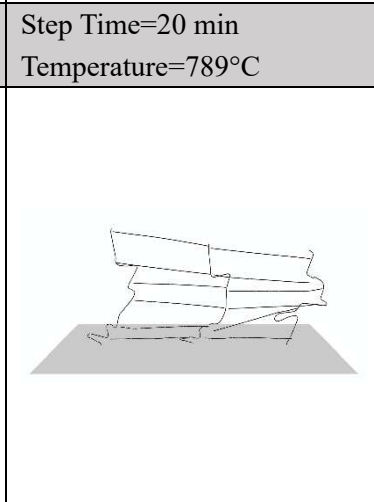
The collapse mechanism of the CBF in Case 5 (CBF and EC3 parametric fire curve in a single compartment) is shown in Table 5.18. As shown in the collapse sequence table, when the step time was at 10 min, the temperature reached 700°C and buckling in one of the braces is noted. Significant buckling of both braces of the first floor was noted at 15 minutes (754.5°C), which was caused by the downward deformation of the frame. Further deformations were noted at 20 min (789°C) and the second floor impacted the ground around 30 minutes (737.5°C) with large tilting of the frame. At 40 minutes (633.3°C), several braces fractured with further tilting of the frame to the right side. The whole frame continued to tilt to the right side at 50 minutes (529°C) with further brace fractures.

Table 5.18 Case-5 CBF Frame B Collapse Sequence

		
Step Time=10min Temperature=700°C	Step Time=15 min Temperature=754.5°C	Step Time=20 min Temperature=789°C
		
Step Time=30 min Temperature=737.5°C	Step Time=40 min Temperature=633.3°C	Step Time=50 min Temperature=529°C

For the gravity frame of Case 5 (CBF and EC3 parametric fire curve in a single compartment), shown in Table 5.19, columns of first floor started to buckle at 10 min (700°C) and the two columns of the left bay excessively buckled at 15 min (754.5°C). At 20 min when the temperature reached 789°C, first floor shear connector failed and the first floor collapsed. Visible separations of the shear connectors of the left bays in all floors was seen at 30 min (737.5°C). Total collapse occurred around 50 min (529°C) with large bending of the columns and more connector separations.

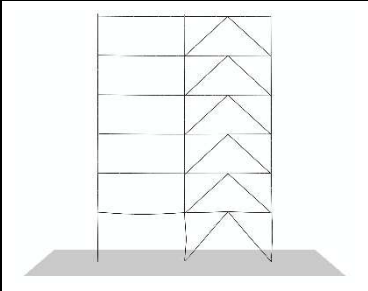
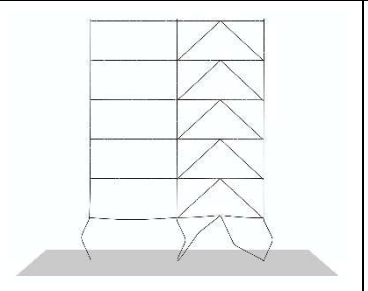
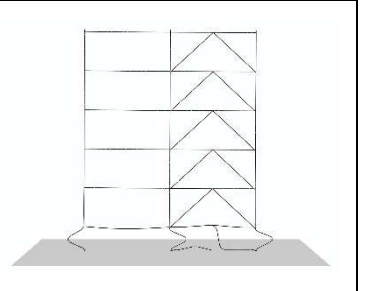
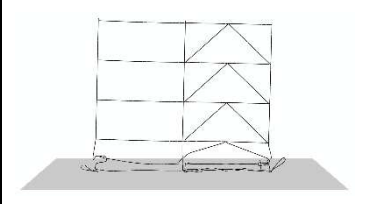
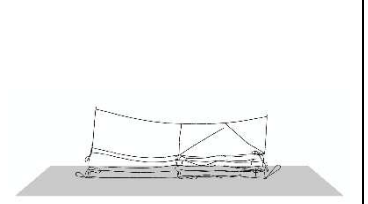
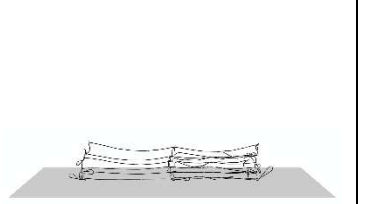
Table 5.19 Case-5 Gravity Frame 2 Collapse Sequence

		
Step Time=10min Temperature=700°C	Step Time=15 min Temperature=754.5°C	Step Time=20 min Temperature=789°C
		
Step Time=30 min Temperature=737.5°C	Step Time=40 min Temperature=633.3°C	Step Time=50 min Temperature=529°C

### 5.6.6 Case 6

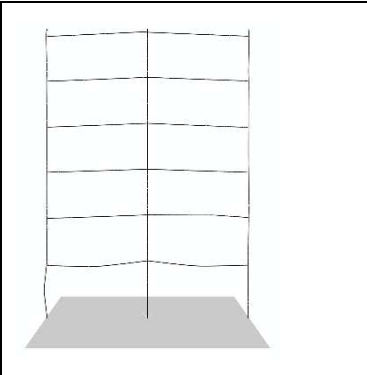
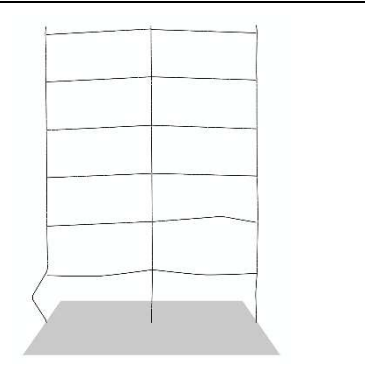
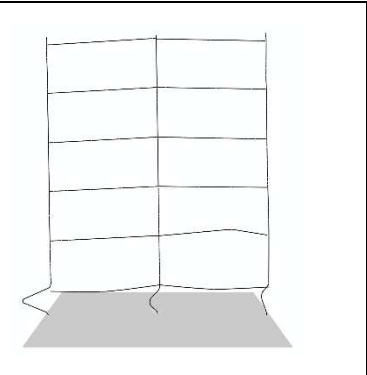
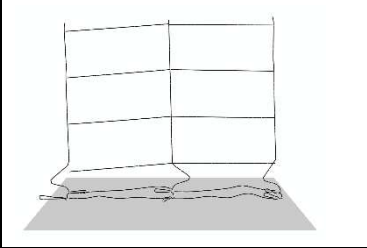
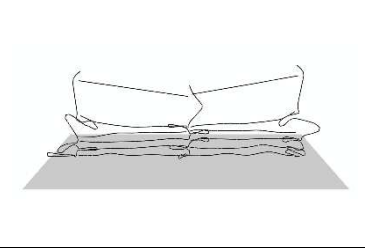
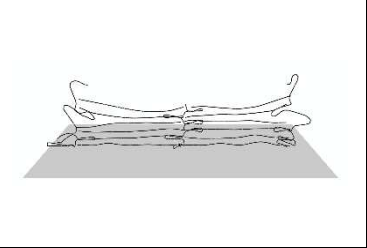
The collapse mechanism of the CBF in Case 6 (CBF and EC3 parametric fire curve in the whole first floor) is shown in Table 5.20. As shown in the collapse sequence table, when the step time is at 10 min, the temperature reached 700°C and the first floor structural members did not experience visible deformations. At 15 minutes (754.5°C), all first floor columns and braces buckled significantly. The left brace of the first floor of the right bay broke at 20 min (789°C). At 30 minutes (737.5°C), the first two floor collapsed and only ten minutes later collapse propagated all the way to fifth floor. The last floor collapsed around 50 minutes (529°C).

Table 5.20 Case-6 CBF Frame B Collapse Sequence

		
Step Time=10 min Temperature=700°C	Step Time=15 min Temperature=754.5°C	Step Time=20 min Temperature=789°C
		
Step Time=30 min Temperature=737.5°C	Step Time=40 min Temperature=633.3°C	Step Time=50 min Temperature=529°C

For the gravity frame of Case 6 (CBF and EC3 parametric fire curve in the whole first floor), shown in Table 5.21, only small deformation can be seen at 10 minutes (700°C), the frame was intact at this point. Plastic hinge generated at the left side column on the first floor at 15 minutes (754.5°C) with the sign of large bending of right side second floor girder cause by unbalance of the frame. The first floor had a drop around 20 minutes (789°C) with visible separation of the first floor left side connection, and first two floors complete collapsed at ten minutes later with columns buckling on the third floor to absorb the collapse energy. At 40 min (633.3°C) and 50 min (529°C), the collapse continues in a progressive manner with clear sign of connector separations on all the floors. Total collapse of the frame occurred at 50.

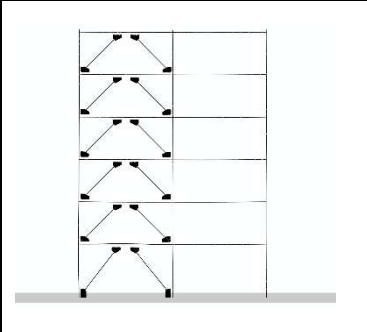
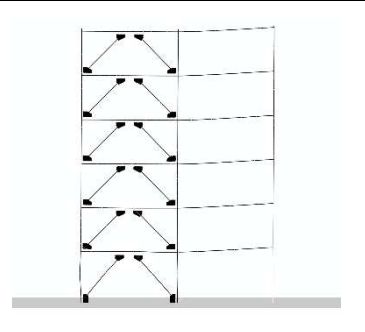
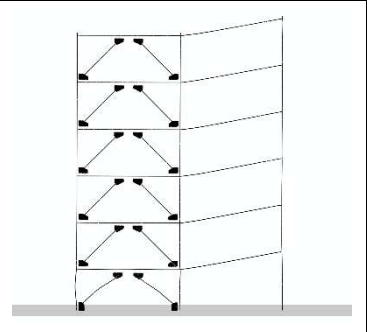
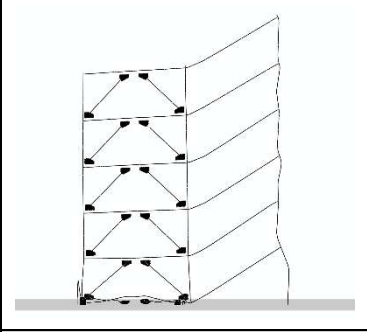
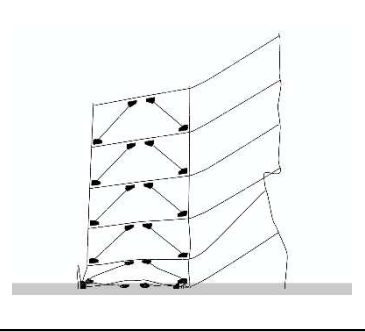
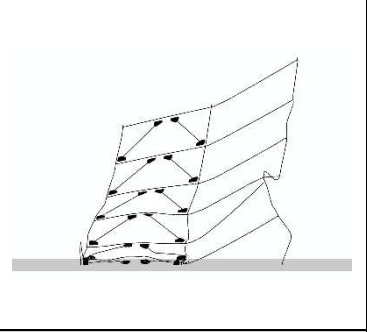
Table 5.21 Case-6 Gravity Frame 2 Collapse Sequence

		
Step Time=10 min Temperature=700°C	Step Time=15 min Temperature=754.5°C	Step Time=20 min Temperature=789°C
		
Step Time=30 min Temperature=737.5°C	Step Time=40 min Temperature=633.3°C	Step Time=50 min Temperature=529°C

### 5.6.7 Case 7

The collapse mechanism of the EBF in Case 7 (EBF and EC3 parametric fire curve in a single compartment) is shown in Table 5.22. The EBF did not undergo large deformation until 20 minutes (789°C). At 30 min (737.5°C), the first floor impacted the ground. The frame bent inward at 40 minutes (633.3°C). The lower two floors collapsed completely around 50 minutes (529°C) with noticeable fold action of the frame.

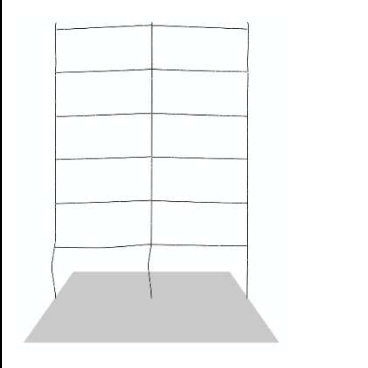
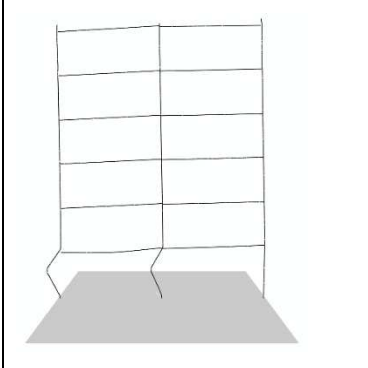
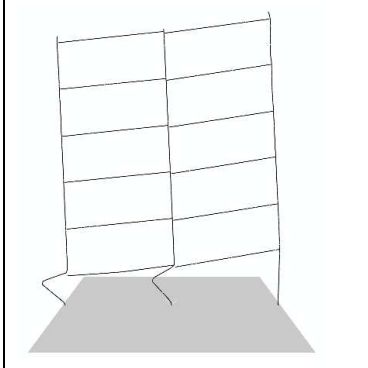
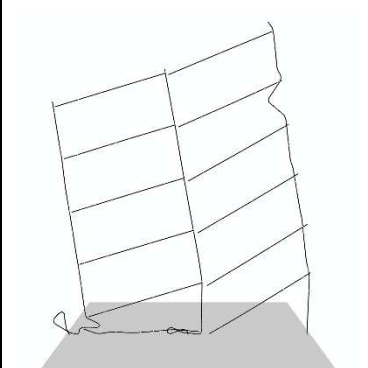
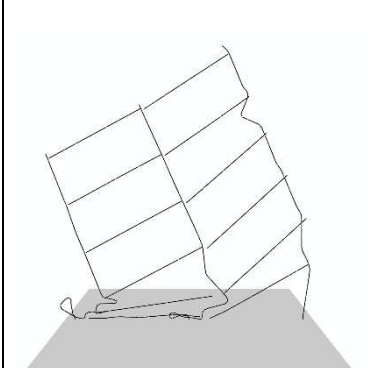
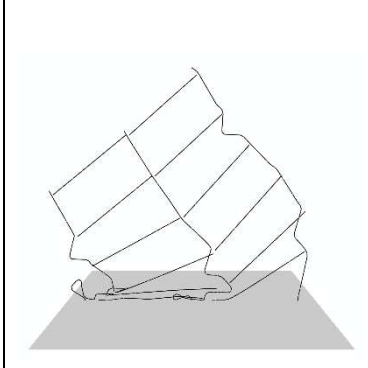
Table 5.22 Case-7 EBF Frame B Collapse Sequence

		
Step Time=10min Temperature=700°C	Step Time=15 min Temperature=754.5°C	Step Time=20 min Temperature=789°C
		
Step Time=30 min Temperature=737.5°C	Step Time=40 min Temperature=633.3°C	Step Time=50 min Temperature=529°C

For the gravity frame of Case 7 (EBF and EC3 parametric fire curve in a single compartment), shown in Table 5.23, two left side columns on first floor starts to have visible bending at 10 min (700°C). Plastic hinges were generated on the same columns and first floor collapsed at 30 minutes (737.5°C). Separations

of shear connectors in the frames can be seen at many points. Third floor hit the ground at 50 minutes (529°C), the frame tilted towards its left side. Plastic hinge also can be found on the right side of columns because the bending of the frame.

Table 5.23 Case-7 Gravity Frame 2 Collapse Sequence

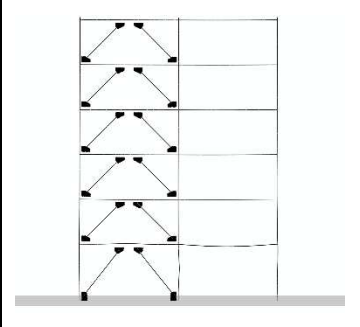
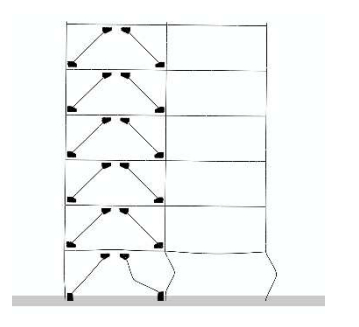
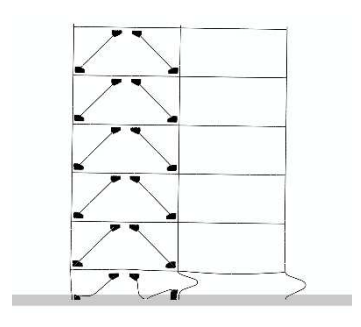
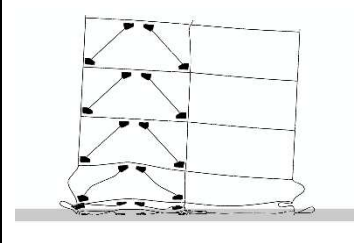
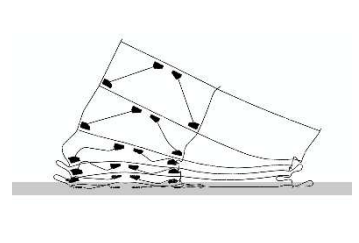
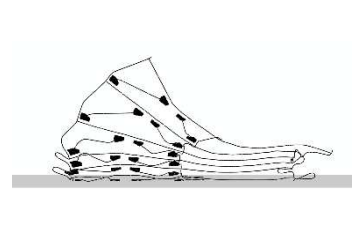
		
Step Time=10min Temperature=700°C	Step Time=15 min Temperature=754.5°C	Step Time=20 min Temperature=789°C
		
Step Time=30 min Temperature=737.5°C	Step Time=40 min Temperature=633.3°C	Step Time=50 min Temperature=529°C

### 5.6.8 Case 8

The collapse mechanism of the EBF in Case 8 (EBF and EC3 parametric fire curve in the whole first floor) is shown in Table 5.24. The building showed no sign of deformations at 10 minutes (700°C) except for small bending of the first floor girder of the right bay. Columns and braces of first floors started to buckle

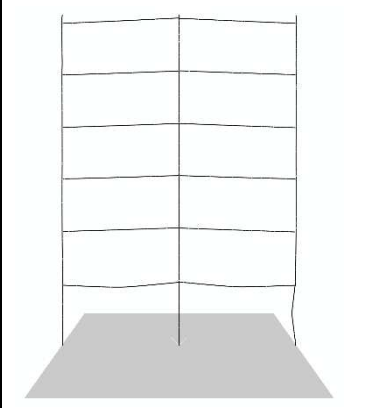
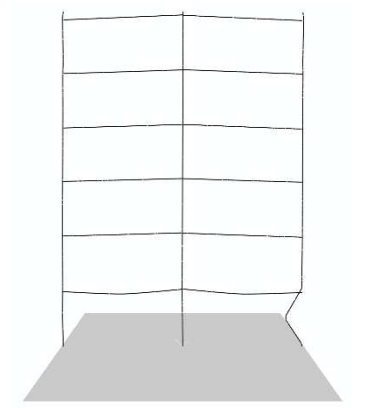
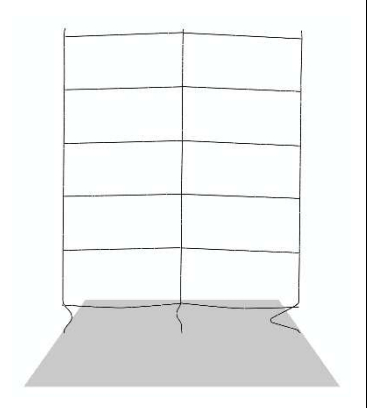
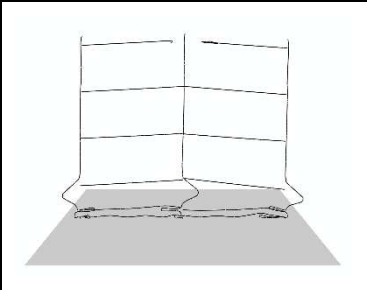
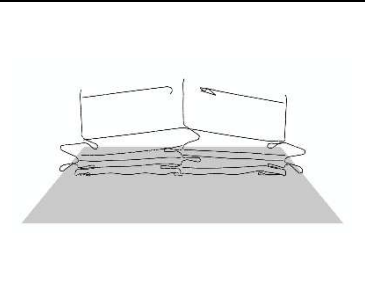
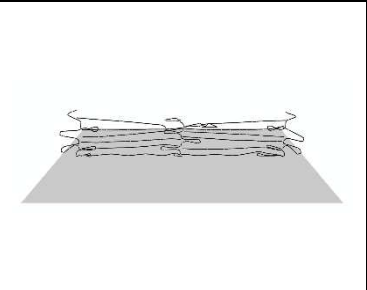
at 15 minutes (754.5°C). The first floor slab dropped to about half of the floor height at 20 minutes (789°C). The lower two floors completely collapsed at 30 min (737.5°C). Total collapse of the frame occurred at 50 min (529°C).

Table 5.24 Case-8 EBF Frame B Collapse Sequence

		
Step Time=10min Temperature=700°C	Step Time=15 min Temperature=754.5°C	Step Time=20 min Temperature=789°C
		
Step Time=30 min Temperature=737.5°C	Step Time=40 min Temperature=633.3°C	Step Time=50 min Temperature=529°C

For the gravity frame of Case 8 (EBF and EC3 parametric fire curve in the whole first floor), shown in Table 5.25, small deformations can be observed at 10 min (700°C) with bending in the first floor beams and buckling in the left bay right column. At 20 min (789°C), the entire first floor columns buckled. The connections at the roof and first story broke at 30 minutes (737.5°C) and complete collapse of the lower two stories was also observed. At 40 min (633.3°C) and 50 min (529°C), total system collapse was observed.

Table 5.25 Case-8 Gravity Frame 2 Collapse Sequence

		
Step Time=10min Temperature=700°C	Step Time=15 min Temperature=754.5°C	Step Time=20 min Temperature=789°C
		
Step Time=30 min Temperature=737.5°C	Step Time=40 min Temperature=633.3°C	Step Time=50 min Temperature=529°C

### 5.6.9 Discussion

For the critical frames selected in this study, similar collapse mechanisms were observed. In the first floor corner compartment fire cases, the frames were shown to bend, lean towards the compartment in which the fire was applied, and fold. On the other hand, in the full first floor fire cases, the floors went straight down and no visible twist was observed during collapse. For the two different fire curves, only minor difference in global deformations was observed since all models started to collapse during the heating phase.

## 5.7 Critical Behavior of Structural Members

### 5.7.1 Column Vertical Displacement

The first floor columns were used in this section to assess system collapse through evaluating their vertical displacements as a function of temperature. Reference points for each column were the element nodes at the first floor height.

#### 5.7.1.1 Case-1

For Case 1 (CBF and E119 in a single compartment), shown in Figure 5.7, with temperature increase, the reference points seem to move slightly upward because of thermal elongation of the steel. At 700°C, the columns of the heated compartment started to move downward. These columns reached their maximum displacement around 820°C to 840°C. The columns, which were not directly subjected to fire started to displace downwards at 842°C. The whole first floor reached its displacement limit as it was in contact with the ground at 927°C.

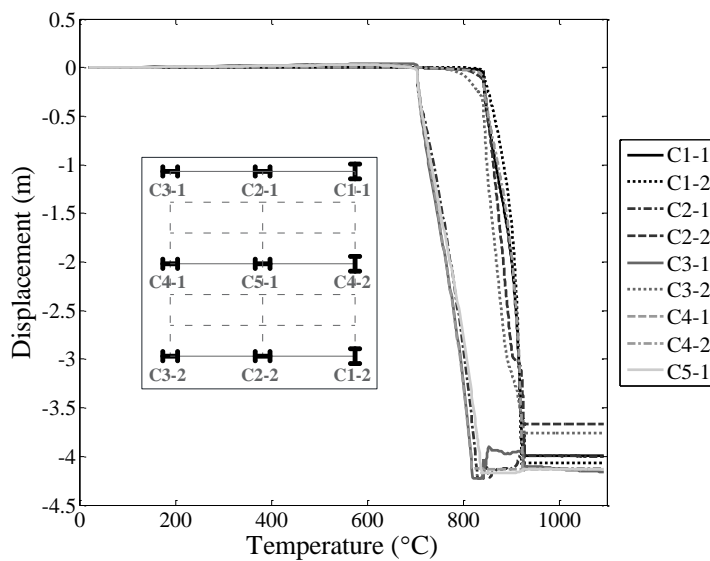


Figure 5.7 Case-1 Vertical Displacements of First Floor Columns

### 5.7.1.2 Case-2

For Case 2 (CBF and E119 in the whole floor), shown in Figure 5.8, the whole first floor was subjected to elevated temperature. A small upward displacement is observed initially due to thermal elongation of the steel. When the temperature reached 700°C, the structural steel lost more than half of its strength and the entire floor started to displace vertically downward as shown in the figure through equal displacement of all columns. Full contact with the ground was reached at 823°C.

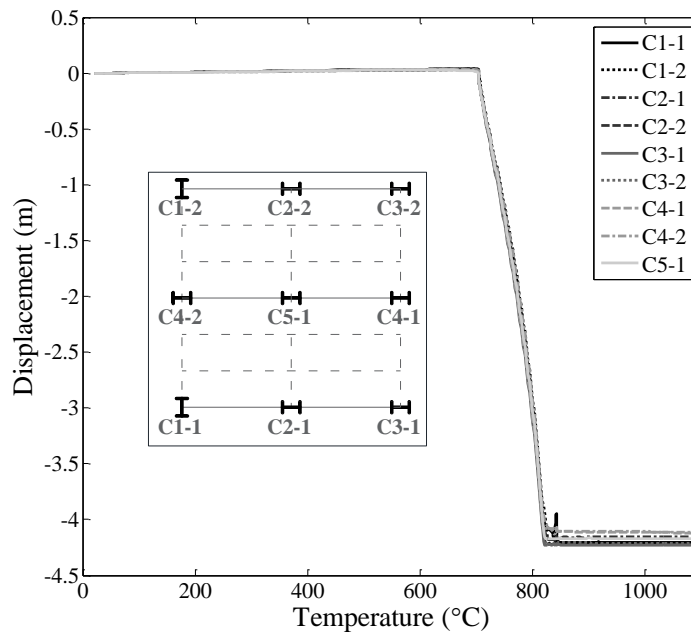


Figure 5.8 Case-2 Vertical Displacements of First Floor Columns

### 5.7.1.3 Case-3

For Case 3 (EBF and E119 in a single compartment), shown in Figure 5.9, the heated compartment started to drop vertically at 700°C and was in contact with the ground at about 840°C. Following this point, the rest of the building started to drop down. Because of the unique collapse mechanism (twist and sway) and

brace type used, the columns did not fail all at once. For example, the corner column far from the fire only had a displacement of 0.233m.

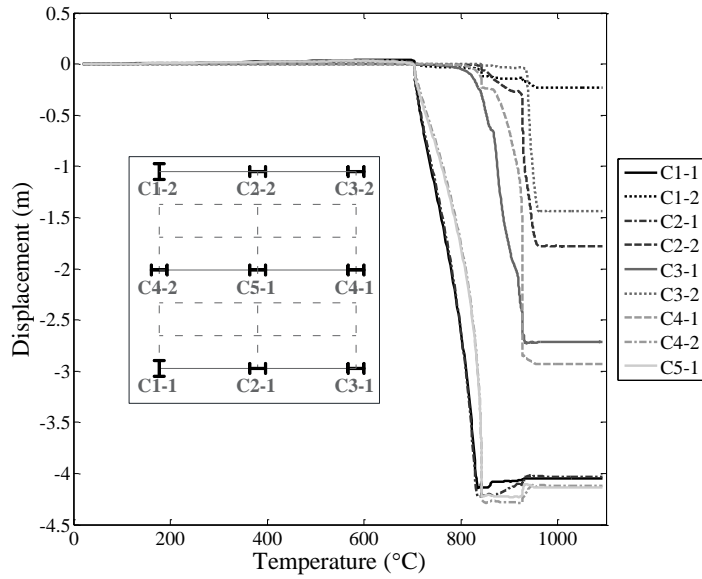


Figure 5.9 Case-3 Vertical Displacements of First Floor Columns

#### 5.7.1.4 Case-4

For Case 4 (EBF and E119 in the whole floor), shown in Figure 5.10, progressive failure of the entire floors is shown to start at approximately 700 °C with complete floor collapse at around 840 °C. All columns sustained the same displacement levels as expected.

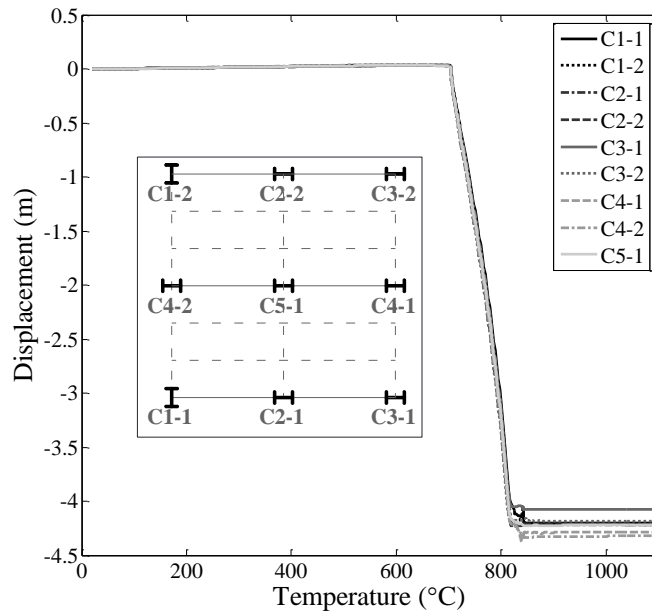


Figure 5.10 Case-4 Vertical Displacements of First Floor Columns

### 5.7.1.5 Case-5

For Case 5 (CBF and EC3 parametric fire curve in a single compartment), shown in Figure 5.11, small thermal elongations of the heated columns were observed before the heated compartment started to drop at 670°C because the EC3 parametric has a slight faster rate of temperature increase. The heated compartment impacted the ground at around 810°C. The system started to cool down following reaching the peak temperature. This is shown in the response curves where the curves end at room temperature.

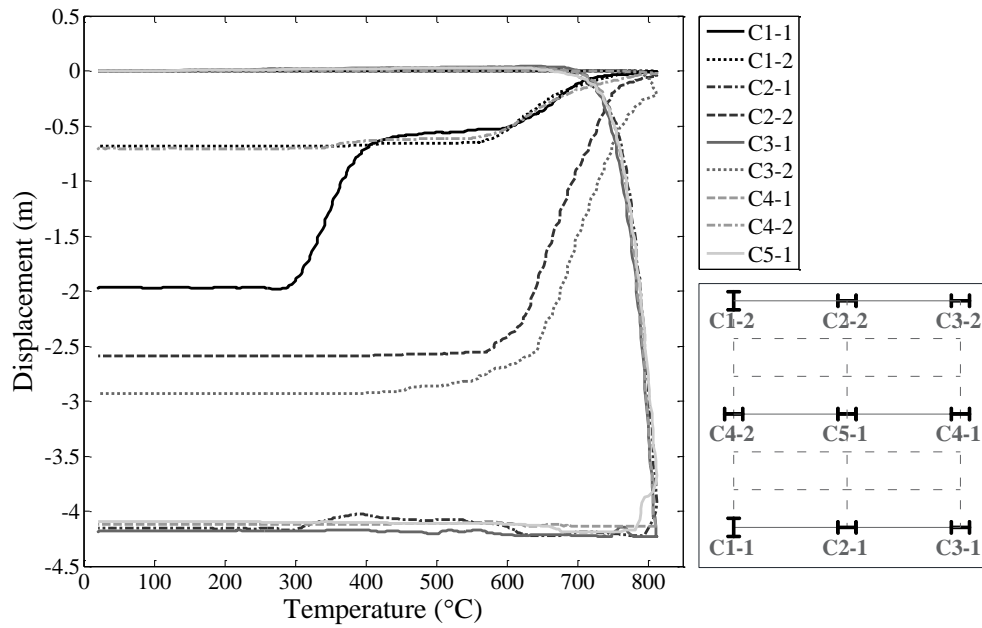


Figure 5.11 Case-5 Vertical Displacements of First Floor Columns

### 5.7.1.6 Case-6

For Case 6 (CBF and EC3 parametric fire curve in the whole first floor), shown in Figure 5.12, all columns sustained the same displacement because of all columns being evenly heated. The structural collapse started at 700 °C with contact with the ground achieved at 810 °C. The results of this fire case were expected and are similar to other whole first floor fire cases.

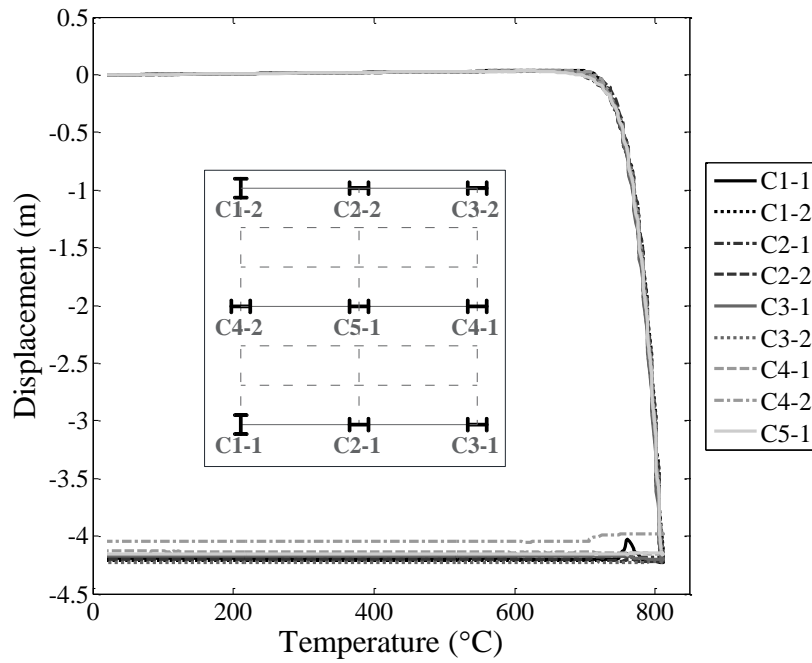


Figure 5.12 Case-6 Vertical Displacements of First Floor Columns

### 5.7.1.7 Case-7

For Case 7 (EBF and EC3 parametric fire curve in a single compartment), shown in Figure 5.13, the heated compartment started to displace downwards at 700°C, and the compartment totally collapsed at around 780°C. The center column C5-1 because the support from non-heated compartment columns reached ground during the cooling phase at 737°C. The corner column C1-2 did not have a large deformation (0.194m) since the building leaned towards the heated compartment.

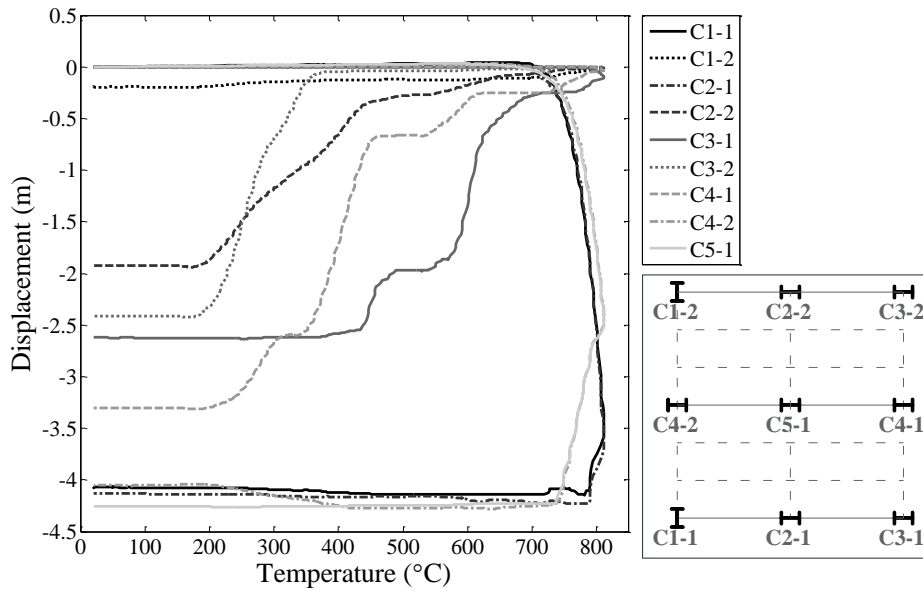


Figure 5.13 Case-7 Vertical Displacements of First Floor Columns

#### 5.7.1.8 Case-8

For Case 8 (EBF and EC3 parametric fire curve in the whole first floor), shown in Figure 5.14, a progressive collapse on the entire floors is shown to start about approximately 700°C with complete floor collapse at around 810 °C. All columns sustained the same displacement levels as expected like other whole floor fire cases.

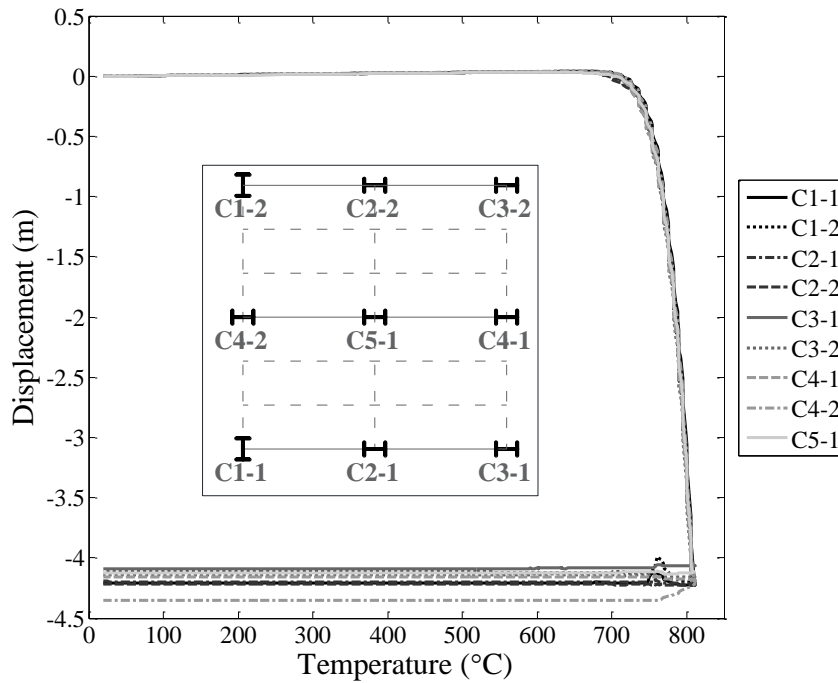


Figure 5.14 Case-8 Vertical Displacements of First Floor Columns

### 5.7.1.9 Discussion

For column vertical displacement, similar patterns are observed for cases where the fire location is the same irrespective of the time-temperature curve used. For the corner compartment fire cases, the columns in the directly heated compartments displaced downwards before other columns in the structure, causing twist of the building. For the full floor fire cases, all the first floor columns seem to move simultaneously downward as expected.

### 5.7.2 Column Axial Force

In this section, the ratio of the demand-to-capacity ratios are plotted for the columns as a function of the changing temperature. The calculations for  $\phi P_n$  followed the equations in Appendix 4 of the *2010 AISC*

*Specifications* (AISC 365-10). Following the presented plots, tables summarizing the demand-to-capacity ratios at key temperature points are presented. In the presented plots and tables, a positive value implies compressive loading while a negative value implies tensile loading.

### 5.7.2.1 Case-1

Figure 5.15 shows demand-to-capacity ratios for Case 1 (CBF and E119 in a single compartment). The ratios of  $P_u/\phi P_n$  of all columns increased at the very beginning. As  $\phi P_n$  decreased with elevated temperature,  $P_u/\phi P_n$  increased further for the compartment columns and decreased for other columns. Around 700°C, the ratios for the fire compartment columns dropped straight down, with other columns' ratios increasing to carry the extra load from the failed columns. The maximum ratio of compression was 2.176 and occurred around 823°C in column C2-1.

For Case 1, the ratios of  $P_u/\phi P_n$  at selected key temperature points, for all first floor columns, are shown in Table 5.26 below. At 600°C, only column C2-1 and C5-1 reached their capacity with a ratio larger than 1. At 700°C, columns C3-1 and C4-1 of the heated compartment reached their capacity limits.

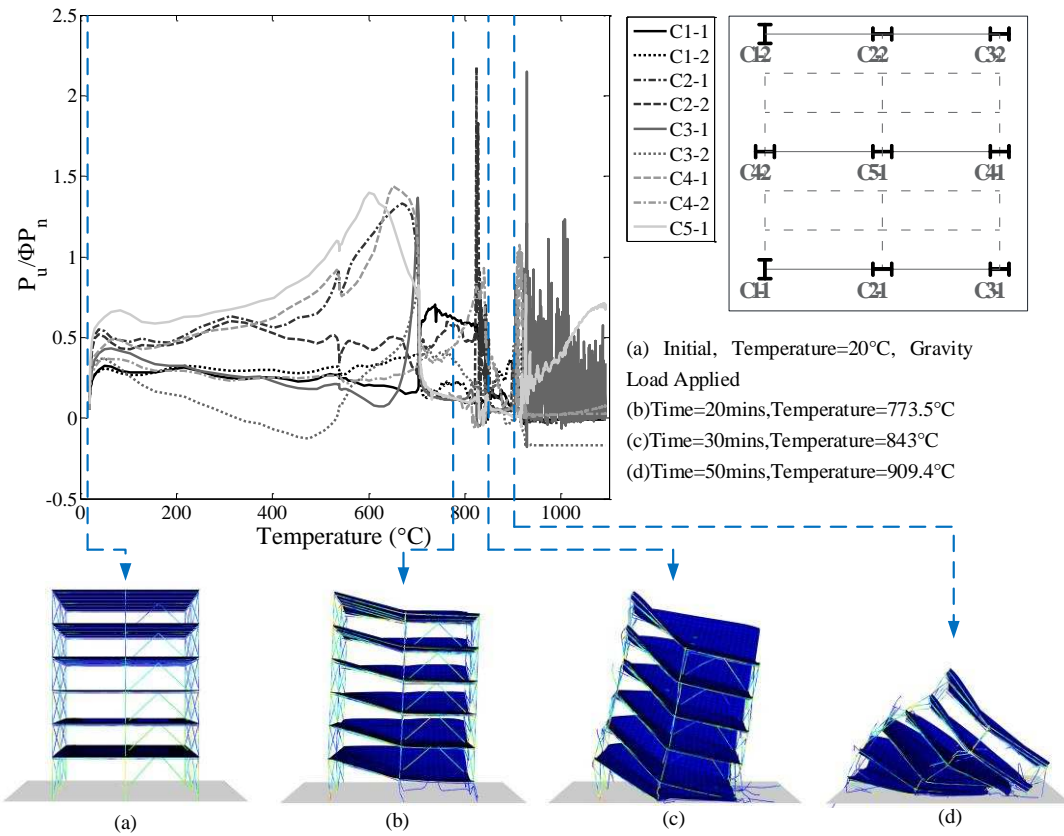


Figure 5.15 Case-1 First Floor Column Axial Forces

Table 5.26 Case-1 Ratios of  $P_u/\Phi P_n$  at Elevated Temperatures

Temperature (°C)	C1-1	C1-2	C2-1	C2-2	C3-1	C3-2	C4-1	C4-2	C5-1
20	0.0501	0.0499	0.0646	0.0646	0.0547	0.0546	0.0793	0.0533	0.0863
100	0.2835	0.2682	0.4746	0.4266	0.4038	0.2582	0.4547	0.3486	0.6429
200	0.3123	0.3223	0.5089	0.4759	0.3220	0.1353	0.4929	0.2913	0.6251
300	0.2496	0.2925	0.6307	0.5995	0.2626	0.0139	0.5560	0.2340	0.6719
400	0.252	0.301	0.5610	0.5251	0.2247	-0.0731	0.6225	0.2543	0.7444
500	0.2631	0.3066	0.6952	0.4775	0.2029	-0.0765	0.8349	0.2634	0.9896
600	0.2044	0.3216	1.1167	0.4269	0.0982	0.2913	0.9744	0.2325	1.3991
700	0.1689	0.3937	0.9727	0.2735	1.3171	0.8088	1.1542	0.3225	0.7587
800	0.5905	0.1895	0.0956	0.4806	0.1188	0.2735	0.0556	0.5788	0.1017
900	0.0743	0.3462	0.0435	0.2718	0.0569	-0.0104	0.0537	0.1566	0.0081
1000	-0.0103	0.0425	-0.0283	0.0982	0.3192	-0.1664	0.0232	0.0237	0.3993

### 5.7.2.2 Case-2

Figure 5.16 shows demand-to-capacity ratios for Case 2 (CBF and E119 in the whole floor). Since the whole floor was subjected to fire loading, the ratios of  $P_u/\phi P_n$  of all columns increased simultaneously at first half of the step. The slight difference in the numbers are due to the unsymmetrical nature of the structure. The ratios for all numbers rapidly decreased at 700 °C. All columns were in contact with the ground at about 820°C. Following that point, a spike in response was observed which was caused by the columns impacting the ground. The maximum ratio of compression occurred at 842°C in column C4-1 is 5.064. Column C1-1 had the maximum ratio of compression was 1.061 occurred at 840°C.

For Case 2, the ratios of  $P_u/\phi P_n$  for all the first floor columns at selected key temperature points are shown in Table 5.27 below. At 600°C, only centerline columns C2-1, C2-2 and C5-1 reached their ratio limit of 1. This is because of the larger tributary areas associated with these columns, which caused them to carry more loads than other columns. At 700°C, all columns of the first floor exceeded their limit as a result of the whole first floor being heated were evenly heated, which marks the onset of collapse of the entire building.

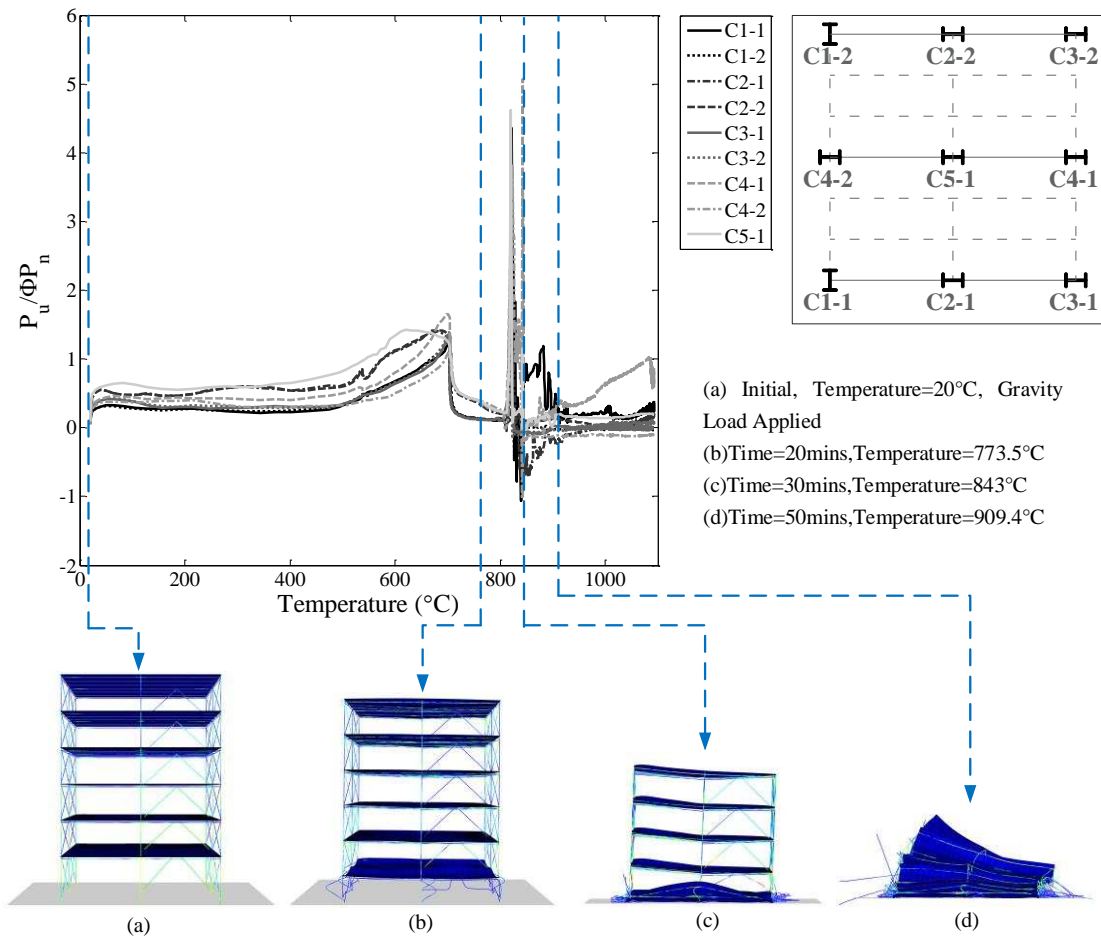


Figure 5.16 Case-2 First Floor Column Axial Forces

Table 5.27 Case-2 Ratios of  $P_u/\Phi P_n$  at Elevated Temperatures

Temperature (°C)	C1-1	C1-2	C2-1	C2-2	C3-1	C3-2	C4-1	C4-2	C5-1
20	0.0501	0.0499	0.0646	0.0646	0.0547	0.0546	0.0793	0.0533	0.0863
100	0.2958	0.2732	0.4778	0.4749	0.3780	0.3803	0.4348	0.3647	0.6220
200	0.2798	0.2726	0.4924	0.4860	0.2988	0.3224	0.4260	0.3979	0.5656
300	0.2308	0.2434	0.6019	0.6006	0.2928	0.2960	0.4113	0.3007	0.5941
400	0.2280	0.2498	0.5342	0.5356	0.3067	0.2858	0.4073	0.3032	0.6475
500	0.3493	0.3569	0.6339	0.6123	0.3680	0.3597	0.5182	0.3318	0.8571
600	0.6795	0.6679	1.1081	1.1297	0.6457	0.6622	0.8019	0.4995	1.3438
700	1.2141	1.2343	1.2815	1.3427	1.3552	1.3739	1.6518	1.0940	1.2476
800	0.1092	0.1106	0.2055	0.1391	0.1062	0.1068	0.2340	0.2601	0.2342
900	0.1821	-0.0205	-0.1463	0.1302	0.0361	-0.0330	0.2645	-0.1254	0.0392
1000	0.2119	-0.0280	0.0319	0.0229	-0.0136	0.0534	0.6426	-0.1022	0.1449

### 5.7.2.3 Case-3

Figure 5.17 shows demand-to-capacity ratios for Case 3 (EBF and E119 in a single compartment). In this case, the columns of the fire compartment started to yield around 700°C and most of the forces redistributed to column C3-1 and C4-1 as shown by the increase in their ratio. Because of the extra strength provided by the EBF, the building collapsed forward, so the first floor did not completely collapse.

For Case 3, the ratios of  $P_u/\phi P_n$  for all first floor columns at selected key temperature points are shown in Table 5.28 below. At 500°C, the center column had exceeded its ratio by approximately 4% due to its larger tributary area. At 600°C, C2-1 and C5-1 had ratios larger than 1 because the load distribution and the increase heating. Two other columns, C3-1 and C4-1, reached their ratio limits at 700°C and 800°C, respectively, because of the collapse of the fire-loaded compartment and the redistribution of the load to the columns close to it.

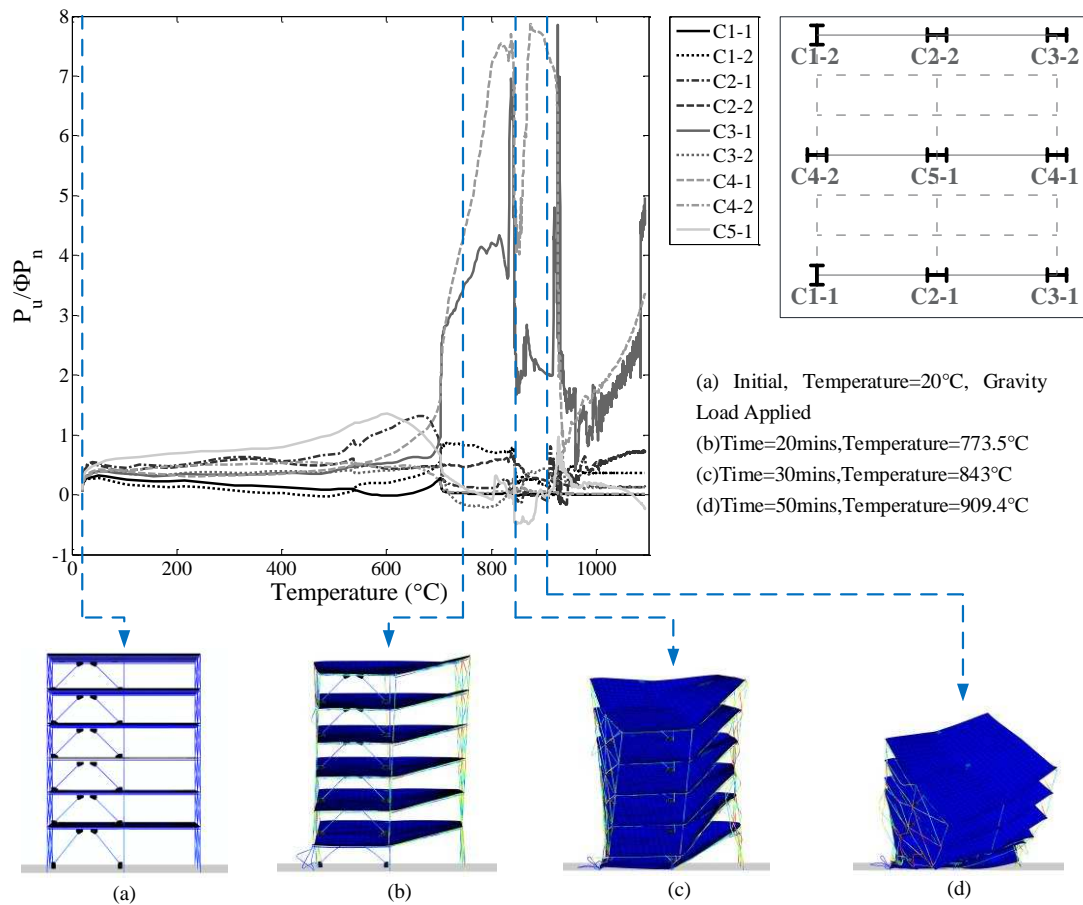


Figure 5.17 Case-3 First Floor Column Axial Forces

Table 5.28 Case-3 Ratios of  $P_u/\phi P_n$  at Elevated Temperatures

Temperature (°C)	C1-1	C1-2	C2-1	C2-2	C3-1	C3-2	C4-1	C4-2	C5-1
20	0.0500	0.0498	0.0646	0.0646	0.0528	0.0526	0.0528	0.0742	0.0787
100	0.2541	0.1740	0.4555	0.4030	0.3497	0.3519	0.3941	0.4023	0.6214
200	0.2425	0.1456	0.5046	0.4754	0.3450	0.3660	0.3094	0.4816	0.6957
300	0.1610	0.0670	0.6289	0.5934	0.3311	0.3675	0.3221	0.5049	0.7467
400	0.1330	0.0221	0.5625	0.5290	0.3649	0.3984	0.3512	0.5263	0.7929
500	0.0919	0.0020	0.6860	0.5167	0.4149	0.3936	0.4452	0.5203	1.0440
600	-0.0173	0.1995	1.0942	0.4405	0.5262	0.4009	0.6525	0.4599	1.3650
700	0.2687	0.5291	0.8963	0.4543	0.9116	0.4751	1.5300	0.2269	0.6906
800	0.0139	0.7111	0.1133	0.5649	4.2206	-0.1988	7.2000	0.0263	-0.0784
900	0.0124	0.1680	-0.0739	0.2492	2.0634	0.4348	7.6560	0.0521	-0.0166
1000	0.0060	0.3683	0.5420	0.1284	1.4235	0.1188	1.7552	0.0140	0.1783

#### 5.7.2.4 Case-4

Figure 5.18 shows demand-to-capacity ratios for Case 4 (EBF and E119 in the whole floor). For this case, same as Case-2, all columns excessively buckled around 700 °C with full collapse of the first floor around 820°C. The extreme tension in columns C4-2 and C5-1 was due to the bending of the lower gusset plate, which was fully welded to them.

For Case 4, the ratios of  $P_u/\phi P_n$  for all first floor columns at selected key temperature points are shown in Table 5.29 below. At 600°C, the centerline columns, C2-1, C2-2 and C5-1, had already reached their load capacity. When the fire temperature increased to 700°C, all first floor columns failed at this point. With the increased temperature, columns C4-2 and C5-1 were subjected to tension because of the large bending in the gusset plates welded to them.

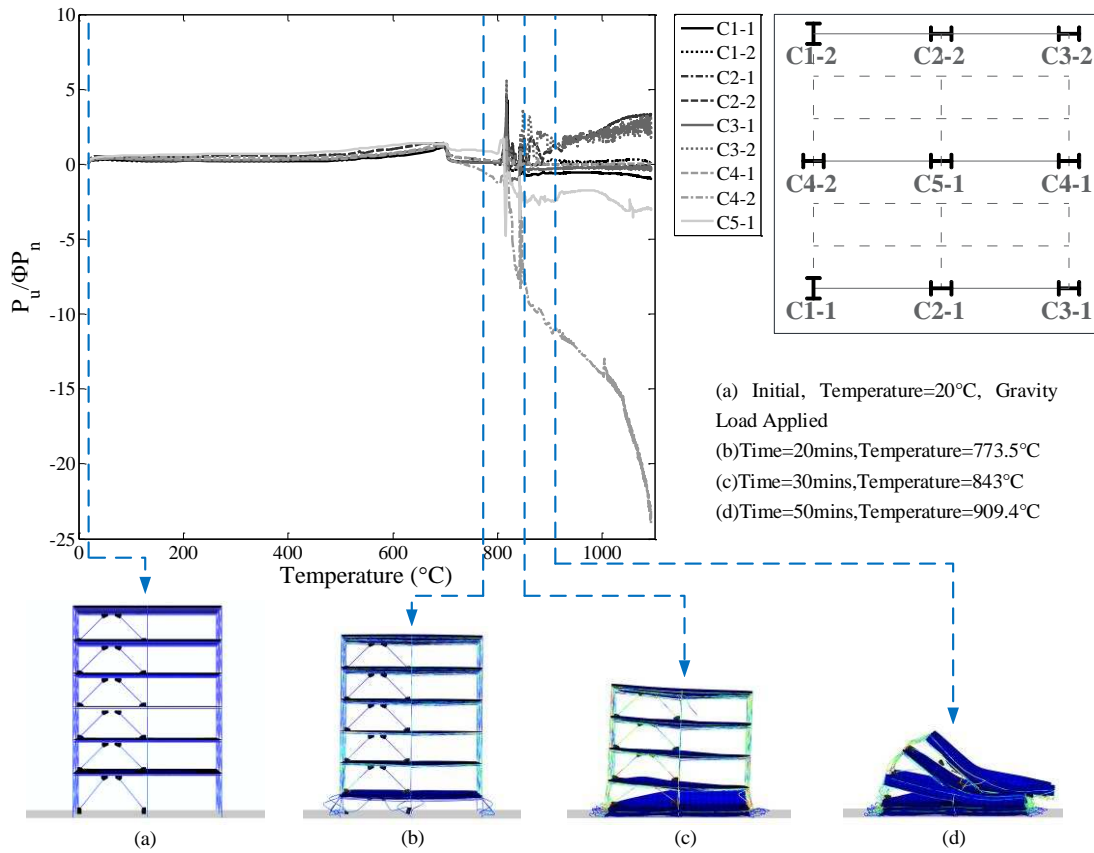


Figure 5.18 Case-4 First Floor Column Axial Forces

Table 5.29 Case-4 Ratios of  $P_u / \phi P_n$  at Elevated Temperatures

Temperature (°C)	C1-1	C1-2	C2-1	C2-2	C3-1	C3-2	C4-1	C4-2	C5-1
20	0.0500	0.0498	0.0646	0.0646	0.0528	0.0526	0.0528	0.0742	0.0787
100	0.2376	0.2157	0.4580	0.4508	0.3147	0.3162	0.3561	0.4058	0.5792
200	0.2454	0.2461	0.4866	0.4805	0.2658	0.2783	0.3292	0.4840	0.6534
300	0.1970	0.2183	0.6001	0.6082	0.2553	0.2633	0.3313	0.4533	0.6724
400	0.2007	0.2228	0.5189	0.5330	0.2971	0.2865	0.3310	0.4394	0.7116
500	0.2884	0.2866	0.6410	0.6430	0.4074	0.3822	0.3927	0.5468	0.9232
600	0.5465	0.5511	1.0344	1.0198	0.7029	0.6829	0.6753	0.7717	1.2772
700	1.2520	1.2561	1.2921	1.0223	1.3252	1.3233	1.2135	1.4167	1.3474
800	0.1129	0.1211	0.2183	-0.0191	0.1050	0.2372	0.2132	-1.2314	0.7690
900	-0.5725	0.2994	0.0072	0.7410	-0.3205	0.8941	-0.0122	-10.7944	-2.4113
1000	-0.5892	0.1833	-0.0204	2.3111	-0.2219	2.1695	0.0113	-14.0869	-1.9617

### 5.7.2.5 Case-5

Figure 5.19 shows demand-to-capacity ratios for Case 5 (CBF and EC3 parametric fire curve in a single compartment). In this case, the values for all fire compartment columns increase 700°C then started to decrease. During the cooling phase, the ratios for the columns were shown to remain constant, which implies that energy from the collapse was absorbed by other floors.

For Case 5, the ratios of  $P_u/\phi P_n$  for all first floor columns at selected key temperature points are shown in Table 5.30 below. At 600°C, three of the four fire-loaded compartment columns had already reach their limits, which led to collapse of the whole building. Column C3-2 had several negative values as shown in the table, which means the column was under tension instead of compression, this was caused by the sway of the building during the collapse.

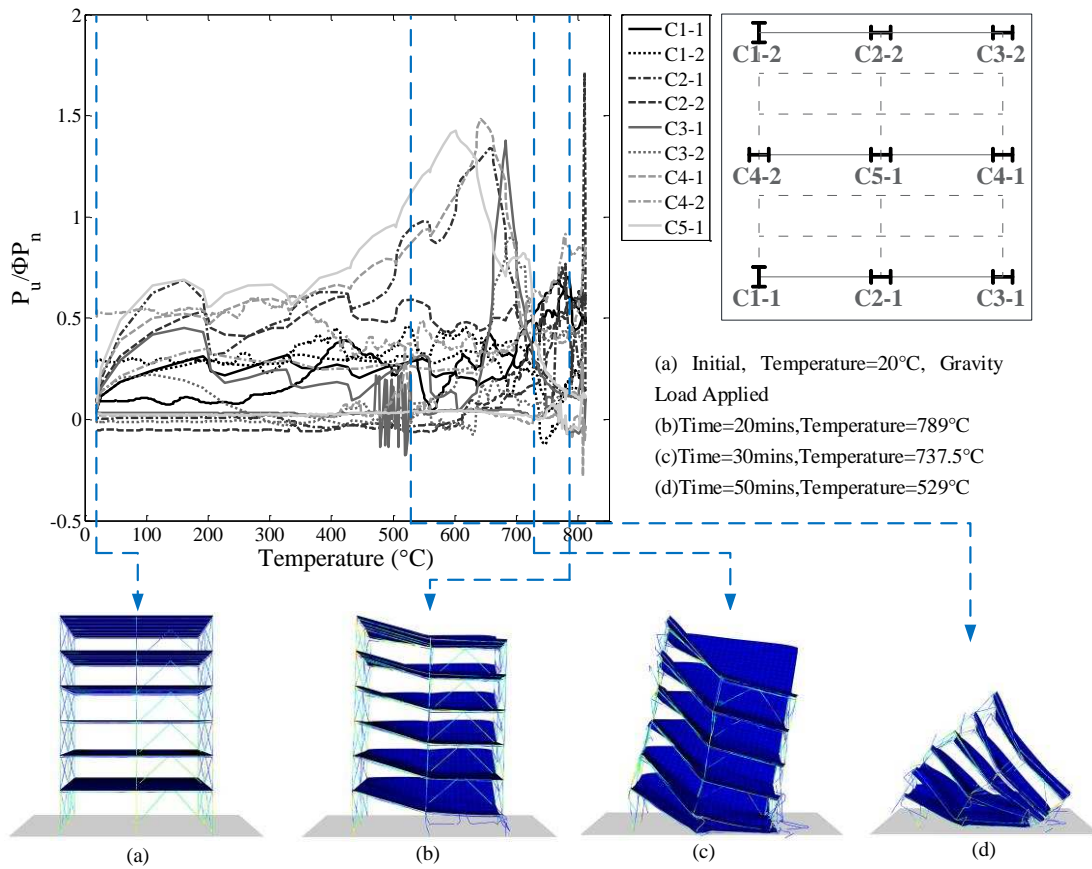


Figure 5.19 Case-5 First Floor Column Axial Forces

Table 5.30 Case-5 Ratios of  $P_u / \phi P_n$  at Elevated Temperatures

Temperature (°C)	C1-1	C1-2	C2-1	C2-2	C3-1	C3-2	C4-1	C4-2	C5-1
20	0.0501	0.0499	0.0646	0.0646	0.0547	0.0546	0.0793	0.0533	0.0863
100	0.2437	0.2368	0.6233	0.4298	0.4208	0.2230	0.4996	0.2808	0.6614
200	0.2933	0.3041	0.4255	0.5151	0.3501	0.1372	0.4685	0.3520	0.5533
300	0.2942	0.2737	0.4685	0.4525	0.2406	-0.0164	0.5943	0.2815	0.6672
400	0.2708	0.2944	0.6278	0.6043	0.1841	-0.0168	0.6649	0.2520	0.7213
500	0.2667	0.2879	0.6984	0.4897	0.2464	-0.0108	0.7899	0.2677	0.9617
600	0.2310	0.3145	1.0268	0.4429	0.1270	0.1681	1.1052	0.2513	1.4246
700	0.3728	0.3698	0.5572	0.5269	0.7506	0.8217	0.6900	0.3890	0.7963
800	0.5535	0.2362	0.1045	0.6207	0.1226	0.4258	0.1088	0.5502	0.1083

### 5.7.2.6 Case-6

Figure 5.20 shows demand-to-capacity ratios for Case 6 (CBF and EC3 parametric fire curve in the whole first floor). This case was the same as the other full floor fire cases. The axial load ratio for all columns decreased around 700°C and floor failure occurred after 800°C. In the cooling phase, the curves showed some random oscillations because the columns were still absorbing energy.

For Case 6, the ratios of  $P_u/\phi P_n$  for all first floor columns at selected key temperature points are shown in Table 5.31 below. The center columns, C2-1 and C5-1, had ratios larger than 1 at 600°C because of their associated larger tributary areas. At 700°C, most columns had their ratio exceed one.

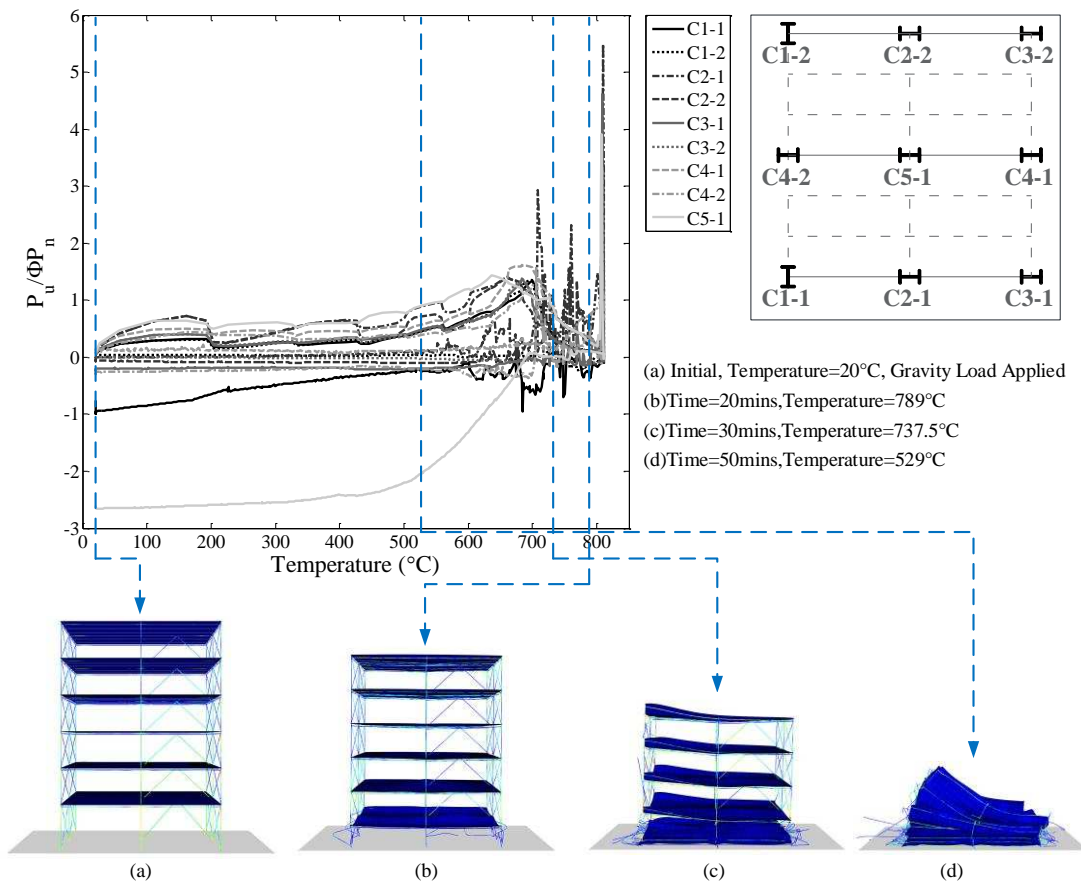


Figure 5.20 Case-6 First Floor Column Axial Forces

Table 5.31 Case-6 Ratios of  $P_u/\phi P_n$  at Elevated Temperatures

Temperature (°C)	C1-1	C1-2	C2-1	C2-2	C3-1	C3-2	C4-1	C4-2	C5-1
20	0.0501	0.0499	0.0646	0.0646	0.0547	0.0546	0.0793	0.0533	0.0863
100	0.2960	0.2967	0.6292	0.6295	0.3901	0.3909	0.4891	0.3457	0.6469
200	0.2641	0.2301	0.4200	0.4177	0.3099	0.3053	0.4352	0.3985	0.5081
300	0.2586	0.2503	0.4514	0.4330	0.2458	0.2707	0.4571	0.3780	0.6063
400	0.2671	0.2987	0.6556	0.6351	0.3511	0.3252	0.4606	0.3458	0.6043
500	0.3717	0.3995	0.6895	0.4824	0.3983	0.3607	0.5277	0.3891	0.7866
600	0.6699	0.6391	1.0134	0.6888	0.6472	0.6718	0.8059	0.5273	1.2021
700	1.3208	1.2933	0.6859	1.0559	0.9092	0.8904	1.5338	1.2752	1.0524
800	0.1281	0.1233	0.1065	0.2343	0.2190	0.1140	0.2309	0.2522	0.2063

### 5.7.2.7 Case-7

Figure 5.21 shows demand-to-capacity ratios for Case 7 (EBF and EC3 parametric fire curve in a single compartment). In this case, the response was similar to that of Case-3 despite the difference in the fire temperature curve. The maximum ratio of compression occurred at 805°C in column C4-1 is 7.412. The ratios of compression were relatively small and close to each other.

For Case 7, the ratios of  $P_u/\phi P_n$  for all first floor columns at selected key temperature points are shown in Table 5.32 below. Column C5-1 was the first columns to fail in this case at 500°C. Columns C5-1 is the center column with the largest tributary area. At 600°C, only columns C2-1 and C5-1 reached their load capacity limits. Other columns, C3-1 and C4-1, far exceeded their limit at 700°C, which was caused by load redistribution of the failed compartment columns.

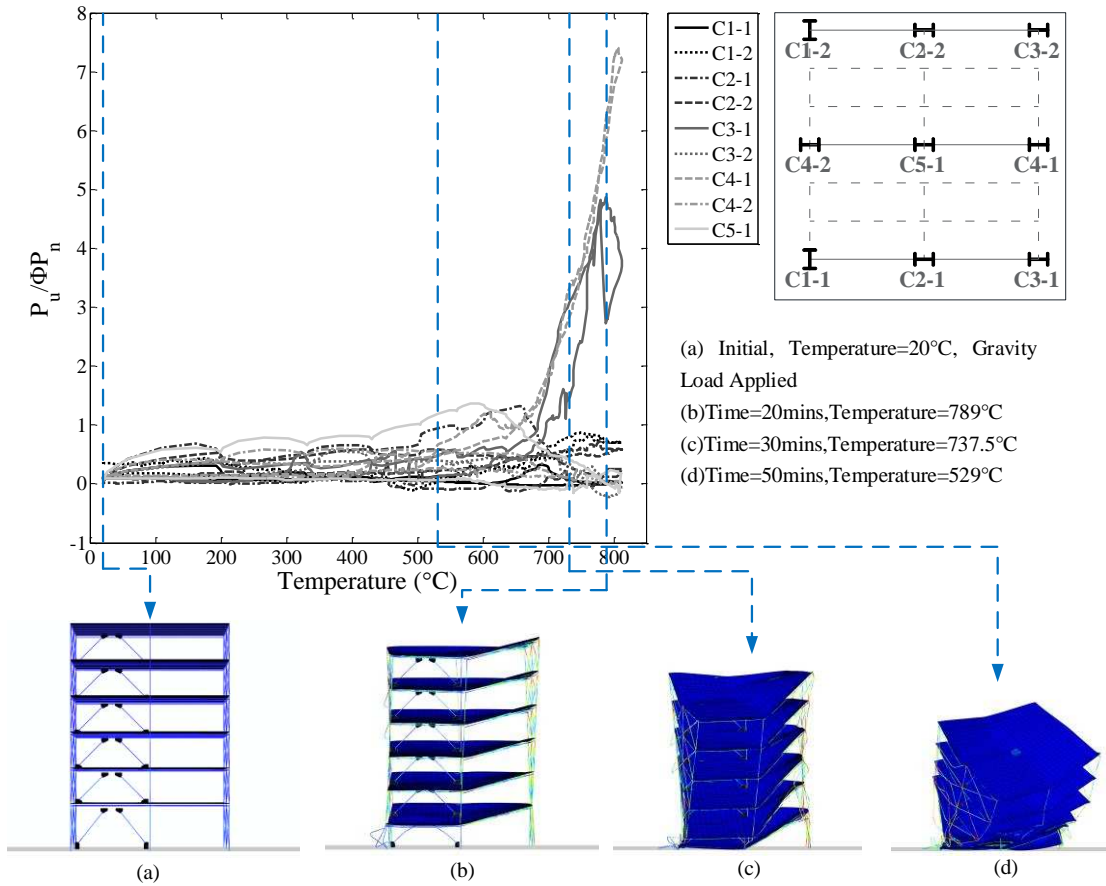


Figure 5.21 Case-7 First Floor Column Axial Forces

Table 5.32 Case-7 Ratios of  $P_u / \phi P_n$  at Elevated Temperatures

Temperature (°C)	C1-1	C1-2	C2-1	C2-2	C3-1	C3-2	C4-1	C4-2	C5-1
20	0.0500	0.0498	0.0646	0.0646	0.0528	0.0526	0.0528	0.0742	0.0787
100	0.2951	0.1791	0.6195	0.4252	0.2909	0.2797	0.2904	0.4045	0.5842
200	0.2403	0.1005	0.4137	0.4945	0.3548	0.3861	0.4026	0.3784	0.5390
300	0.1927	0.0334	0.4845	0.4312	0.3328	0.3350	0.3349	0.5668	0.7693
400	0.1238	0.0736	0.6565	0.5843	0.3657	0.3755	0.3374	0.5779	0.8158
500	0.1286	0.0461	0.6768	0.4994	0.4272	0.3775	0.4455	0.5520	1.0216
600	0.0307	0.1903	1.0730	0.4903	0.6307	0.4223	0.7296	0.5082	1.3311
700	0.2332	0.6227	0.5605	0.5123	1.8601	0.4768	1.9568	0.1930	0.5125
800	0.0143	0.7071	0.1186	0.5632	4.5317	-0.1829	7.2448	0.0274	-0.0613

### 5.7.2.8 Case-8

Figure 5.22 shows demand-to-capacity ratios for Case 8 (EBF and EC3 parametric fire curve in the whole first floor). The response of the columns in this case was similar to that of Case-4 even though the fire curve included a cooling phase. As previously indicated, the tension in columns C4-2 and C5-1 was caused by deformation in the welded gusset plate.

For Case 8, the ratios of  $P_u/\phi P_n$  for all first floor columns at selected key temperature points are shown in Table 5.33 below. The ratios for the centerline columns C2-1, C2-2 and C5-1 exceeded a value of one at 600°C as expected. At 700°C, all columns exceeded their ratio limits, then the collapse of the building began.

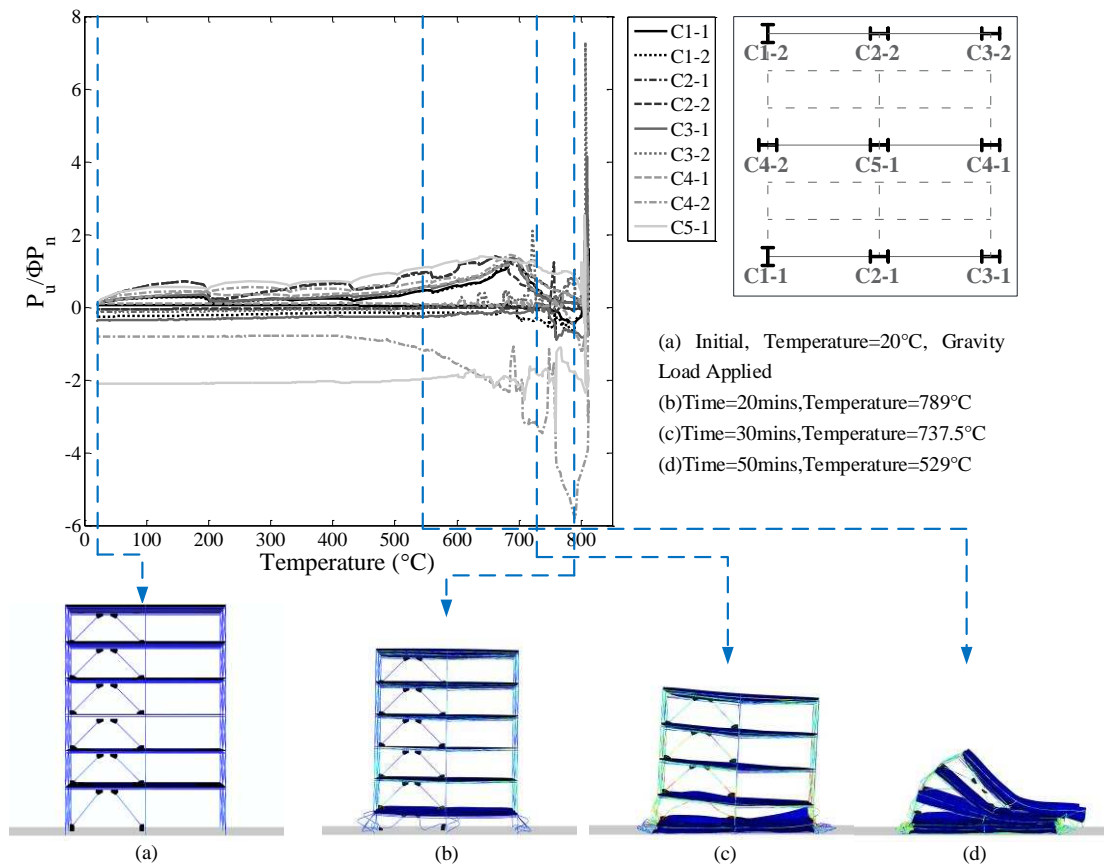


Figure 5.22 Case-8 First Floor Column Axial Forces

Table 5.33 Case-8 Ratios of  $P_u / \phi P_n$  at Elevated Temperatures

Temperature (°C)	C1-1	C1-2	C2-1	C2-2	C3-1	C3-2	C4-1	C4-2	C5-1
20	0.0500	0.0498	0.0646	0.0646	0.0528	0.0526	0.0528	0.0742	0.0787
100	0.2746	0.2720	0.6241	0.6236	0.3042	0.3058	0.3060	0.4287	0.5511
200	0.2236	0.1922	0.4082	0.4067	0.2799	0.2750	0.4109	0.3805	0.4841
300	0.2365	0.2236	0.4635	0.4544	0.2204	0.2339	0.3443	0.5265	0.6996
400	0.2383	0.2616	0.6550	0.6618	0.3075	0.3105	0.3709	0.5022	0.7194
500	0.3079	0.3341	0.6674	0.6632	0.4035	0.4032	0.4393	0.5969	0.9242
600	0.6027	0.5686	1.0286	1.0358	0.7200	0.7296	0.7141	0.8240	1.2799
700	1.2628	1.2594	1.0446	0.6702	1.0499	1.0587	1.3594	1.2625	1.2487
800	0.1129	0.1189	0.2051	-0.0537	0.1053	0.3033	0.2176	-1.1720	0.4274

### 5.7.2.9 Discussion

In this section, plots of demand-to-capacity ratio for all first floor columns for all eight cases were presented. The response is typically governed by three main characteristic responses; namely 1) loss of strength of the columns with larger tributary areas; 2) load shedding to other columns that ultimately lose their strength together; and 3) large inelastic deformation of all columns that lead to floor collapse. In addition, the difference in performance between the of EBF and CBF frames is due to the presence of the gusset plates in the EBF frames, which caused large forces to develop. In addition to the plots, tables were provided summarizing the demand-to-capacity ratios at different key temperatures. In general, the analyses shows that failure typically starts in columns with larger tributary areas then spread to other columns due to load shedding. For the corner bay fire case, when the fire-loaded compartment collapsed, the load was redistributed to the columns close to it, which also caused column over load.

### 5.7.3 Column End Moment Diagram

First floor columns' strong- and weak-axis end moments were captured from the models as mentioned before and used to plot demand-to-capacity ratios. The calculation of  $\phi M_n$  followed the equations in Appendix 4 of the *2010 AISC Specifications* (AISC 365-10). Screenshots for moment frame B, which is shown in the building plan view of Figure 3.1, were selected to highlight frame deformations at various points. Specifically, Figure 5.23-5.30 (a), (b), (c) were used for the screenshots of frame B from time 20 min, 40 min, and 50 min, respectively, of the step time sequence. In addition, tables are presented with summary of the calculated demand-to-capacity ratios at key temperature points for both strong- and weak-axis end moments.

### 5.7.3.1 Case-1

For Case 1 (CBF and E119 in a single compartment), shown in Figure 5.23, the absolute value of the ratios increased for the columns about both the x- and y-axis. The positive values imply negative moment while the negative values imply positive moment. The change in signs for some columns during the response is due to the fact that through initial heating and because of the unsymmetrical nature of the loading and the structural configuration, the columns in the compartment are bending in one direction (i.e. columns expanding causing end rotation in one direction due to unsymmetrical loading). This direction is reversed when the columns lose their strength and are dragged down during collapse.

Table 5.34 and 5.35 show the ratios of columns' end moments at selected temperature points for the x-axis and y-axis. At 500°C, the value of column C3-1 had already exceeded one about the x-axis. The ratios did not exceed one for other columns until a temperature of about 900°C. This implies that bending about the x-axis was not very critical in this case. Instead, as shown in the table, bending about the y-axis was more critical as various ratios had already exceeded one at 800°C. This is expected as the building was leaning forward during the collapse process.

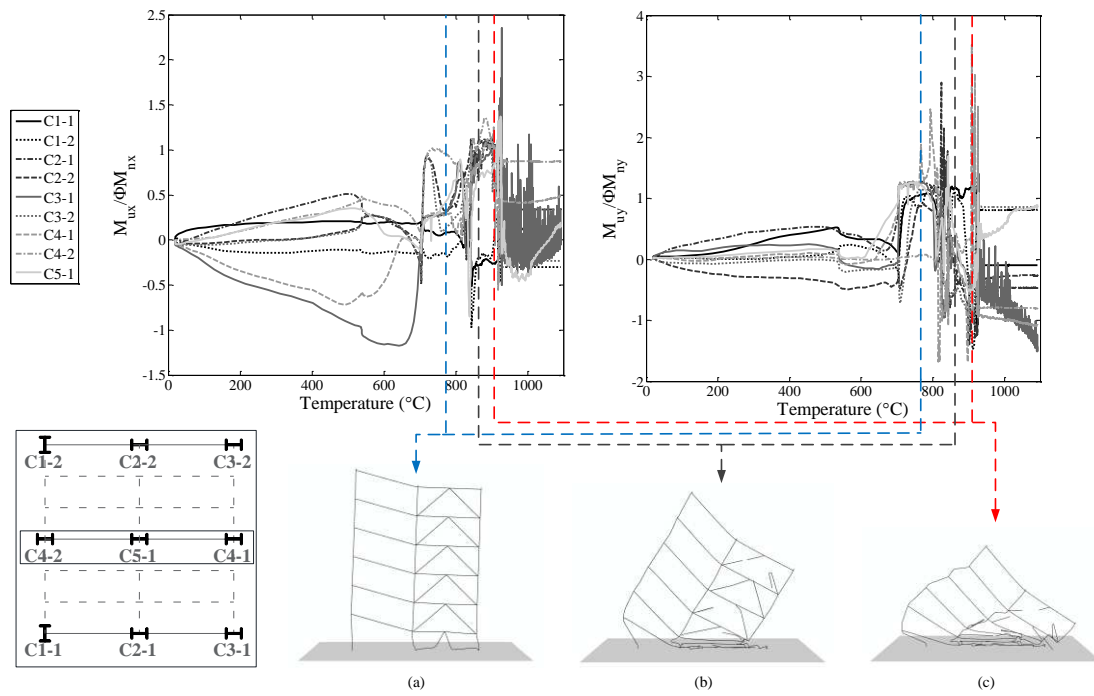


Figure 5.23 Case-1 First Floor Column End Moment

Table 5.34 Case-1 Ratios of  $M_{ux}/\phi M_{nx}$  at Elevated Temperature

Temperature (°C)	C1-1	C1-2	C2-1	C2-2	C3-1	C3-2	C4-1	C4-2	C5-1
20	0.0001	-0.0001	0.0000	0.0000	-0.0052	-0.0052	-0.0051	0.0055	0.0000
100	0.1423	-0.0838	0.0751	-0.0379	-0.2587	-0.0514	-0.1721	0.0256	0.0136
200	0.1793	-0.1333	0.2220	-0.0032	-0.4844	-0.0250	-0.3631	0.1092	0.1154
300	0.1908	-0.1438	0.3337	0.0027	-0.5928	-0.0029	-0.4734	0.2103	0.1995
400	0.2027	-0.1200	0.4189	0.0322	-0.7016	0.0259	-0.5568	0.2829	0.2563
500	0.2069	-0.1139	0.5115	0.1095	-0.9287	0.0887	-0.6969	0.3908	0.3533
600	0.1969	-0.1346	0.2448	0.2477	-1.1583	0.2459	-0.4661	0.3934	0.0733
700	0.1950	-0.1268	-0.0302	-0.2480	-0.1184	-0.2166	-0.0056	0.0928	-0.1121
800	0.0787	-0.0811	0.3659	0.5605	0.5604	0.2600	0.0855	0.8336	0.6676
900	-0.2571	-0.1852	1.1277	0.9966	0.9939	0.9881	1.1618	1.1021	0.7526
1000	-0.0895	-0.3017	0.0841	0.3375	0.1122	-0.2349	0.4134	0.8732	-0.3840

Table 5.35 Case-1 Ratios of  $M_{uy}/\phi M_{ny}$  at Elevated Temperature

Temperature (°C)	C1-1	C1-2	C2-1	C2-2	C3-1	C3-2	C4-1	C4-2	C5-1
20	0.0056	0.0056	0.0029	-0.0029	0.0005	-0.0003	-0.0001	0.0000	0.0000
100	0.0561	0.0258	0.2259	-0.1582	0.1450	-0.0655	-0.0105	0.0249	0.0365
200	0.1260	0.0009	0.3497	-0.2517	0.1970	-0.0673	0.0107	0.0207	0.0651
300	0.2728	0.0093	0.4479	-0.2864	0.2327	-0.0377	0.0565	0.0151	0.1109
400	0.4008	0.0399	0.5021	-0.3080	0.2282	-0.0103	0.0811	0.0357	0.1414
500	0.4984	0.0980	0.5189	-0.3699	0.2022	-0.0106	0.0877	0.0313	0.1630
600	0.3272	0.2040	0.3591	-0.4592	-0.1372	-0.1729	-0.0578	-0.0024	0.0104
700	0.1180	-0.1698	0.6683	-0.3741	-0.0616	-0.1460	0.7587	0.0169	0.9193
800	0.9930	1.1748	1.0744	0.7797	0.8670	1.1154	1.8105	0.0048	0.9210
900	1.1455	-0.4658	-0.3811	-1.3248	-0.2678	-0.8606	-0.7296	0.3265	-0.5197
1000	-0.0999	0.8111	-0.2777	-0.4703	-0.6488	0.8607	-0.9817	-0.7932	0.5761

### 5.7.3.2 Case-2

For Case 2 (CBF and E119 in the whole floor), the ratios are shown in Figure 5.24. As previously indicated the change in signs for some columns during the response is due to the fact that the columns in the compartment are bending in one direction during initial and bending in another direction during collapse. Although the heating is uniform, the bending is due to the unsymmetrical nature of the structure because of the presence of the bracing only in one bay.

Table 5.36 and 5.37 summaries the ratios of columns' end moments at selected temperature points for the x-axis and y-axis. Column C4-2 was the first to reach its flexure capacity about the x-axis at 400°C. This is because it is located in the left end of the left bay and therefore is undergoing the largest moment during heating. The moment, as indicated previously, is due to the structure being unsymmetrical although the heating is. Although columns C1-1 and C1-2 are also located in the left end of the left bays, they did not

reach their ratio limit about the x-axis due to their orientation. Instead, they were the first to reach their limit about the y-axis as expected, which was at 500°C.

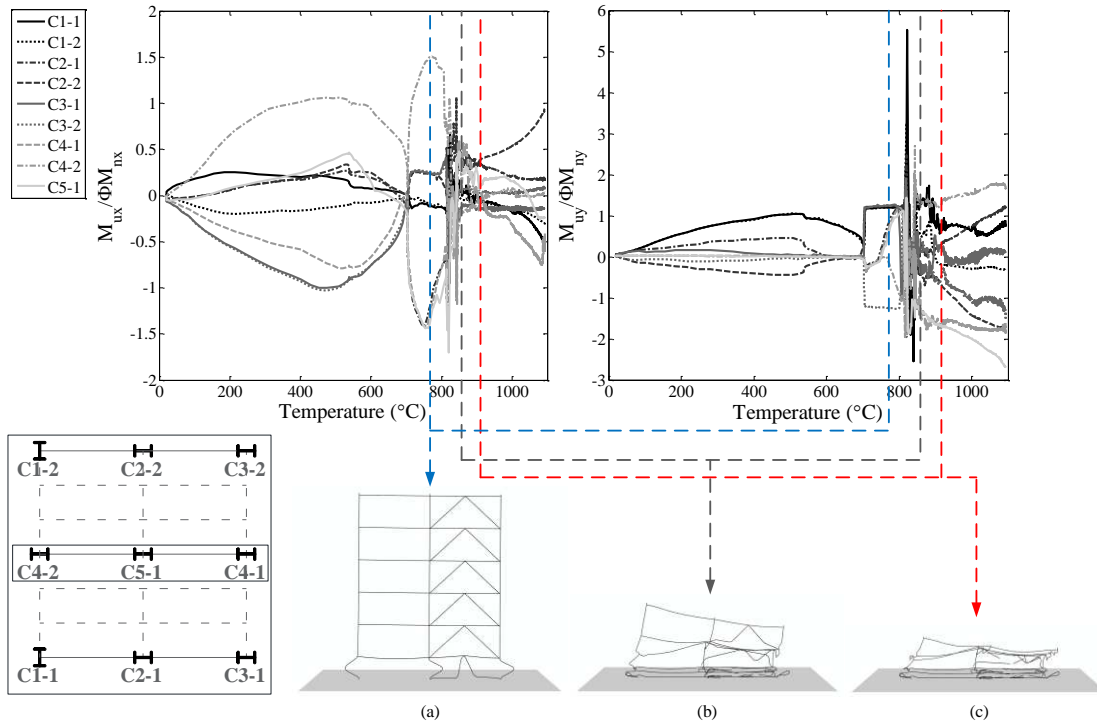


Figure 5.24 Case-2 First Floor Column End Moment

Table 5.36 Case-2 Ratios of  $M_{ux}/\phi M_{nx}$  at Elevated Temperature

Temperature (°C)	C1-1	C1-2	C2-1	C2-2	C3-1	C3-2	C4-1	C4-2	C5-1
20	0.0001	-0.0001	0.0000	0.0000	-0.0052	-0.0052	-0.0051	0.0055	0.0000
100	0.1817	-0.1179	-0.0132	-0.0109	-0.3000	-0.3038	-0.1939	0.2466	-0.0271
200	0.2504	-0.1994	0.0733	0.0797	-0.5725	-0.5843	-0.3887	0.7022	0.0941
300	0.2223	-0.1743	0.1390	0.1431	-0.7672	-0.7895	-0.5078	0.9388	0.1725
400	0.2035	-0.1623	0.1724	0.1848	-0.9060	-0.9306	-0.5870	1.0120	0.2458
500	0.1862	-0.1151	0.2550	0.3074	-0.9820	-1.0029	-0.7853	1.0606	0.4153
600	0.0745	-0.0780	0.1937	0.2427	-0.7544	-0.7531	-0.6585	0.9324	0.1384
700	0.0174	-0.0297	-0.1399	0.0113	-0.0722	-0.0624	0.0110	0.3864	-0.1731
800	-0.1277	-0.1212	-0.7733	0.1683	0.2905	0.2574	-0.7819	1.3725	-1.0762
900	-0.0077	-0.0601	0.3105	0.3400	-0.1489	0.0308	0.0348	-0.0547	0.2737
1000	-0.1699	-0.1402	0.2123	0.5336	-0.1332	0.0238	-0.3248	0.0717	0.1554

Table 5.37 Case-2 Ratios of  $M_{uy}/\phi M_{ny}$  at Elevated Temperature

Temperature (°C)	C1-1	C1-2	C2-1	C2-2	C3-1	C3-2	C4-1	C4-2	C5-1
20	0.0056	0.0056	0.0029	-0.0029	0.0005	-0.0003	-0.0001	0.0000	0.0000
100	0.2740	0.2743	0.1809	-0.1481	0.1171	-0.0569	0.0275	0.0273	0.0234
200	0.6000	0.6006	0.2803	-0.2516	0.1677	-0.1103	0.0260	0.0188	0.0273
300	0.8079	0.8055	0.3822	-0.3423	0.1440	-0.1013	0.0276	0.0143	0.0208
400	0.9144	0.9067	0.4254	-0.3980	0.0785	-0.0772	0.0178	0.0233	0.0169
500	1.0422	1.0529	0.4505	-0.4358	0.0408	-0.0361	0.0092	0.0186	0.0077
600	0.8600	0.8706	0.0280	-0.0922	0.0250	-0.0130	0.0004	0.0131	-0.0075
700	0.3264	0.3013	-0.0470	0.2072	0.0014	-0.0043	-0.0451	0.0150	-0.0590
800	1.2182	1.2301	1.2334	1.1821	0.7781	-1.2518	1.1919	-0.9264	1.0493
900	0.7266	-0.0375	0.2327	-0.4884	0.4414	-0.5584	-1.6264	1.2998	-1.6527
1000	0.6429	-0.2945	0.7524	-1.4243	0.0264	-1.0798	-1.7317	1.5428	-1.9913

### 5.7.3.3 Case-3

For Case 3 (EBF and E119 in a single compartment), shown in Figure 5.25, similar response is observed where the values change from positive to negative. Similar to the axial load response, the gusset plates of the EBF imposed additional demand on the columns, causing the moment ratios to exceed one about the x-axis at an early loading stage (300°C). Bending about y-axis did not control until higher temperatures were reached.

Table 5.38 and 5.39 show the ratios of columns' end moment at selected temperature points for the x-axis and y-axis. Large end moments of column C4-1 and C5-1 of their strong axis can be observed at 300°C, where the values were just over one, which was again expected because of the additional demand imposed by the gusset plates as they further bent the gussets as a result of bending in the braces. Columns C2-1, C3-1, and C5-1 were the first to exceed their ratio about the y-axis as expected. This occurred, however, at

800°C, which implies that the response was dominated first by x-axis bending until a later stage of loading

where the y-axis response played a noticeable role.

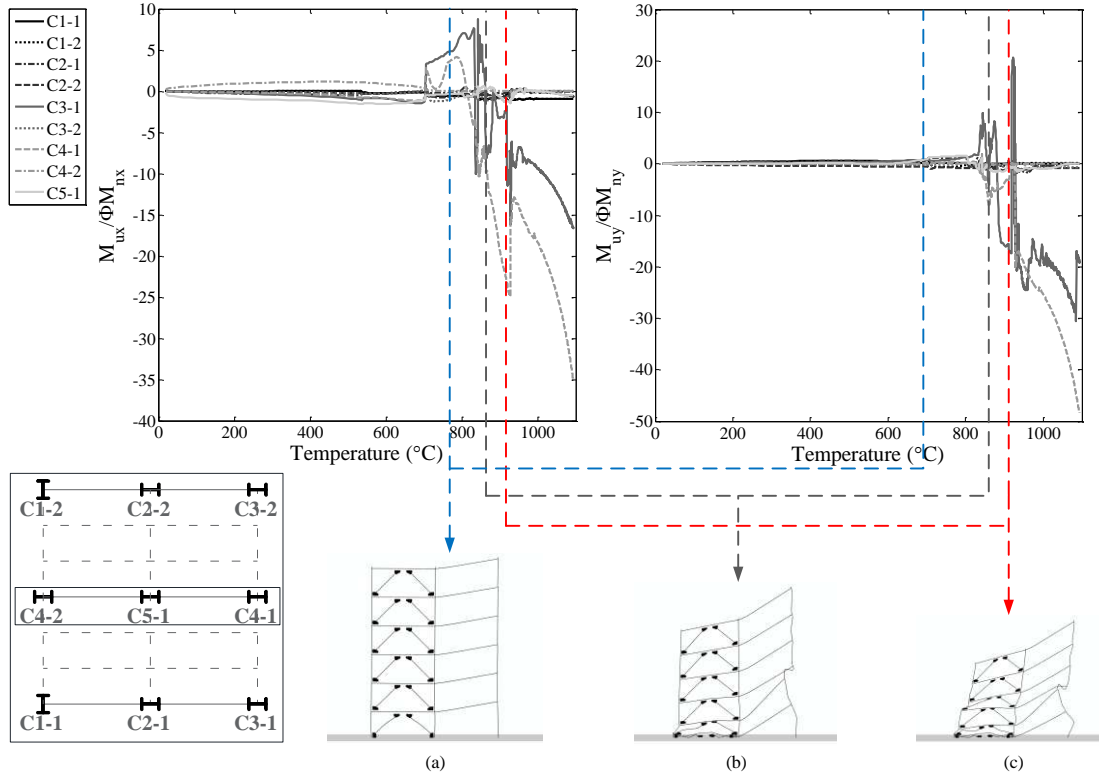


Figure 5.25 Case-3 First Floor Column End Moment

Table 5.38 Case-3 Ratios of  $M_{ux}/\phi M_{nx}$  at Elevated Temperature

Temperature (°C)	C1-1	C1-2	C2-1	C2-2	C3-1	C3-2	C4-1	C4-2	C5-1
20	0.0025	-0.0025	0.0000	0.0000	-0.0053	-0.0053	-0.0054	0.0954	-0.0963
100	0.2093	-0.0729	-0.1399	-0.0309	-0.1033	-0.0537	-0.0756	0.6660	-0.8085
200	0.3348	-0.0510	-0.2785	-0.0505	-0.2488	-0.0773	-0.1559	0.9396	-0.9338
300	0.3746	0.0121	-0.3533	-0.0755	-0.4170	-0.1012	-0.2488	1.0690	-1.0366
400	0.3653	0.0551	-0.4068	-0.1322	-0.5555	-0.1480	-0.3580	1.1549	-1.1292
500	0.2589	0.0604	-0.4817	-0.2184	-0.8811	-0.2341	-0.6290	1.1091	-1.4437
600	-0.0389	-0.2002	-0.2071	-0.2645	-0.9010	-0.2761	-0.8390	0.8757	-1.5266
700	0.0042	-0.1451	0.0295	0.1120	-1.2492	0.1063	-0.7161	0.3994	-1.0585
800	-0.0412	-0.5295	0.2212	-0.2916	6.9788	-0.4903	3.1568	-0.0101	-0.2847
900	-0.0171	-0.7092	-0.8400	-0.2485	-3.2529	-0.8331	-19.4819	0.0555	-0.6802
1000	-0.0048	-0.9062	-0.1299	-0.0347	-9.3829	0.0006	-18.4152	0.0488	0.0556

Table 5.39 Case-3 Ratios of  $M_{uy}/\phi M_{ny}$  at Elevated Temperature

Temperature (°C)	C1-1	C1-2	C2-1	C2-2	C3-1	C3-2	C4-1	C4-2	C5-1
20	0.0055	0.0055	0.0033	-0.0033	0.0068	-0.0066	-0.0001	0.0000	0.0000
100	0.2162	0.0277	0.2506	-0.1584	0.1546	-0.0845	0.0107	0.0046	0.0330
200	0.3857	-0.0232	0.4175	-0.2814	0.2429	-0.1303	0.0211	0.0025	0.0571
300	0.4770	-0.0475	0.4790	-0.3264	0.2449	-0.1545	0.0063	0.0124	0.0870
400	0.5694	-0.0770	0.5259	-0.3727	0.2373	-0.1737	0.0197	-0.0004	0.1166
500	0.5858	-0.1427	0.5506	-0.4144	0.3050	-0.1715	0.0737	-0.0135	0.1088
600	0.4572	-0.1968	0.3777	-0.5299	0.5228	-0.1727	-0.0007	-0.0659	0.0150
700	0.0846	0.0921	0.7535	-0.5234	0.8724	-0.2087	0.0095	0.1901	0.9270
800	0.1309	-0.2783	1.1345	-0.7531	1.2681	0.0745	0.1465	0.2132	1.6020
900	0.0079	-0.4431	-0.0701	-1.1588	-15.8599	-0.5031	-3.5975	0.0043	-1.3528
1000	0.0120	0.1366	-0.3129	-0.6820	-18.7610	-0.6075	-25.3910	-0.0243	-0.8998

#### 5.7.3.4 Case-4

For Case 4 (EBF and E119 in the whole floor), shown in Figure 5.26, the response is very similar to that of Case-2 despite the difference in frame types. In addition, because an EBF is used in Case 4, similar to Case-3, the first floor gusset plates also caused large end moments to develop in C4-2 and C5-1 about the x-axis at lower temperatures. At higher temperatures, the response about the y-axis for other columns started to dominate.

Table 5.40 and 5.41 show the ratios of columns' end moment at selected temperature points for the x-axis and y-axis. Columns C4-1 and C5-1 reached their load capacity at rather low temperature of approximately 300°C. At 800°C, other columns started to experience large demand about the y-axis.

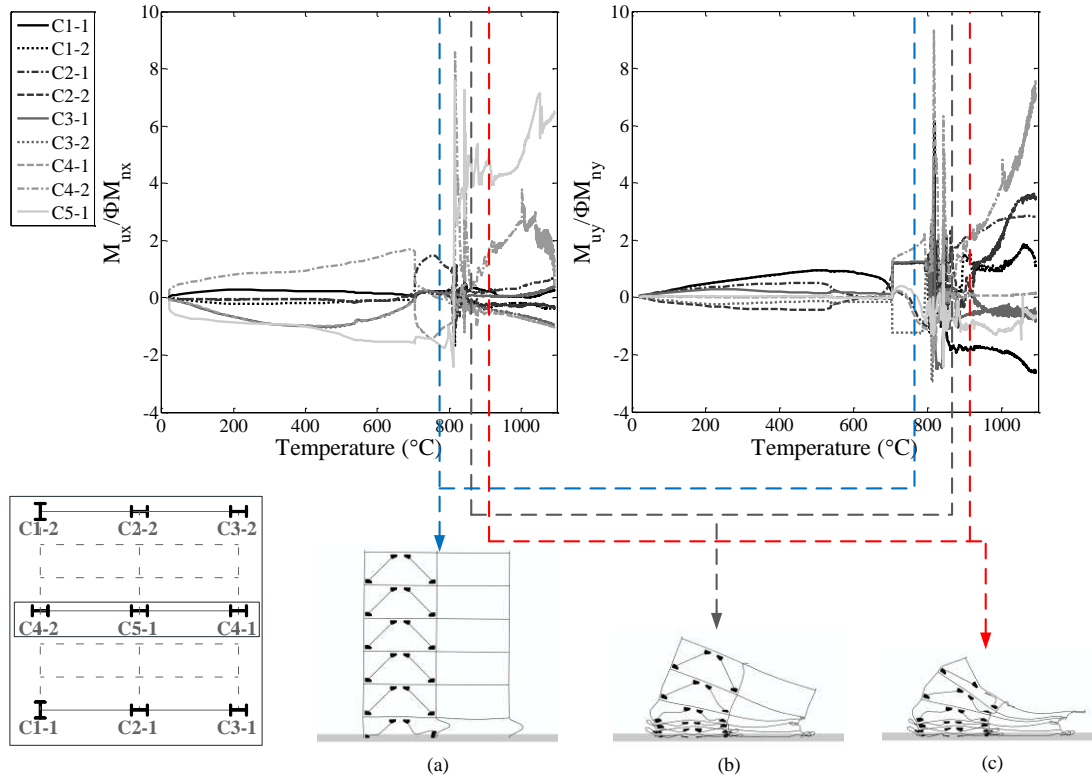


Figure 5.26 Case-4 First Floor Column End Moment

Table 5.40 Case-4 Ratios of  $M_{ux}/\phi M_{nx}$  at Elevated Temperature

Temperature (°C)	C1-1	C1-2	C2-1	C2-2	C3-1	C3-2	C4-1	C4-2	C5-1
20	0.0025	-0.0025	0.0000	0.0000	-0.0053	-0.0053	-0.0054	0.0954	-0.0963
100	0.2040	-0.1365	-0.0498	-0.0487	-0.3447	-0.3422	-0.2887	0.5976	-0.7317
200	0.2749	-0.2086	-0.0478	-0.0608	-0.7097	-0.7158	-0.7201	0.8321	-0.8638
300	0.2623	-0.2115	-0.0426	-0.0431	-0.9143	-0.9241	-0.9289	0.8910	-0.9245
400	0.2333	-0.1735	-0.0346	-0.0395	-0.9876	-0.9952	-0.9619	0.9359	-1.0009
500	0.2172	-0.1374	-0.1138	-0.1094	-0.9594	-0.9820	-0.9590	1.1760	-1.3405
600	0.1543	-0.1000	-0.0847	-0.0906	-0.6955	-0.7157	-0.6955	1.4261	-1.5326
700	0.0542	-0.0799	0.1886	0.0534	-0.0932	-0.0952	-0.1867	1.6720	-1.5467
800	0.2523	0.2961	1.0207	0.0366	0.1635	0.0739	-0.9317	-0.1726	-1.2478
900	0.2498	-0.3811	0.2163	-0.2845	0.0597	-0.4005	-0.5483	1.4334	4.5845
1000	0.0527	-0.1869	0.3651	-0.2799	0.0796	-0.6140	-0.7031	2.6259	4.8943

Table 5.41 Case-4 Ratios of  $M_{uy}/\phi M_{ny}$  at Elevated Temperature

Temperature (°C)	C1-1	C1-2	C2-1	C2-2	C3-1	C3-2	C4-1	C4-2	C5-1
20	0.0055	0.0055	0.0033	-0.0033	0.0068	-0.0066	-0.0001	0.0000	0.0000
100	0.2510	0.2481	0.2348	-0.1895	0.1705	-0.1107	0.0278	0.0316	0.0287
200	0.5069	0.4964	0.3660	-0.3187	0.2847	-0.2298	0.0197	0.0260	0.0314
300	0.6795	0.6800	0.4489	-0.4009	0.2553	-0.2045	0.0156	0.0211	0.0293
400	0.8081	0.7968	0.4827	-0.4168	0.1906	-0.1626	0.0093	0.0267	0.0324
500	0.9486	0.9555	0.4969	-0.4287	0.1569	-0.1306	0.0064	0.0294	0.0399
600	0.8786	0.8787	0.0579	-0.0680	0.1623	-0.1598	0.0038	0.0189	-0.0172
700	0.2741	0.2707	-0.0544	0.6404	0.1096	-0.1465	-0.0135	0.0353	-0.0135
800	1.2106	0.5907	-1.0281	1.0989	1.2559	0.9192	-1.1303	0.8865	-0.2010
900	-1.7573	1.4283	2.0418	-0.2931	-0.6646	0.2444	0.0036	1.9382	-1.1179
1000	-1.8989	1.0208	2.7161	2.1060	-0.3986	-0.6173	0.0633	3.8492	-1.1653

### 5.7.3.5 Case-5

For Case 5 (CBF and EC3 parametric fire curve in a single compartment), shown in Figure 5.27, the demand on the columns about both the x-axis and y-axis is somewhat similar to that of Case-1. Table 5.42 and 5.43 show the ratios for the columns' end moment at selected temperature points for the x-axis and y-axis. As shown in the tables, only column C3-1 was found to have reached its capacity limit about the x-axis. About the y-axis, C2-1 was the first to reach its limit at 700°C. Various other columns reached their capacity about the same axis at 800°C.

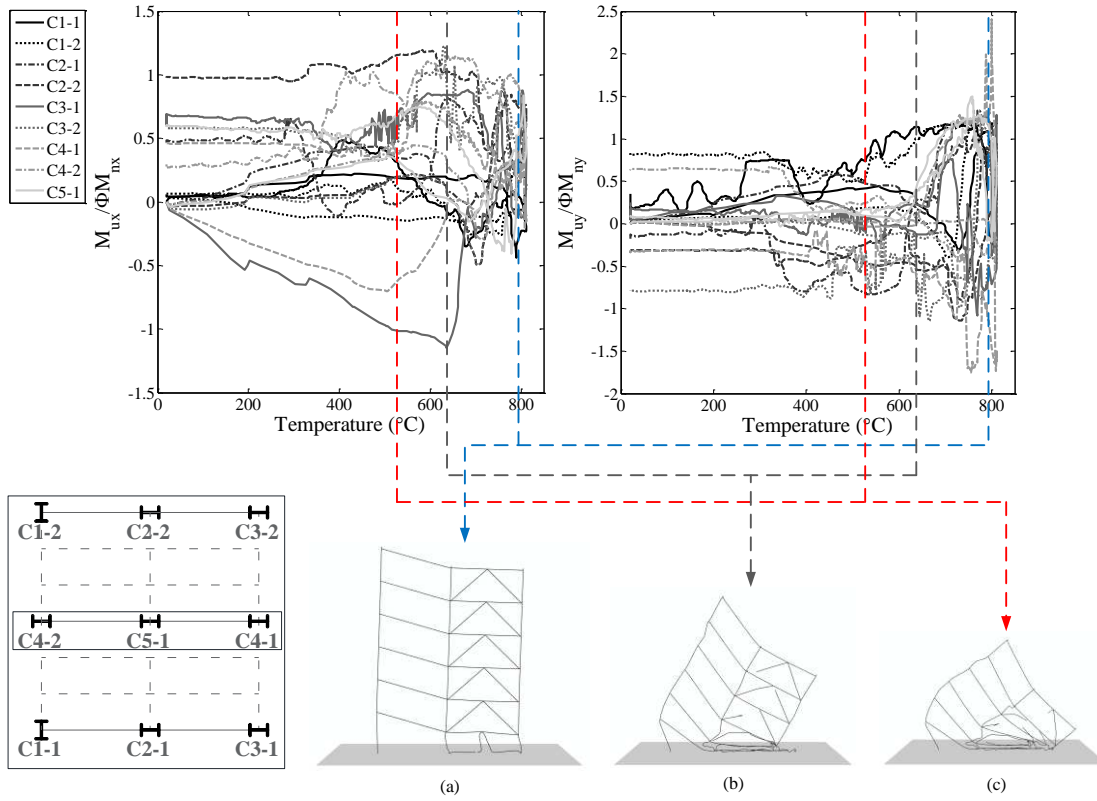


Figure 5.27 Case-5 First Floor Column End Moment

Table 5.42 Case-5 Ratios of  $M_{ux}/\phi M_{nx}$  at Elevated Temperature

Temperature (°C)	C1-1	C1-2	C2-1	C2-2	C3-1	C3-2	C4-1	C4-2	C5-1
20	0.0001	-0.0001	0.0000	0.0000	-0.0052	-0.0052	-0.0051	0.0055	0.0000
100	0.0452	0.0122	0.0385	-0.0281	-0.2559	-0.0576	-0.1789	0.0103	-0.0045
200	0.1005	-0.0461	0.1817	0.0199	-0.5016	0.0188	-0.3192	0.0870	0.1017
300	0.1481	-0.1173	0.3151	0.0313	-0.6463	0.0052	-0.4565	0.2022	0.1918
400	0.2178	-0.1198	0.4101	0.0523	-0.7567	0.0299	-0.5723	0.2968	0.2716
500	0.2044	-0.1317	0.4252	0.1505	-0.9736	0.1353	-0.6994	0.3774	0.3414
600	0.1983	-0.1274	0.3202	0.1886	-1.0566	0.1889	-0.3707	0.4259	0.0643
700	0.1978	-0.1094	0.0675	-0.4816	-0.2430	-0.4835	-0.1160	-0.2391	-0.0824
800	0.0176	-0.0609	0.3900	0.3091	0.5840	0.2797	0.2347	0.8403	0.6008

Table 5.43 Case-5 Ratios of  $M_{uy}/\phi M_{ny}$  at Elevated Temperature

Temperature (°C)	C1-1	C1-2	C2-1	C2-2	C3-1	C3-2	C4-1	C4-2	C5-1
20	0.0056	0.0056	0.0029	-0.0029	0.0005	-0.0003	-0.0001	0.0000	0.0000
100	0.0858	0.0601	0.0959	0.0005	0.1321	-0.0056	-0.0138	0.0205	0.0196
200	0.1026	0.0807	0.2213	-0.0574	0.1743	0.0023	-0.0105	0.0315	0.0379
300	0.2855	0.0609	0.3615	-0.1118	0.2442	0.0109	0.0231	0.0132	0.0800
400	0.3677	0.0457	0.4660	-0.2689	0.2705	0.0057	0.0526	0.0412	0.1286
500	0.4142	0.1326	0.5495	-0.4148	0.1507	-0.0864	0.0040	0.0442	0.1172
600	0.3728	0.1697	0.4166	-0.4612	-0.0197	-0.1162	-0.0318	0.0387	0.0160
700	-0.0746	-0.3816	1.1514	-0.5120	0.9047	-0.1557	0.9742	0.0320	1.1008
800	0.8109	1.1114	1.1608	0.8624	0.6301	0.6454	2.1744	-0.0498	1.0104

### 5.7.3.6 Case-6

For Case 6 (CBF and EC3 parametric fire curve in the whole first floor), shown in Figure 5.28, all curves of moment demand-to-capacity ratios moved more or less simultaneously because the floor was heated evenly. Table 5.44 and 5.45 show the ratios of columns' end moment at selected temperature points for the x-axis and y-axis. Only two columns have values larger than one about the x-axis. It is important however, to note that the listed values in the tables are at increments of 100°C, which resulted in some of the ratios not being captured as they exceeded a value of one.

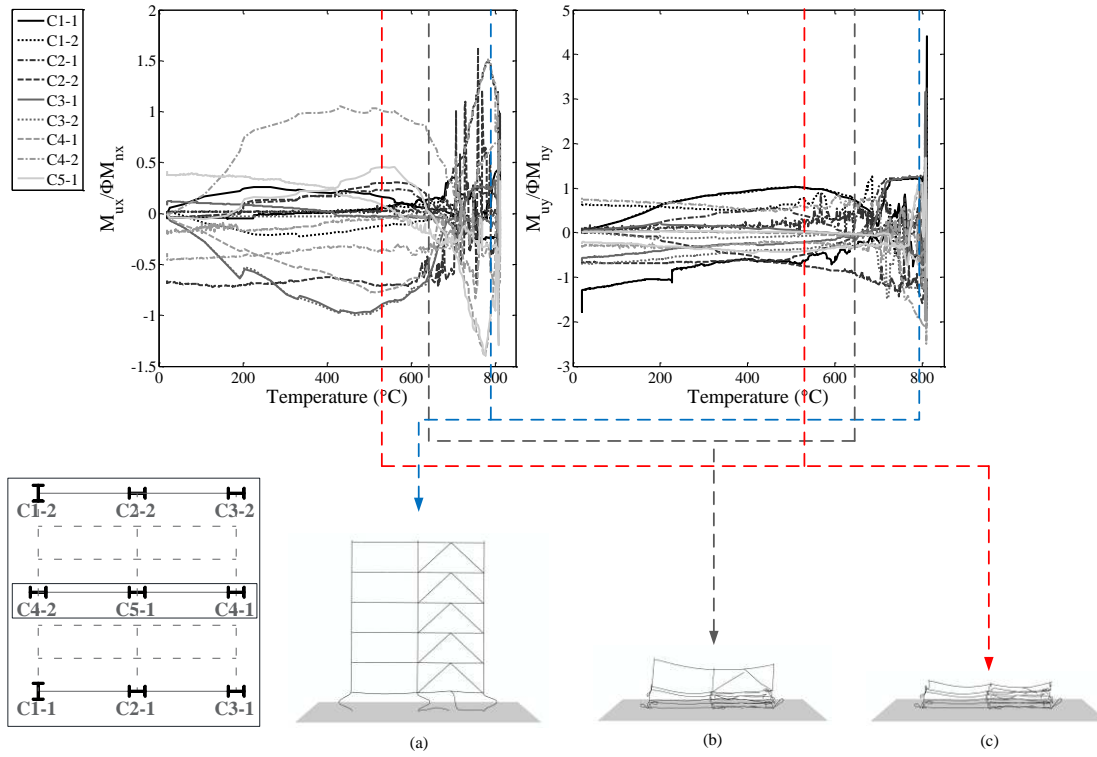


Figure 5.28 Case-6 First Floor Column End Moment

Table 5.44 Case-6 Ratios of  $M_{ux}/\phi M_{nx}$  at Elevated Temperature

Temperature (°C)	C1-1	C1-2	C2-1	C2-2	C3-1	C3-2	C4-1	C4-2	C5-1
20	0.0001	-0.0001	0.0000	0.0000	-0.0052	-0.0052	-0.0051	0.0055	0.0000
100	0.1658	-0.0932	-0.0228	-0.0216	-0.2771	-0.2789	-0.1866	0.1865	-0.0570
200	0.2407	-0.1784	0.0331	0.0452	-0.5995	-0.5923	-0.3638	0.7026	0.1084
300	0.2314	-0.1971	0.1235	0.1372	-0.7934	-0.7862	-0.4987	0.9112	0.1665
400	0.1979	-0.1946	0.1651	0.1742	-0.9327	-0.9462	-0.5973	0.9980	0.2324
500	0.1928	-0.1413	0.2120	0.2666	-0.9652	-0.9828	-0.7675	0.9948	0.4100
600	0.0787	-0.1004	0.2209	0.2837	-0.7641	-0.7370	-0.6371	0.9058	0.2920
700	-0.0343	-0.0071	-0.0992	0.4412	-0.1882	-0.1818	-0.1980	0.2133	-0.3644
800	-0.2184	-0.2208	0.1921	1.2237	0.2022	0.2496	-0.3817	1.2734	-0.9545

Table 5.45 Case-6 Ratios of  $M_{uy}/\phi M_{ny}$  at Elevated Temperature

Temperature (°C)	C1-1	C1-2	C2-1	C2-2	C3-1	C3-2	C4-1	C4-2	C5-1
20	0.0056	0.0056	0.0029	-0.0029	0.0005	-0.0003	-0.0001	0.0000	0.0000
100	0.2524	0.2514	0.0803	-0.0366	0.1160	-0.0597	0.0287	0.0251	0.0229
200	0.5963	0.6021	0.2066	-0.1447	0.2212	-0.0642	0.0262	0.0272	0.0294
300	0.8222	0.8222	0.3698	-0.3301	0.1518	-0.1126	0.0244	0.0178	0.0352
400	0.9413	0.9203	0.4810	-0.5148	0.0892	-0.0952	0.0036	0.0120	0.0127
500	1.0202	1.0157	0.4994	-0.5862	0.0573	-0.0925	-0.0141	0.0087	0.0246
600	0.8836	0.9026	0.1271	-0.2857	-0.0204	-0.0351	-0.0622	-0.0068	-0.0110
700	0.2195	0.2873	1.0338	0.0716	0.7196	-0.7822	-0.0618	-0.0206	-0.0283
800	1.2069	1.2536	1.2782	0.8571	-0.8305	-1.2514	0.8866	-1.0887	1.1132

### 5.7.3.7 Case-7

For Case 7 (EBF and EC3 parametric fire curve in a single compartment), shown in Figure 5.29, the response was similar to that of the other single compartment fire cases. Table 5.46 and 5.47 show the ratios of columns' end moment at selected temperature points for the x-axis and y-axis. Columns C4-2 and C5-1 reached their limit about the x-axis at rather low temperature due to the unbalanced deformation of the building. Columns C2-1, C3-1, and C5-1 reached their limit about the y-axis, as expected, at around 700°C.

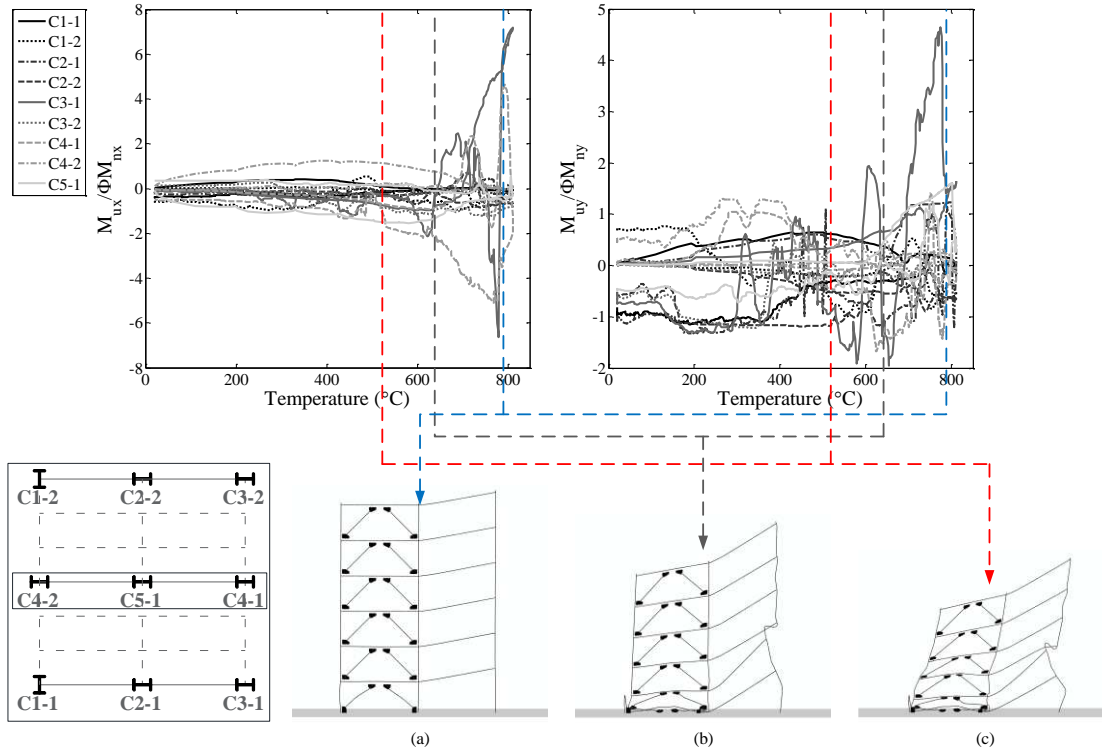


Figure 5.29 Case-7 First Floor Column End Moment

Table 5.46 Case-7 Ratios of  $M_{ux}/\phi M_{nx}$  at Elevated Temperature

Temperature (°C)	C1-1	C1-2	C2-1	C2-2	C3-1	C3-2	C4-1	C4-2	C5-1
20	0.0025	-0.0025	0.0000	0.0000	-0.0053	-0.0053	-0.0054	0.0954	-0.0963
100	0.1907	0.0149	-0.1087	-0.0435	-0.0970	-0.0707	-0.0835	0.6634	-0.7704
200	0.2926	0.0140	-0.2441	-0.1032	-0.1743	-0.1278	-0.1628	0.7705	-0.7679
300	0.3800	0.0329	-0.3329	-0.1137	-0.3821	-0.1327	-0.2564	1.1247	-1.0641
400	0.3682	0.0434	-0.3825	-0.1510	-0.5074	-0.1706	-0.3423	1.2270	-1.1509
500	0.1716	-0.0461	-0.3866	-0.2736	-0.6732	-0.2774	-0.5879	1.1557	-1.4180
600	-0.0079	-0.1145	-0.2319	-0.2536	-0.9711	-0.2818	-0.9279	0.8726	-1.4933
700	0.0060	-0.1287	-0.0478	0.5860	0.1041	0.6200	1.2328	0.2945	-0.6950
800	-0.0418	-0.4050	0.0628	-0.4109	6.3839	-0.5911	3.8850	-0.0218	-0.3750

Table 5.47 Case-7 Ratios of  $M_{uy}/\phi M_{ny}$  at Elevated Temperature

Temperature (°C)	C1-1	C1-2	C2-1	C2-2	C3-1	C3-2	C4-1	C4-2	C5-1
20	0.0055	0.0055	0.0033	-0.0033	0.0068	-0.0066	-0.0001	0.0000	0.0000
100	0.2199	0.0477	0.0667	0.0008	0.0557	-0.0075	0.0209	-0.0139	0.0195
200	0.4089	-0.0348	0.2139	-0.0600	0.1341	-0.0632	0.0230	-0.0126	0.0389
300	0.5070	-0.0444	0.3913	-0.1362	0.1720	-0.1075	0.0158	-0.0038	0.0730
400	0.6177	-0.1091	0.5064	-0.2871	0.2683	-0.1486	0.0103	-0.0153	0.0983
500	0.6381	-0.1930	0.5955	-0.4842	0.3286	-0.1862	0.0465	-0.0655	0.0713
600	0.4423	-0.1906	0.4154	-0.5218	0.5443	-0.1960	0.0811	-0.0501	0.0874
700	0.1397	0.4605	1.1505	-0.3934	0.9941	-0.1675	0.1671	0.2251	1.1410
800	0.1296	-0.3152	1.1944	-0.6226	1.5470	0.0823	0.0345	0.2033	1.6079

### 5.7.3.8 Case-8

For Case 8 (CBF and EC3 parametric fire curve in the whole first floor), shown in Figure 5.30, same phenomenon can be seen here as in the other cases of EBF where the gusset plates induced large moments to the columns. Since the building collapsed almost straight down due to the uniform full first floor fire, all curves seems to respond together. It is however clear that columns C3-1, C3-2, C4-2, and C5-1 exhibited larger response about their x-axis early on as noted before with continued demand on C4-2, and C5-1 with higher temperature. It was not until later where many other columns experienced higher demand about the y-axis.

Table 5.48 and 5.49 show the ratios of columns' end moment at selected temperature points for the x-axis and y-axis. Columns C4-1 and C5-1 reached their load capacity at about 400°C. Various other columns reached their limit about the y-axis at about 800°C.

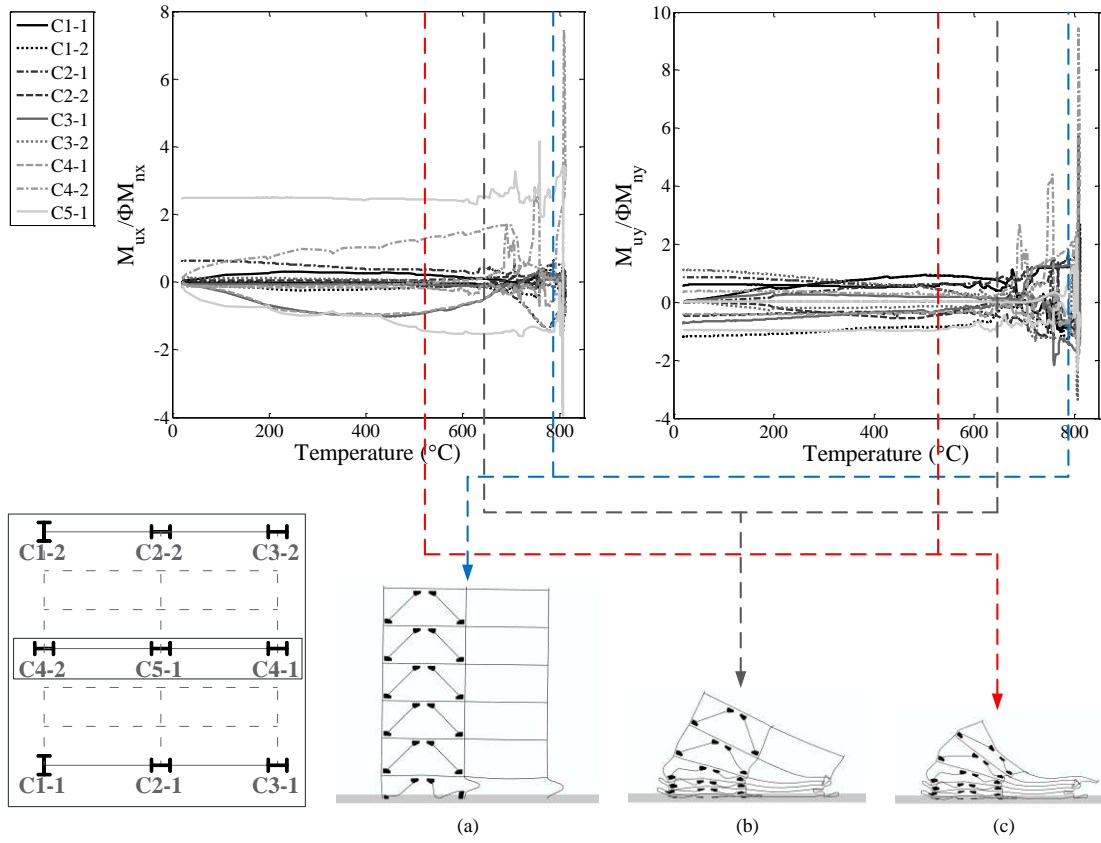


Figure 5.30 Case-8 First Floor Column End Moment

Table 5.48 Case-8 Ratios of  $M_{ux}/\phi M_{nx}$  at Elevated Temperature

Temperature (°C)	C1-1	C1-2	C2-1	C2-2	C3-1	C3-2	C4-1	C4-2	C5-1
20	0.0025	-0.0025	0.0000	0.0000	-0.0053	-0.0053	-0.0054	0.0954	-0.0963
100	0.2018	-0.1273	-0.0388	-0.0409	-0.2930	-0.2937	-0.2616	0.6105	-0.7116
200	0.2590	-0.1998	-0.0594	-0.0522	-0.6832	-0.6893	-0.7531	0.6612	-0.6914
300	0.2832	-0.2267	-0.0502	-0.0389	-0.9303	-0.9314	-0.9143	0.9523	-0.9619
400	0.2556	-0.2010	-0.0132	-0.0037	-0.9916	-0.9908	-0.9407	1.0282	-0.9932
500	0.2316	-0.1560	-0.0765	-0.0689	-0.9474	-0.9496	-0.9049	1.2269	-1.3232
600	0.1341	-0.0987	-0.0988	-0.1025	-0.6774	-0.6681	-0.6567	1.4648	-1.5317
700	-0.0133	-0.0451	-0.3962	0.1276	-0.0768	-0.0975	-0.0383	1.6091	-1.4373
800	0.2259	0.2328	-0.8864	0.0268	0.1983	0.1334	-0.9398	-0.2084	-0.1257

Table 5.49 Case-8 Ratios of  $M_{uy}/\phi M_{ny}$  at Elevated Temperature

Temperature (°C)	C1-1	C1-2	C2-1	C2-2	C3-1	C3-2	C4-1	C4-2	C5-1
20	0.0055	0.0055	0.0033	-0.0033	0.0068	-0.0066	-0.0001	0.0000	0.0000
100	0.2376	0.2366	0.0785	-0.0392	0.1783	-0.1199	0.0229	0.0280	0.0306
200	0.5091	0.4999	0.2131	-0.1588	0.3676	-0.2262	0.0201	0.0299	0.0281
300	0.6623	0.6804	0.3987	-0.3584	0.2558	-0.2041	0.0156	0.0288	0.0277
400	0.8362	0.8327	0.5298	-0.4897	0.2030	-0.1766	0.0133	0.0244	0.0241
500	0.9383	0.9433	0.5506	-0.5309	0.1813	-0.1533	0.0159	0.0344	0.0364
600	0.8398	0.8485	0.1983	-0.1922	0.1627	-0.1550	0.0124	0.0117	0.0204
700	0.3255	0.3215	-0.0550	1.0526	0.6378	-0.6612	0.0100	0.3271	-0.0010
800	1.2284	1.1283	-1.1743	0.4406	1.2352	-0.0611	-1.1412	1.0817	0.0349

### 5.7.3.9 Discussion

For the moment demand-to-capacity ratios, the response shown in all figures, for the EBF, can be characterized by a large demand on columns C4-2 and C5-1 about the x-axis, starting at lower temperatures. The demand in the y-axis became evident for various columns but only at a very later stage where collapse had already started. For the CBF, the system was much more forgiving than the EBF frame. This is because the welded gusset plates of the EBF imposed large demand on the columns due to large deformation in the braces and the fact that the gusset plates are welded to the columns.

### 5.7.4 Interaction Diagram

The beam-columns are members that are subjected to combined axial loads and moments, which should be evaluated using the interaction equation specified in Chapter H of the *2010 AISC Specifications* (AISC 365-10). This section presents a simplified interaction curve that was developed to ensure members are able to withstand the combined forces, the curves are based on the following AISC equations:

$$\text{For } \frac{P_r(T)}{P_c(T)} \geq 0.2$$

$$\frac{P_r(T)}{P_c(T)} + \frac{8}{9} \left( \frac{M_{rx}(T)}{M_{cx}(T)} + \frac{M_{ry}(T)}{M_{cy}(T)} \right) \leq 1.0$$

$$\text{For } \frac{P_r(T)}{P_c(T)} < 0.2$$

$$\frac{P_r(T)}{2P_c(T)} + \left( \frac{M_{rx}(T)}{M_{cx}(T)} + \frac{M_{ry}(T)}{M_{cy}(T)} \right) \leq 1.0$$

Where,

$P_r$  is the required axial compressive strength

$P_c$  is the available axial compressive strength

$M_r$  is the required flexural strength

$M_c$  is the available flexural strength

For this study, the axial forces and moments used in the interaction equation were taken as the actual data collected during the simulations to determine if the demand exceeded the design requirement. Furthermore, the available capacity of the structural member changes throughout the fire as the material degrades due to the temperature effect. Therefore, the values for each column attained during the simulation is plotted using the AISC interaction equation.

#### 5.7.4.1 Case-1

For Case 1 (CBF and E119 in a single compartment), shown in Figure 5.31 and Table 5.50, the curves representing the response of the four fire compartment columns reached failure (value=1) before all other curves surpassing the value of 1. In addition, column C2-1 was the most critical column as the ratio exceeded one at 200°C.

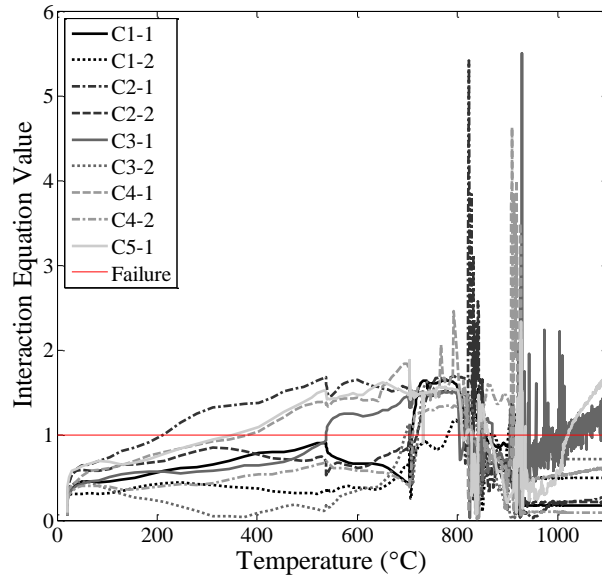


Figure 5.31 Case-1 Interaction Equation Value

Table 5.50 Case-1 Interaction Equation Value at Key Temperature Points

Temperature (°C)	C1-1	C1-2	C2-1	C2-2	C3-1	C3-2	C4-1	C4-2	C5-1
20	0.0552	0.0548	0.0672	0.0672	0.0589	0.0595	0.0838	0.0581	0.0863
100	0.4599	0.3196	0.7422	0.6009	0.5049	0.3621	0.6170	0.3936	0.6875
200	0.5837	0.4399	1.0171	0.7025	0.5775	0.2174	0.8061	0.4067	0.7855
300	0.6617	0.4121	1.3254	0.8516	0.5827	0.0500	0.9266	0.4343	0.9478
400	0.7884	0.3722	1.3796	0.7702	0.6455	0.0870	1.0453	0.5375	1.0979
500	0.8901	0.3207	1.6111	0.7090	0.8487	0.1459	1.3763	0.6386	1.4485
600	0.6702	0.3832	1.6535	0.6149	1.2498	0.3562	1.4400	0.5801	1.4735
700	0.4471	0.6573	1.5399	0.8264	1.4771	1.1311	1.8235	0.4200	1.4762
800	1.5432	1.1617	1.3759	1.6719	1.3875	1.4961	1.7410	1.3241	1.5138
900	0.8640	0.9248	0.7072	0.5636	0.7023	0.1237	0.4379	1.4265	0.2151
1000	0.1787	0.4953	0.2003	0.2163	0.7961	0.7228	0.5284	0.0949	0.5701

### 5.7.4.2 Case-2

For Case 2 (CBF and E119 in the whole floor), shown in Figure 5.32 and Table 5.51, The demand overall is higher than that of Case-1. In addition, column C1-1 and C4-2 were the first to exceed a ratio of one at 200°C. At 600°C, all columns have exceeded a ratio of one as shown in the table.

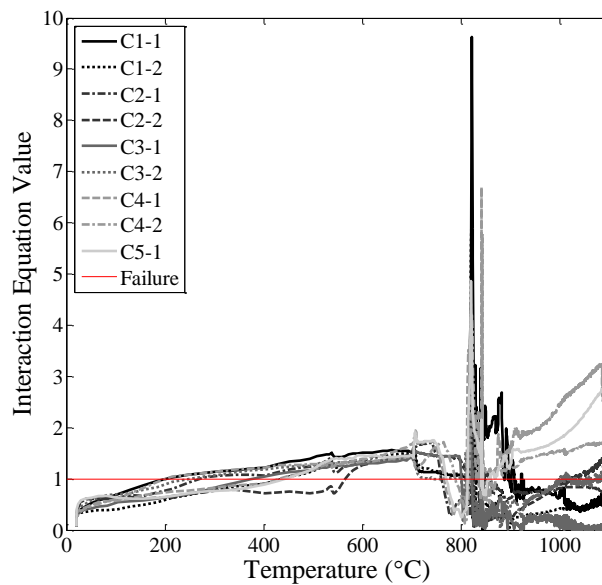


Figure 5.32 Case-2 Interaction Equation Value

Table 5.51 Case-2 Interaction Equation Value at Key Temperature Points

Temperature (°C)	C1-1	C1-2	C2-1	C2-2	C3-1	C3-2	C4-1	C4-2	C5-1
20	0.0552	0.0548	0.0672	0.0672	0.0589	0.0595	0.0838	0.0581	0.0863
100	0.7009	0.4123	0.6268	0.6162	0.5406	0.7009	0.5827	0.6082	0.6252
200	1.0357	0.6292	0.8067	0.6388	0.6586	0.9398	0.7484	1.0387	0.6735
300	1.1466	0.8044	1.0652	0.7776	0.8467	1.0879	0.8381	1.1480	0.7659
400	1.2217	0.9114	1.0656	0.7252	1.0422	1.1816	0.9133	1.2234	0.8810
500	1.4412	1.1904	1.2610	0.7265	1.2046	1.2833	1.2080	1.2911	1.2331
600	1.5102	1.3724	1.3052	1.2636	1.2940	1.3433	1.3869	1.3399	1.4601
700	1.5197	1.4757	1.4477	1.5369	1.4181	1.4332	1.6821	1.4508	1.4538
800	1.0785	1.0963	0.6144	1.3395	1.0560	0.9906	0.5984	0.6567	0.2582
900	0.8212	0.1074	0.6291	0.2622	0.2961	0.5020	1.6793	1.2321	1.2650
1000	0.6324	0.4145	0.8894	0.8147	0.1085	0.9921	2.4706	1.5374	1.7769

### 5.7.4.3 Case-3

For Case 3 (EBF and E119 in a single compartment), shown in Figure 5.33 and Table 5.52, with columns C4-2 and C5-1 undergoing the most demand as early as 100°C. At 600°C and higher various other columns have experienced very large demand as well.

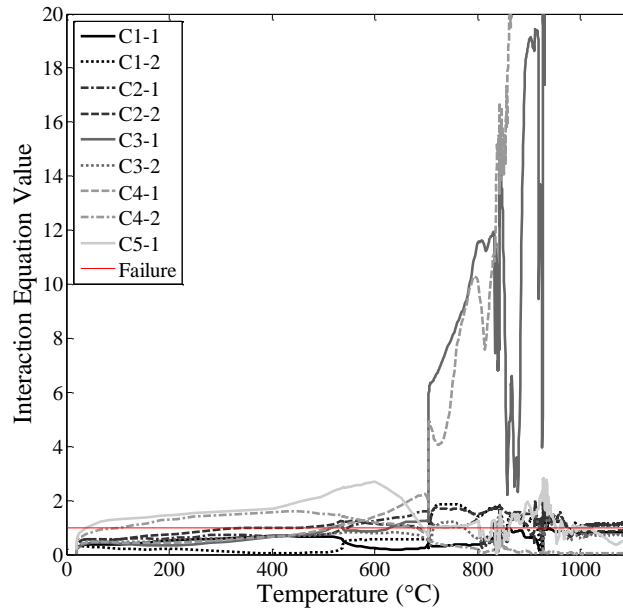


Figure 5.33 Case-3 Interaction Equation Value

Table 5.52 Case-3 Interaction Equation Value at Key Temperature Points

Temperature (°C)	C1-1	C1-2	C2-1	C2-2	C3-1	C3-2	C4-1	C4-2	C5-1
20	0.0571	0.0525	0.0674	0.0675	0.0541	0.0632	0.0577	0.1589	0.1643
100	0.6324	0.2142	0.5539	0.5713	0.3953	0.4747	0.4518	0.9983	1.3107
200	0.8829	0.2116	0.6282	0.7704	0.3503	0.5505	0.4291	1.3190	1.4750
300	0.9180	0.0985	0.7406	0.9506	0.4841	0.5948	0.5376	1.4661	1.5908
400	0.9639	0.0415	0.6683	0.9778	0.6477	0.6843	0.6520	1.5525	1.6930
500	0.8428	0.0752	0.7474	1.0793	0.9270	0.7541	0.9389	1.4942	2.2305
600	0.3891	0.5523	1.2458	1.1466	0.8624	0.7998	1.3990	1.1796	2.7086
700	0.3476	0.5762	1.5924	0.8200	1.2466	0.5661	2.1581	0.7509	0.8074
800	0.0937	1.4292	1.3184	1.4935	11.5511	0.5685	10.1362	0.2068	1.2494
900	0.0205	1.1922	0.8829	1.5002	19.0526	1.6225	28.1710	0.1053	1.8238
1000	0.0124	1.0524	0.9357	0.7655	26.4404	0.6582	40.6941	0.0358	0.9287

#### 5.7.4.4 Case-4

For Case 4 (EBF and E119 in the whole floor), shown in Figure 5.34 and Table 5.53, all response curves passed the failure line with columns C5-1 exceeding the limit again as early as 100°C. Other columns followed at 200°C and 300°C. At 500°C, all columns, except one) had reached their limit, making the EBF with a whole floor fire being the worst case thus far.

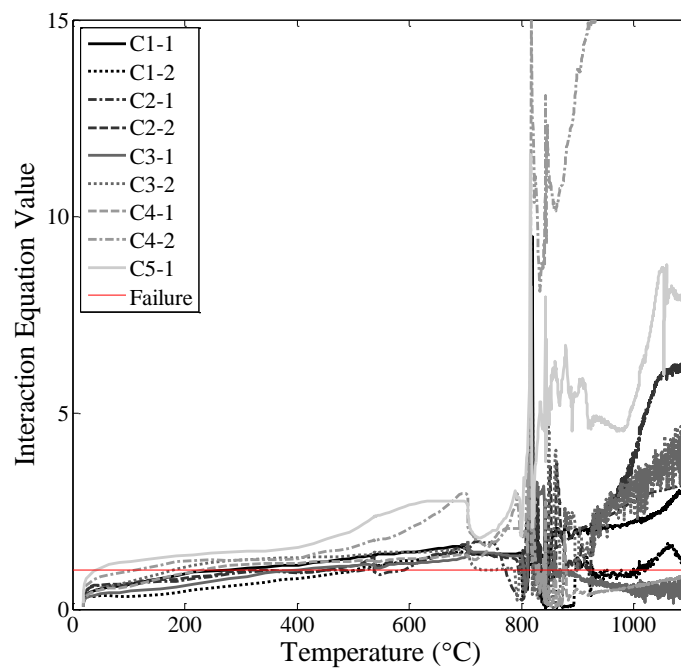


Figure 5.34 Case-4 Interaction Equation Value

Table 5.53 Case-4 Interaction Equation Value at Key Temperature Points

Temperature (°C)	C1-1	C1-2	C2-1	C2-2	C3-1	C3-2	C4-1	C4-2	C5-1
20	0.0571	0.0525	0.0674	0.0675	0.0541	0.0632	0.0577	0.1589	0.1643
100	0.6421	0.3148	0.6224	0.6626	0.4694	0.7188	0.5881	0.9650	1.2041
200	0.9404	0.5019	0.7694	0.8178	0.6435	1.1188	0.9518	1.2468	1.3934
300	1.0341	0.6348	0.9613	1.0029	0.8410	1.2665	1.1431	1.2641	1.4682
400	1.1264	0.7768	0.9172	0.9386	1.0055	1.3156	1.1777	1.2950	1.5725
500	1.3246	1.0138	0.9815	1.1212	1.1208	1.3712	1.2394	1.6182	2.0792
600	1.4645	1.2433	1.0582	1.1607	1.1769	1.4611	1.2902	2.0562	2.6548
700	1.5439	1.4258	1.4115	1.6390	1.3398	1.5382	1.3914	2.9343	2.7342
800	1.4133	0.9094	0.2249	1.0284	1.3668	1.1200	2.0461	1.8660	2.0568
900	1.9125	1.2303	2.0144	1.2545	0.8582	1.0329	0.4963	13.7914	5.4927
1000	2.2303	0.9245	2.7592	3.9343	0.5055	3.2640	0.5800	19.8425	5.2763

#### 5.7.4.5 Case-5

For Case 5 (CBF and EC3 parametric fire curve in a single compartment), shown in Figure 5.35 and Table 5.54, the curves representing the response of the four fire compartment columns reached failure (value=1) before all other curves. Column C-2 was under the most demand as shown by its ratio exceeding one at 300°C. At 400°C, columns C4-1 and C5-1 also surpassed the ratio of one.

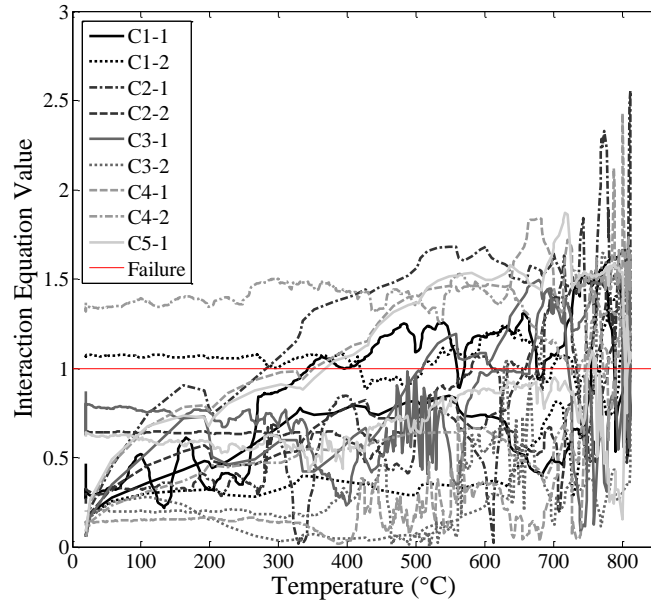


Figure 5.35 Case-5 Interaction Equation Value

Table 5.54 Case-5 Interaction Equation Value at Key Temperature Points

Temperature (°C)	C1-1	C1-2	C2-1	C2-2	C3-1	C3-2	C4-1	C4-2	C5-1
20	0.0552	0.0548	0.0672	0.0672	0.0589	0.0595	0.0838	0.0581	0.0863
100	0.3602	0.3011	0.7428	0.4543	0.5308	0.2792	0.6710	0.3082	0.6747
200	0.4739	0.3348	0.7837	0.5484	0.6410	0.1560	0.7615	0.4574	0.6773
300	0.6797	0.3239	1.0699	0.5240	0.5981	0.0308	0.9795	0.4729	0.9089
400	0.7912	0.3603	1.4065	0.7969	0.6163	0.0485	1.1269	0.5524	1.0770
500	0.8166	0.2886	1.5648	0.7246	0.9778	0.0543	1.4081	0.6424	1.3694
600	0.7386	0.3521	1.6816	0.6852	1.0837	0.2328	1.4630	0.6643	1.4959
700	0.4822	0.8062	1.6407	1.4101	1.3388	1.3899	1.4528	0.5730	1.7015
800	1.2900	1.1699	1.4829	1.6621	1.2019	1.2482	2.2502	1.2529	1.5405

### 5.7.4.6 Case-6

For Case 6 (CBF and EC3 parametric fire curve in the whole first floor), shown in Figure 5.36 and Table 5.55, all response curves reached to failure line almost concurrently at about 700°C as shown in the table. The demand on C1-1 and C4-2 was rather larger as shown by their ratio exceeding a value of one early on at 200°C.

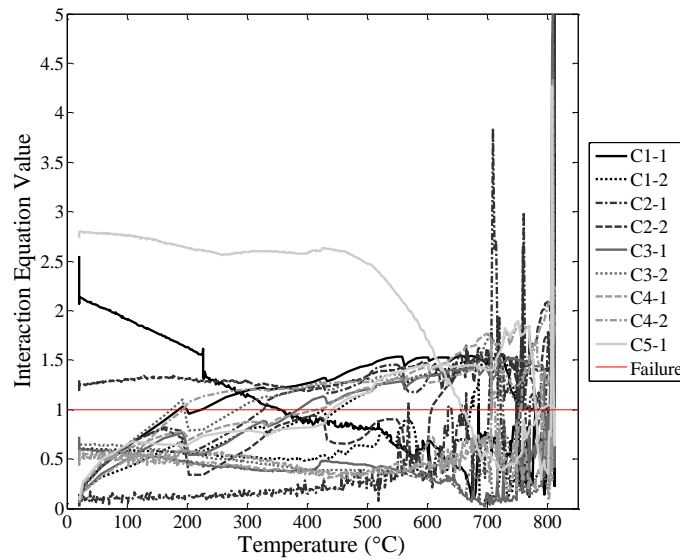


Figure 5.36 Case-6 Interaction Equation Value

Table 5.55 Case-6 Interaction Equation Value at Key Temperature Points

Temperature (°C)	C1-1	C1-2	C2-1	C2-2	C3-1	C3-2	C4-1	C4-2	C5-1
20	0.0552	0.0548	0.0672	0.0672	0.0589	0.0595	0.0838	0.0581	0.0863
100	0.6677	0.4373	0.6804	0.6812	0.5332	0.6919	0.6295	0.5338	0.6773
200	1.0082	0.6067	0.6331	0.5062	0.6463	0.8888	0.7353	1.0472	0.6306
300	1.1951	0.8059	0.8899	0.6045	0.8161	1.0696	0.8787	1.2038	0.7856
400	1.2797	0.9438	1.2299	0.9377	1.1009	1.2509	0.9884	1.2436	0.8221
500	1.4499	1.1768	1.3219	0.7666	1.2054	1.3166	1.2225	1.2811	1.1730
600	1.5253	1.3522	1.3227	0.6906	1.3446	1.3581	1.4275	1.3264	1.4518
700	1.4854	1.5424	1.5166	1.5118	1.3815	1.7473	1.7648	1.4465	1.4015
800	1.0068	1.0414	1.4134	2.0839	0.7774	1.0045	0.6797	0.4164	0.3474

### 5.7.4.7 Case-7

For Case 7 (EBF and EC3 parametric fire curve in a single compartment), shown in Figure 5.37 and Table 5.56. The demand was most concentrated on column C5-1 and C4-2 as expected with the ratios being exceeded at temperature as low as 100°C. Again, this is due to the impose demand from the gusset plates that are welded to the braces. Various other columns started to experience large demand at temperature of 600°C.

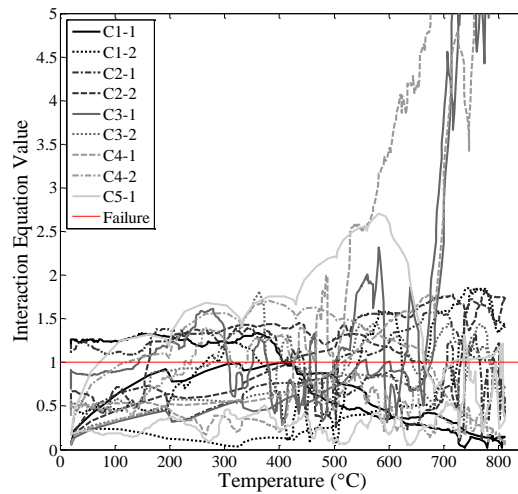


Figure 5.37 Case-7 Interaction Equation Value

Table 5.56 Case-7 Interaction Equation Value at Key Temperature Points

Temperature (°C)	C1-1	C1-2	C2-1	C2-2	C3-1	C3-2	C4-1	C4-2	C5-1
20	0.0571	0.0525	0.0674	0.0675	0.0541	0.0632	0.0577	0.1589	0.1643
100	0.6601	0.2348	0.6567	0.4630	0.3276	0.3492	0.3460	0.9818	1.2517
200	0.8639	0.1189	0.4405	0.6396	0.3905	0.5559	0.5269	1.0521	1.1870
300	0.9811	0.0437	0.5365	0.6533	0.5196	0.5485	0.5488	1.5631	1.6503
400	1.0001	0.1320	0.7667	0.9738	0.5782	0.6592	0.6326	1.6549	1.7514
500	0.8483	0.2586	0.8625	1.1730	0.7334	0.7896	0.9268	1.5211	2.2186
600	0.4168	0.4615	1.2361	1.1796	1.0101	0.8470	1.4823	1.2394	2.5809
700	0.3627	0.9177	1.5407	0.6834	2.8363	0.8790	3.2011	0.6549	0.9090
800	0.0924	1.3473	1.2361	1.4819	11.5814	0.6352	10.7289	0.1887	1.1572

### 5.7.4.8 Case-8

For Case 8 (EBF and EC3 parametric fire curve in the whole first floor), shown in Figure 5.38 and Table 5.57, all response curves reached failure almost concurrently. At 400°C, all columns, except for C1-2, had exceeded their limit.

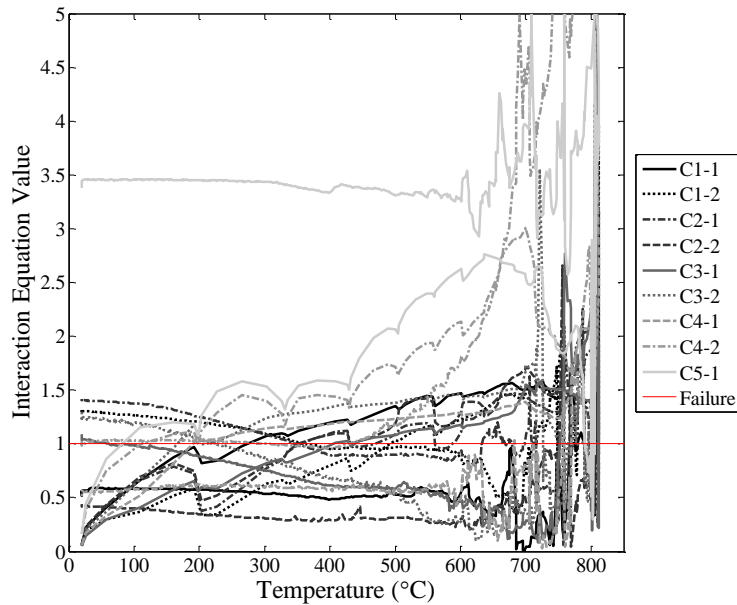


Figure 5.38 Case-8 Interaction Equation Value

Table 5.57 Case-8 Interaction Equation Value at Key Temperature Points

Temperature (°C)	C1-1	C1-2	C2-1	C2-2	C3-1	C3-2	C4-1	C4-2	C5-1
20	0.0571	0.0525	0.0674	0.0675	0.0541	0.0632	0.0577	0.1589	0.1643
100	0.6652	0.3692	0.6594	0.6947	0.4062	0.6735	0.5182	0.9963	1.1564
200	0.9063	0.4589	0.5448	0.5943	0.5604	1.0888	1.0624	0.9947	1.0737
300	1.0770	0.6270	0.7733	0.8076	0.8199	1.2433	1.1431	1.3986	1.5300
400	1.2089	0.8231	1.1141	1.1004	1.0085	1.3481	1.1952	1.4380	1.5808
500	1.3477	1.0339	1.0888	1.1964	1.0844	1.3836	1.2295	1.7180	2.0680
600	1.4684	1.2351	1.1170	1.2977	1.1775	1.4612	1.2869	2.1364	2.6233
700	1.5403	1.5051	1.4456	1.7194	1.5485	1.7331	1.3846	2.9836	2.5272
800	1.4055	1.3289	2.0368	0.4692	1.3796	0.3675	2.0674	1.9482	0.5081

#### **5.7.4.9 Discussion**

Since this is a collapse analysis, it is reasonable that all the interaction equation values would ultimately pass the limit. The challenging aspect of representing the results is defining the “final” point for which the results should be plotted. Plotting the results at the onset of exceeding a value of one in any of the columns might be an alternative. However, it is arguably a conservative approach since failure of one column does not necessarily imply failure of the entire system as was seen in the analysis. For example, in some cases the limit ratio of one was exceeded at as low of a temperature as 100oC. However, the deformation of the frames at that point was minimal and collapse was not imminent. Generally, the EBF experienced higher ratios, which was due to the additional demand imposed by the columns.

#### **5.7.5 Shear Connector Failure**

The shear connector model used in this study was describe in detail in Chapter 4. The shear model utilized a failure mechanism to break the connector at a certain separation distance of the connector nodes. Horizontal and vertical separation of a selected connector (marked in Figure 5.39) of the first floor were obtained from the simulation results and plotted for each case as shown below.

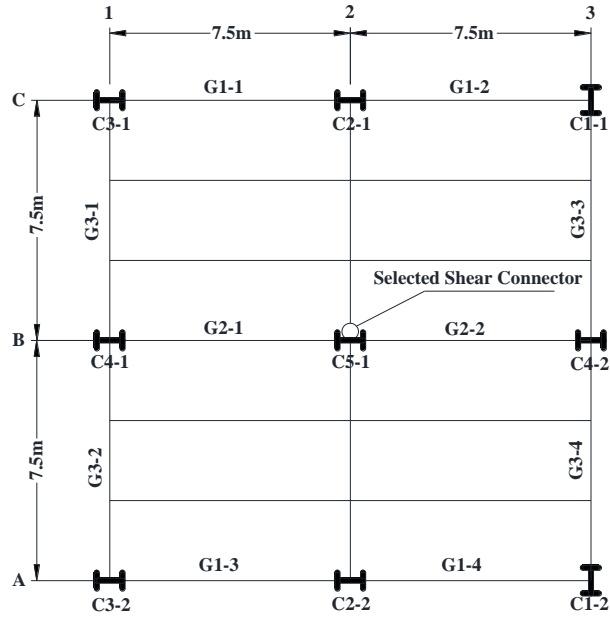


Figure 5.39 Floor Plan of the Buildings showing the Selected Shear Connector

### 5.7.5.1 Case-1

Figure 5.40 shows the shear connector node separation for Case 1 (CBF and E119 in a single compartment).

The selected shear connector reached its failure point around 730°C. Following that point, the separation value suddenly increased to a value of 1m, implying a complete breakage of the connector. The enlarged view in the figure shows the connector behavior before the sudden large separation (i.e. before collapsed).

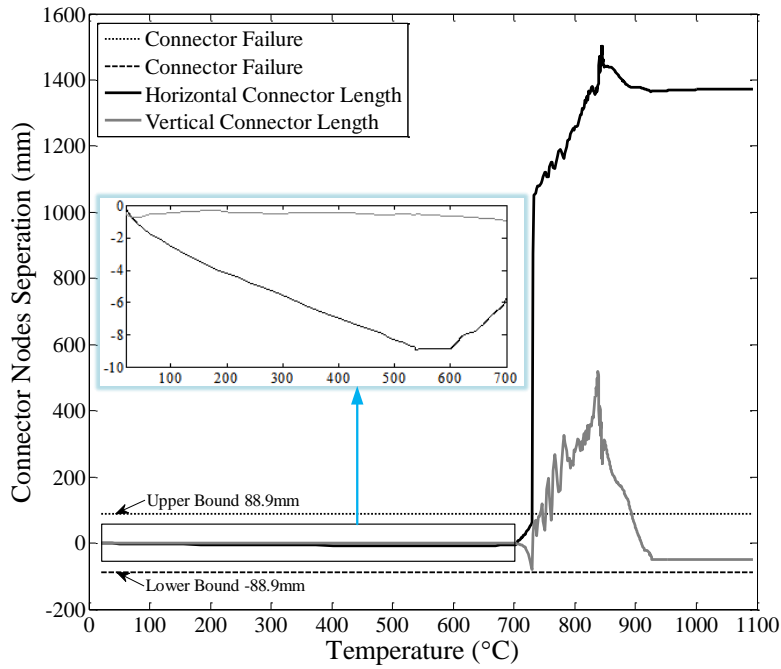


Figure 5.40 Case-1 First Floor Shear Connector Nodes Separation

### 5.7.5.2 Case-2

Figure 5.41 shows the shear connector nodes separation for Case 2 (CBF and E119 in the whole floor).

Because the floor went straight down in Case-2, there was no relative vertical movement between the girder and the column. Some horizontal separation can be seen in the figure, which is due to the slight tilting of the system, which caused separation of the joint. Overall, the connector did not fail in either directions.

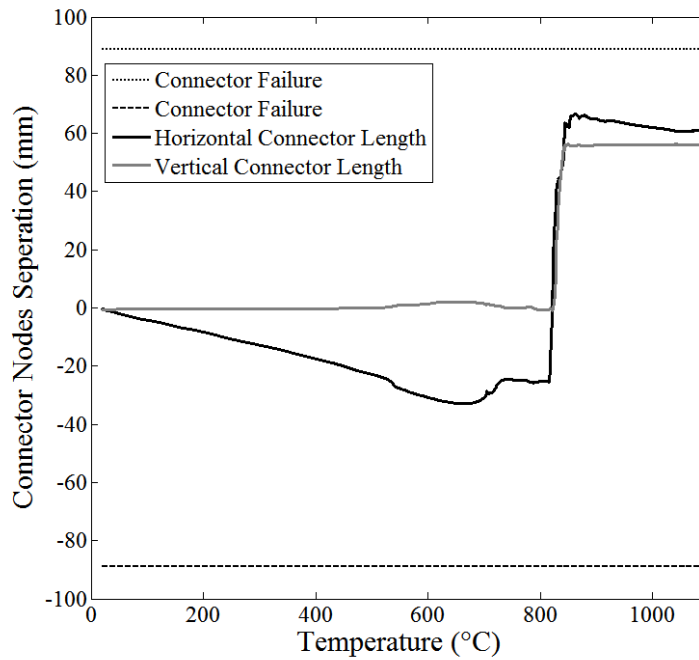


Figure 5.41 Case-2 First Floor Shear Connector Nodes Separation

### 5.7.5.3 Case-3

Figure 5.42 shows the shear connector node separation for Case 3 (EBF and E119 in a single compartment).

There was no sudden increase in the separation value until reaching the critical temperature point of about 700°C. This is because the concrete slab provided the continuity needed to limit the separation at the girder-to-column joint.

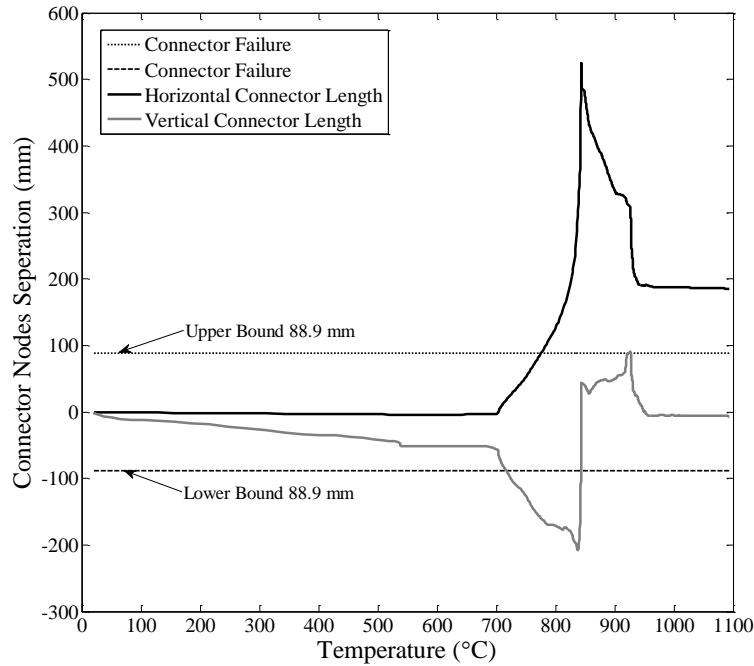


Figure 5.42 Case-3 First Floor Shear Connector Nodes Separation

#### 5.7.5.4 Case-4

Figure 5.43 shows the shear connector nodes separation for Case 4 (EBF and E119 in the whole floor). The shear connector failure in the vertical direction occurred around 538°C. Following that failure point, the separation value suddenly increased to a value of 165 mm, implying a complete breakage of the connector. In the horizontal direction, while the separation started to increase at the early stage of loading, failure did not occur until approximately 800°C.

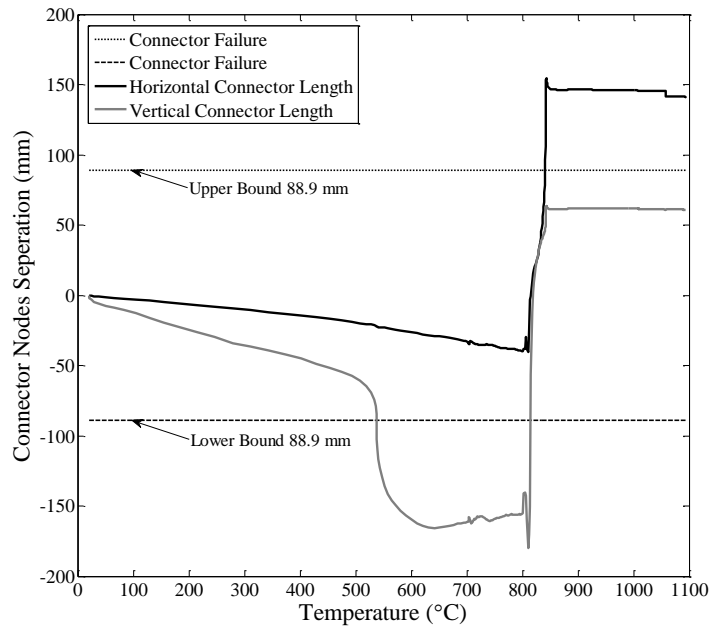


Figure 5.43 Case-4 First Floor Shear Connector Nodes Separation

#### 5.7.5.5 Case-5

Figure 5.44 shows the shear connector nodes separation for Case 5 (CBF and EC3 parametric fire curve in a single compartment). At 769°C, the selected shear connector reached its deformation limit in both directions. Following this point, the separation value suddenly increased horizontally, implying a complete breakage of the connector, which is consistent with the large lateral deformation resulting from the compartment fire.

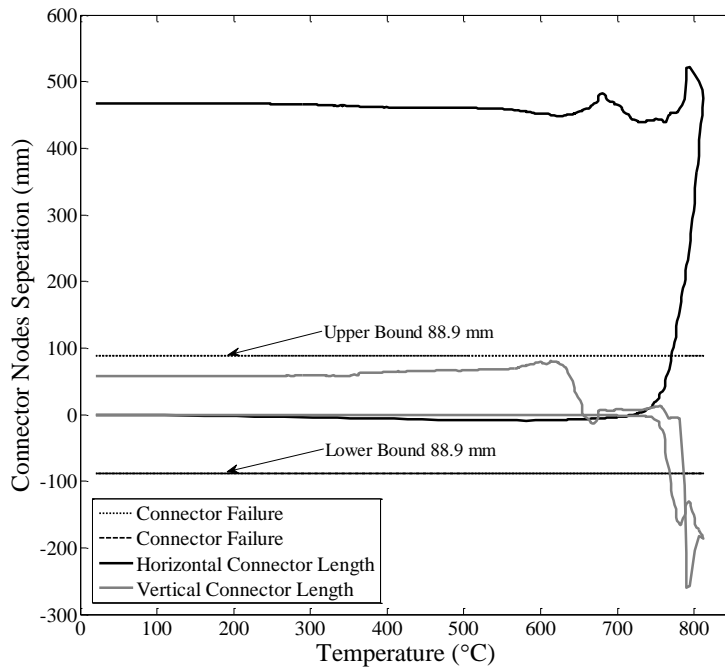


Figure 5.44 Case-5 First Floor Shear Connector Nodes Separation

### 5.7.5.6 Case-6

Figure 5.45 shows the shear connector nodes separation for Case 6 (CBF and EC3 parametric fire curve in the whole first floor). Because of the vertical collapse mechanism of this case, there was no relative vertical movement between girder and column during the heating phase. Separation that is more evident in the horizontal direction, as shown, due to the slight tilting of the system. The separation value is however below the failure value. The failure lines are not drawn in this figure as was in the case in the previous figures.

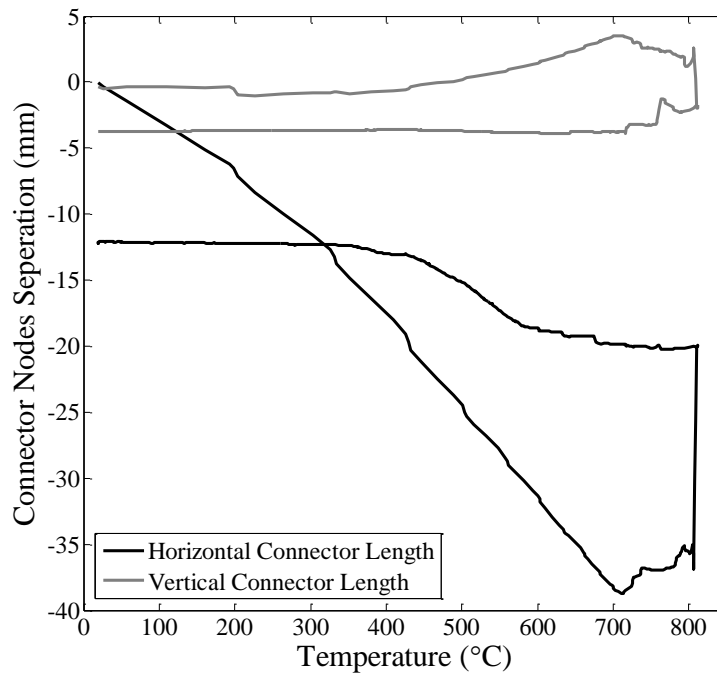


Figure 5.45 Case-6 First Floor Shear Connector Nodes Separation

### 5.7.5.7 Case-7

Figure 5.46 shows the shear connector nodes separation for Case 7 (EBF and EC3 parametric fire curve in a single compartment). The shear connector reached its vertical deformation limit state at 755°C. At this point, two nodes were separated, the nodes separation after that point was useless in this study.

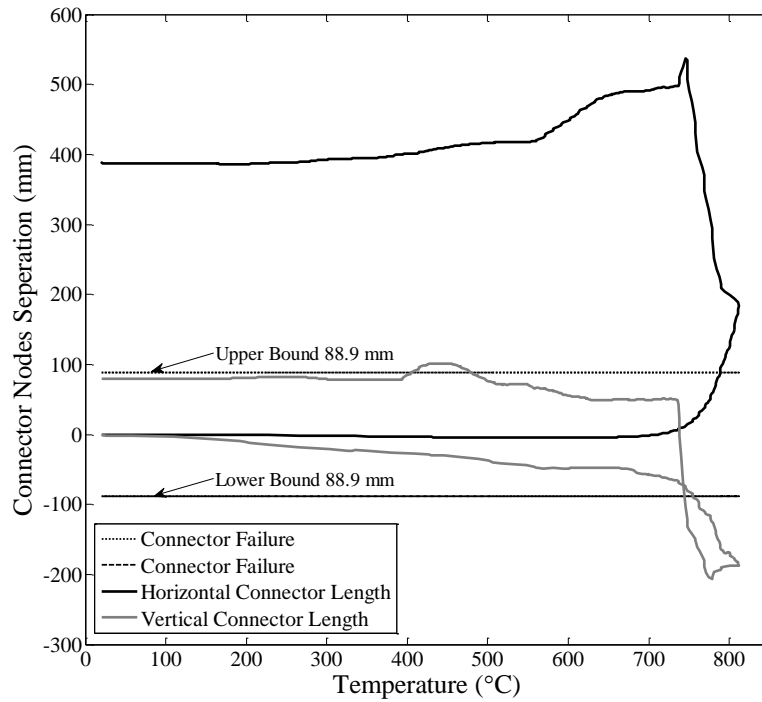


Figure 5.46 Case-7 First Floor Shear Connector Nodes Separation

### 5.7.5.8 Case-8

Figure 5.47 shown the shear connector nodes separation for Case 8 (EBF and EC3 parametric fire curve in the whole first floor). The shear connector failure in the horizontal direction occurred at 810°C, which is the end of the heating phase in this case. Suddenly increased separations in both directions can be observed following this point, implying a complete breakage of the connector. In the vertical direction, separation took place at 806°C.

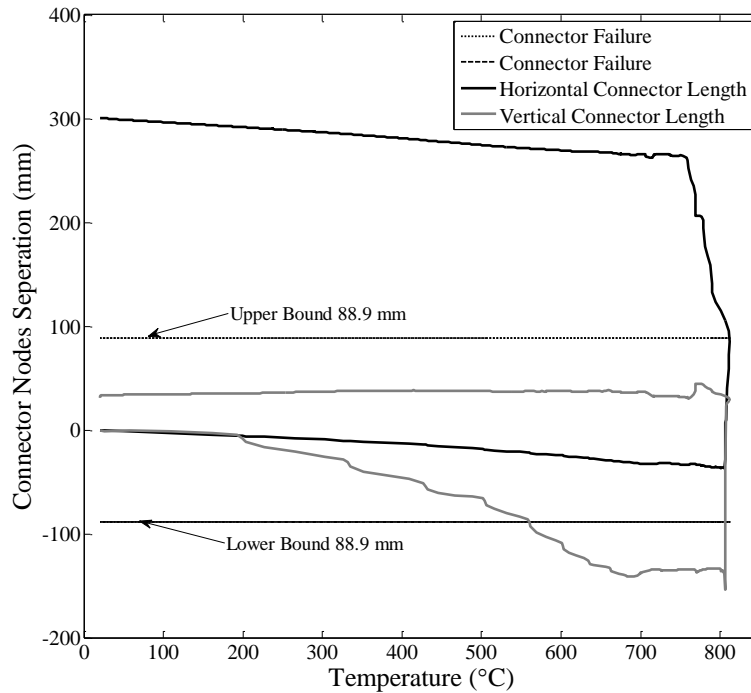


Figure 5.47 Case-8 First Floor Shear Connector Nodes Separation

### 5.7.5.9 Discussion

The shear connector model used in this study was such that it can only move vertically and horizontally. Once the specified separation limit in either direction was reached, the connection between the two nodes released. In general, the shear connectors in the corner compartment fire cases were severed at the onset of collapse of the compartment. For full floor fire cases, the connector either stay intact or broke around the total collapse occurred.

### 5.7.6 Moment Connector Rotation

For this section, the moment connector of the first floor at the center of the structure (Figure 5.48) was the focus. As previously indicated, failure in the moment connection was introduced when rotation of the connector reached 0.06 radius.

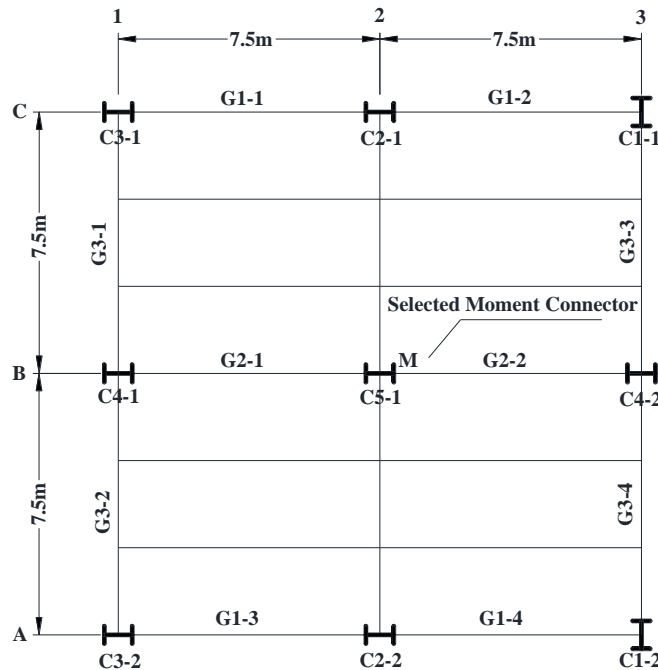


Figure 5.48 Selected Moment Connector

Figure 5.49 shows first floor moment connector rotation versus temperature for all cases. From this figure it can be seen that the connector did not fail only in Case-1, 2, and 6. For Case-1, 2 and 6, large connector rotation was observed around 700°C, which was the onset of the initial collapse. Large rotation also can be seen around 800°C, which was the point where the first floor fully collapsed..

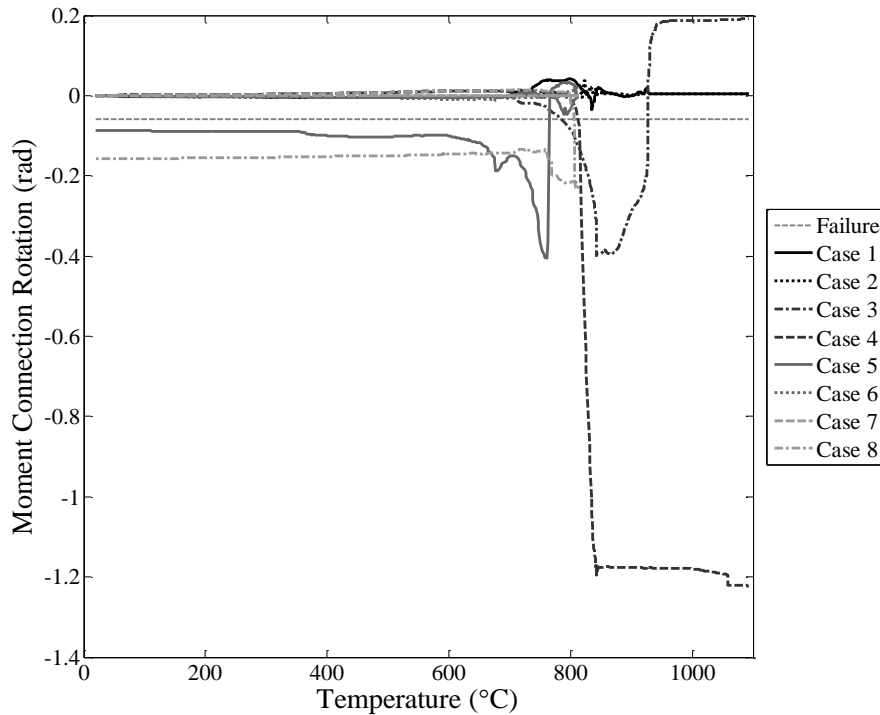


Figure 5.49 Moment Connector Rotation

## 5.8 Comparison

In this section, several comparisons of some of the previously discussed responses for the eight cases were made to show the effect of 1) fire scenario, 2) bracing system, and 3) fire curve on the collapse behavior of the building..

### 5.8.1 Different Fire Scenarios – Case 1 VS. Case 2

For Case-1 and Case-2, the simulation models were the same except for the location in which the fires were applied. Figure 5.50 show the displacement of columns for the two cases. For Case 1, the collapse started with the buckling of the columns in the heated compartment manifested by their vertical downward deformation, which was followed by large downward displacement of the remaining columns at higher

temperature. For Case 2, collapse was triggered by failure of all columns simultaneously and the system collapse entirely prior to Case 1. This response resulted in higher demand on the columns in Case 2 in comparison to Case 1.

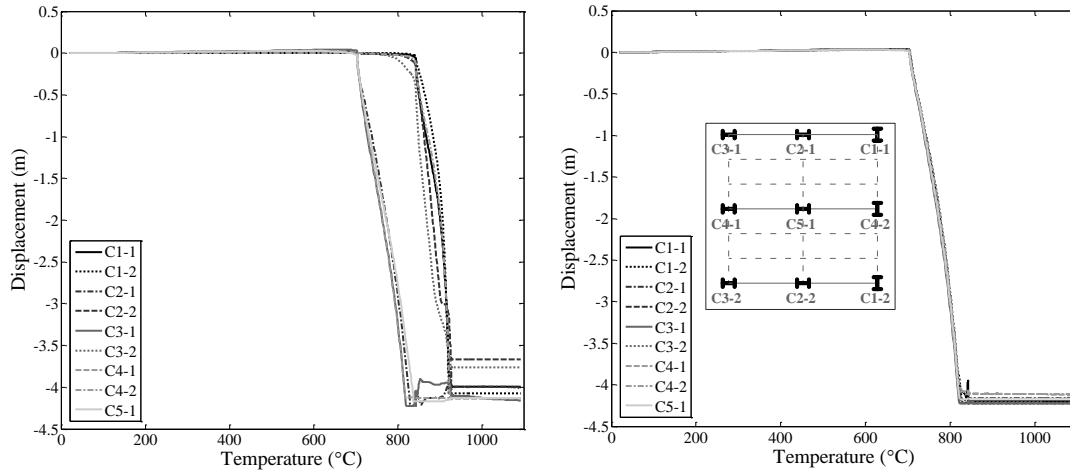


Figure 5.50 Column Vertical Displacement – Case 1 (Left) VS. Case 2 (Right)

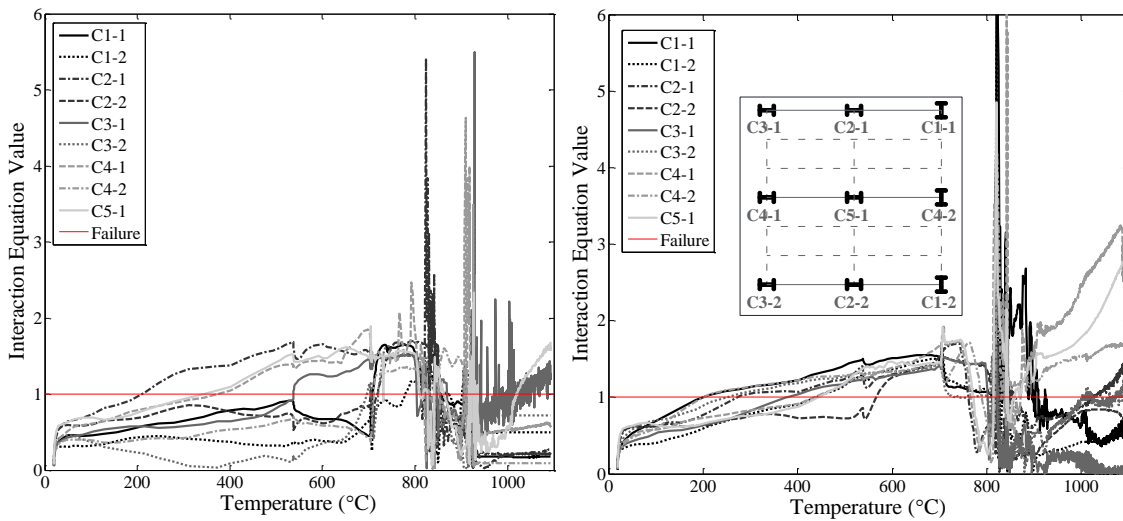


Figure 5.51 Column Interaction Equation – Case 1 (Left) VS. Case 2 (Right)

### 5.8.2 Different Bracing System – Case 6 VS. Case 8

The only difference between Case 6 and Case 8 was the use of different bracing frame (CBF and EBF).

Figure 5.52 shows almost identical downward displacement for the first floor columns. However, Figure 5.53 shows higher force demand on the EBF frame. This is because of the effect of the welded gusset plate on increasing the demand on the columns.

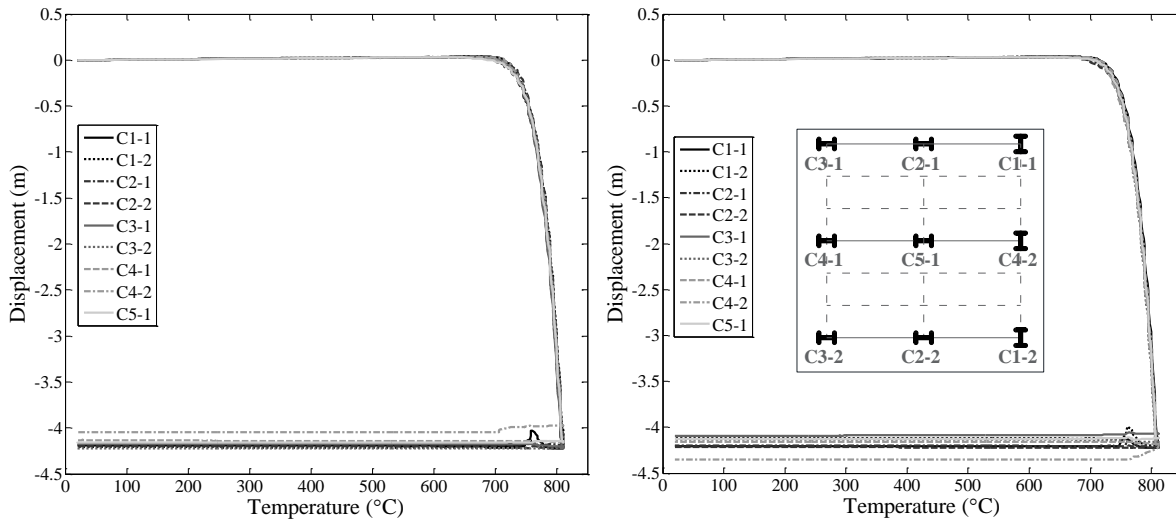


Figure 5.52 Column Vertical Displacement – Case 6 (Left) VS. Case 8 (Right)

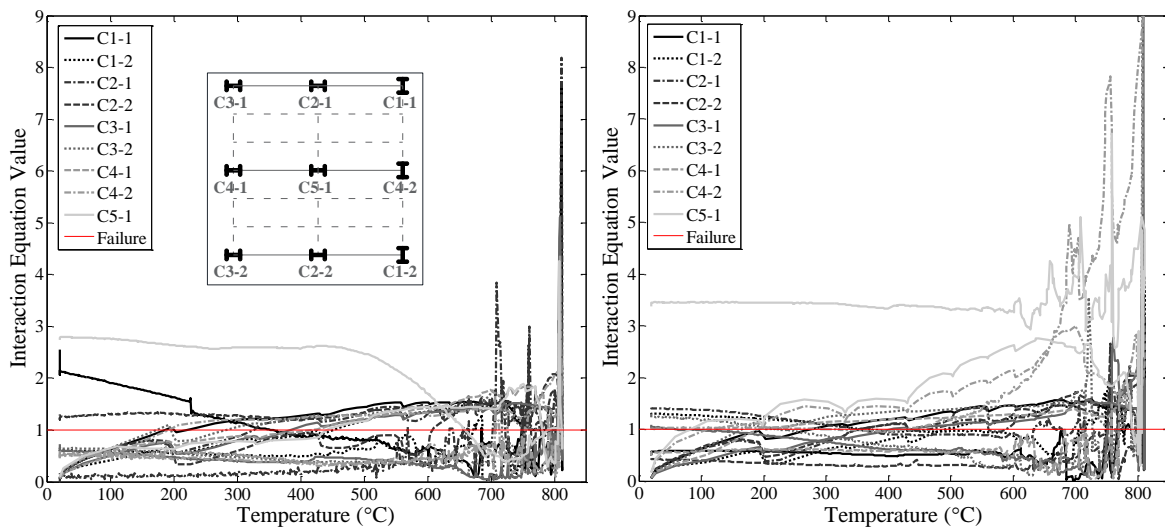


Figure 5.53 Column Interaction Equation – Case 6 (Left) VS. Case 8 (Right)

### 5.8.3 Different Fire Curves – Case 3 VS. Case 7

Two fire curves were chosen in this study, which were ASTM E119 and Eurocode 3 parametric fire curves.

The objective of using a fire curve with a cooling phase was to capture the behavior of the various elements during cooling. However, for this study, the onset of system collapse took place during the heating phase, which made the cooling phase irrelevant. Figure 5.54 below shows the similarity in the column vertical displacements (cooling is omitted from Case 7). Similarity in response, during the heating phase, can also be seen in the interaction equation values during as shown in Figure 5.55.

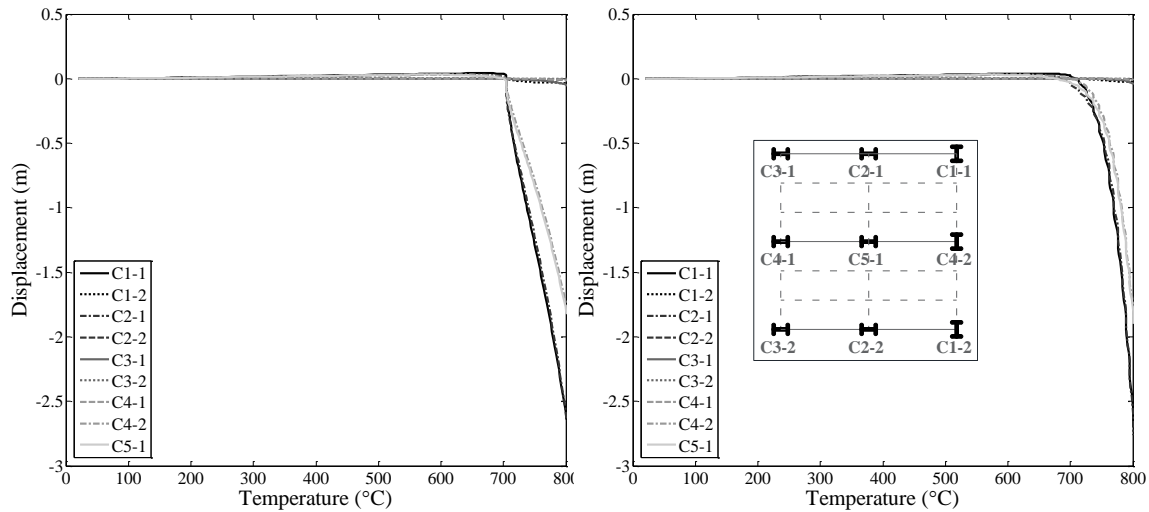


Figure 5.54 Column Vertical Displacement – Case 3 (Left) VS. Case 7 (Right)

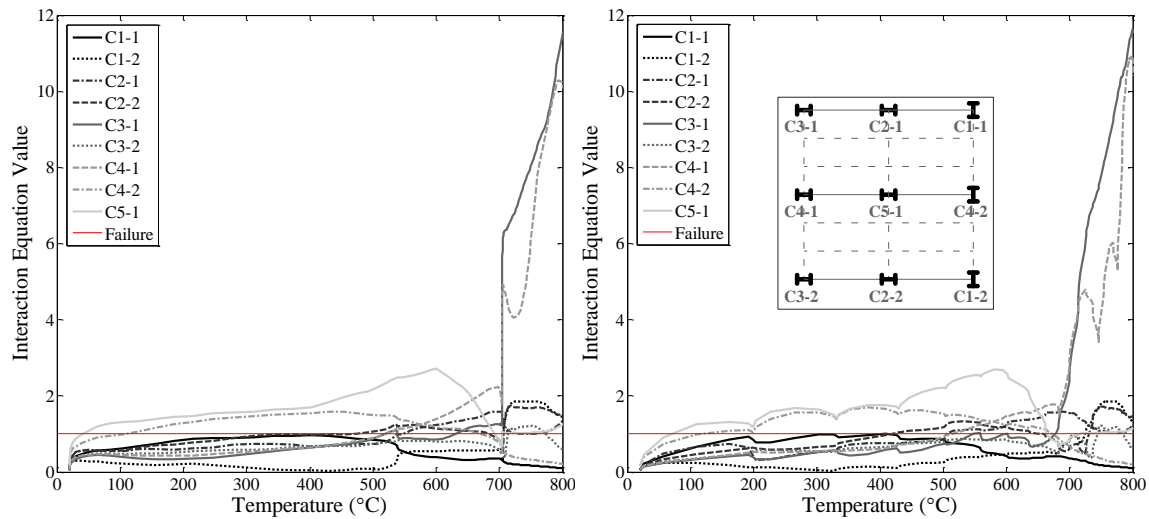


Figure 5.55 Column Interaction Equation – Case 3 (Left) VS. Case 7 (Right)

#### 5.8.4 Discussion

In this section, three pairs of cases were compared to each other for the purpose of showing the effect of using different fire scenarios, different bracing systems, and different fire curves on the response. The effect of the fire scenario is shown through “earlier” downward displacement of some columns in the case of the compartment fire. For the whole floor fire, all columns displaced vertically almost equally. Comparison of the different framing systems showed the equal displacements for both frames but larger forces being developed in the EBF due to the demand imposed by the bracings onto the columns through the welded gusset plates. The use of different fire curves in this study had almost no impact on the response during the heating phase since both curves had identical heating portions during which collapse was initiated.

## 5.9 Summary

In this chapter, the response of two 3D full structural systems that comprise of moment frames, braced frames (CBF in one building and EBF in the other building), and gravity frames were evaluated up to and including collapse when subjected to two different time-temperature curves with different fire scenarios. The overall collapse behavior and sequences for both building systems were discussed. In addition, other performance parameters were presented including axial force and bending moment demands-to-capacity ratios as well as the observed damage pattern in the shear connections during the fire. In addition, the imposed demand on the subassemblies when exposed to fire are compared to the nominal strength values specified by the *2010 AISC Specifications* (AISC 365-10). Three pairs of case comparisons were made to show the difference caused by the simulation conditions. A summary of the conclusions that can be drawn from these results as well as recommendations for future studies are presented in the following chapter.

## CHAPTER 6 CONCLUSION

### 6.1 General

In this research, the main objective is to better understand the system-level behavior of 3D steel buildings with braced frames during progressive collapse induced by fire events. This was realized through employing detailed finite element simulations to assess the behavior of individual members such as girders, beams, columns and braces as well as the whole system response that is controlled by the interaction between the various elements and components.

Experimental testing of structural system up to and including collapse is indeed the most reliable way for assessing the collapse potential for the structures. However, issues of limited laboratory capabilities and funding hinder the ability to perform such tests. On the other hand, numerical simulations with acceptable level of accuracy can be relied upon for evaluating collapse of various structural systems under different loading scenarios. In this study, detailed finite element models of 3D steel building structures with braced frames were created using the commercial software ABAQUS (2014) and utilized for the collapse simulations.

This chapter provides a summary of the study and conclusions that can be drawn from the research, recommendations based on the findings of the project as well as suggestions for additional work that could be performed to extend the study.

## 6.2 Summary

In this section, a brief summary of tasks performed for this study was given as following:

- 1) Two building systems with different bracing types (CBF and EBF) were selected for the simulations in this study. The buildings were 6-story structures, previously tested by Foutch, Roeder, and Goel (1986) in the laboratory under earthquake loading.
- 2) The first building was two bays in each direction, designed with two exterior moment frames in one direction and an interior CBF frame in the same direction. Three gravity frames with shear-tab connections were utilized in the other directions. The other building was identical in design and configuration except it included an intermediate EBF frame instead of the CBF frame.
- 3) The gravity loads used in this study were obtained from the previous test report (Foutch, Roeder, and Goel 1986). For the purpose of this study, a load combination was used to account for the added fire loads.
- 4) Two time-temperature curves were selected to simulate fire temperature, which are ASTM E-119 standard fire curve (ASTM, 2015) and EC3 parametric fire curve (Eurocode 3 EN 1993-1-2, 2005), which included a cooling phase.
- 5) The fire curves were utilized in two different scenarios including a first floor corner compartment and whole first floor for different fire scenarios.
- 6) Steel material properties at elevated temperature were taken from Eurocode 3 (Eurocode 3 EN 1993-1-8, 2005).
- 7) For the concrete slab, the properties at elevated temperature, including the reinforcing steel, were neglected in this simulation based on the assumption that concrete is a good thermal insulator.

- 8) Damage models were utilized in the models to capture failure of structure members and connections including separations and fractures.

### **6.3 Conclusions**

The main findings and general conclusions obtained from this research are summarized in the following key points.

- 1) From the background and literature review chapter, several past fire events were reviewed. It was found that in most cases, with the exception of WTC-7, most of structures suffered only partial collapse when subjected to severe fire events.
- 2) The two selected fire curves caused collapse for all building models. Depending on fire locations, two types of collapse mechanisms can be seen in simulations. In first floor corner compartment fire cases, the building models is shown to twist, lean towards the compartment in which the fire is applied, and laterally sway. On the other hand, in the full first floor fire cases, the building models went straight down and no visible twist was observed during collapse.
- 3) Large axial forces were developed in girders and beams at elevated temperature then transmitted to beam-column connections, which are not typically considered in traditional building code provisions.

- 4) Large axial forces also were observed in the columns during the simulations. With increase in temperature, the columns in the directly heated areas experienced thermal expansion with essentially significant reduction in modulus of elasticity and yield strength. The simulation results show the columns in the directly heated area to have deformed significantly around 700°C, which is onset of building collapse.
- 5) Large horizontal and vertical deformations were observed in the shear-tab connections, which led to connector failure.
- 6) Large rotation of the moment connectors was also observed in several cases, which is caused by the relative deformation that is imposed during collapse.
- 7) The structural response of the building, structural members and connections during the events can be predicted with reasonable accuracy with advanced finite element analysis.

## **6.4 Recommendations**

### **6.4.1 Design Recommendations**

In the review of past events of steel building systems subjected to fire it is evident that fire insulation of members is key to the robustness of structural systems under elevated temperature. In this study, however, it is assumed that fire insulations were completely consumed and provided no barrier between the fire and the exposed steel. While this allowed conservative results to be obtained, the extreme high temperature of steel led to building collapse, which might have otherwise been prevented given proper level of insulation, is included. That being said, moving towards performance based design dictates that fireproofing be

specified only when needed to but in a manner that would ensure structural safety. This could lead to substantial savings and could ultimately lead to steel building construction being an attractive alternative in a competitive market place.

The analysis conducted showed failure of the shear connectors in the simulations, which suggests the need for new design provisions to improve the composite action between the slab and the beams in the case when large lateral deformation is expected during confined compartment fires.

#### **6.4.2 Analytical Modeling Recommendation and Future Work**

The advantage of using line elements to model wide flange sections lies in the computational efficiency offered by line elements. However, some shortcomings can result from using simplified line element models including the inability to capture some behavioral aspects includes for example, local buckling of webs or flanges. In addition, the use of line elements does not allow for proper representation of thermal distribution along the cross section of a member. Including the properties of concrete at elevated temperature was ignored in this study due to lack of data in the literature. More accurate simulation results can be achieved if the material properties of concrete are included in the analyses. Fire insulations should also be included in future simulations to eliminate overestimation of steel temperature due to direct exposure to fire.

Due to the computational effort associated with conducting the simulations, only limited fire scenarios were evaluated. Future work should include the possibility of additional fire scenarios so that the fire location that causes the building to be most vulnerable can be determined. The developed models can be utilized in future analysis to assess multi hazard response of the buildings under fire following by earthquakes.

## REFERENCES

- ABAQUS v6.14, (2014). Dassault Systems, Providence, RI. ([www.simulia.com](http://www.simulia.com)).
- ANSI/AISC 360-05: "Specification for Structural Steel Buildings." (2005c). American Institute of Steel Construction, Chicago, IL.
- ASTM A992/A992M-11. American Society of Testing and Materials (ASTM), (2011) West Conshohocken, PA.
- ASTM International. *ASTM E119-16 Standard Test Methods for Fire Tests of Building Construction and Materials*. West Conshohocken, PA: ASTM International, 2016.
- Agarwal, Anil, and Amit H. Varma. 2013. "Fire Induced Progressive Collapse of Steel Building Structures: The Role of Interior Gravity Columns." *Engineering Structures*.
- British Steel. (1999). "The Behavior of Multi-Storey Steel Framed Buildings in Fire", (1999).
- EC1: Actions on Structures – Part 1.2: General Actions – Actions on Structures Exposed to Fire. (2002). British Standards Institution, London, UK.
- Ellingwood, Bruce R., and Ross B. Corotis. 1991. "Load Combinations for Buildings Exposed to Fires." *Engineering Journal* 28 (1): 37–44.
- En, Cen. 2005. 1-2, *Eurocode 3: Design of Steel Structures, Part 1.2: General Rules—structural Fire Design*. London: British Standards Institution. Vol. 2.
- En, Cen. 2005. 1-8, *Eurocode 3: Design of Steel Structures, Part 1.8: Design of Joints*. London: British Standards Institution. Vol. 8.
- FEMA 350: Recommended Seismic Design Criteria for New Steel Moment-Frame Buildings. (2000). Federal Emergency Management Agency, Washington, D.C.
- Foutch, D.A., C.W. Roeder, and S.C. Goel. 1986. "Preliminary Report on Seismic Testing of A. Full-Scale Six-Story Steel Building."
- Hu, Guanyu, and Michael D. Engelhardt. "Behavior of Steel Single-Plate Beam End Framing Connections in Fire." In *Structures Congress 2010*, pp. 1554-1565. ASCE, 2010.

- ISO. (1975). "Fire resistance tests-elements of building construction." International Standard ISO 834, Geneva.
- Jankowiak, Tomasz, and Tomasz Lodygowski. "Identification of parameters of concrete damage plasticity constitutive model." *Foundations of civil and environmental engineering* 6, no. 1 (2005): 53-69.
- Jiang, Jian, Guo-Qiang Li, and Asif Usmani. "Progressive collapse mechanisms of steel frames exposed to fire." *Advances in Structural Engineering* 17, no. 3 (2014): 381-398.
- Johnson, Gordon R., and William H. Cook. 1985. "Fracture Characteristics of Three Metals Subjected to Various Strains, Strain Rates, Temperatures and Pressures." *Engineering Fracture Mechanics* 21 (1): 31-48.
- Khandelwal, Kapil, Sherif El-Tawil, and Fahim Sadek. 2009. "Progressive Collapse Analysis of Seismically Designed Steel Braced Frames." *Journal of Constructional Steel Research* 65 (3). Elsevier Ltd: 699-708.
- Mao, C.J., Y.J. Chiou, P.a. Hsiao, and M.C. Ho. 2009. "Fire Response of Steel Semi-Rigid Beam-column Moment Connections." *Journal of Constructional Steel Research* 65 (6). Elsevier Ltd: 1290-1303.
- Memari, Mehrdad, and Hussam Mahmoud. 2014. "Performance of Steel Moment Resisting Frames with RBS Connections under Fire Loading." *Engineering Structures* 75. Elsevier Ltd: 126-38.
- Memari, Mehrdad, Collin Turbert, and Hussam Mahmoud. 2013. "Effects of Fire Following Earthquakes on Steel Frames with Reduced Beam Sections." *Structures Congress 2013*, 2555-65.
- Murray, Thomas M, and Emmett A Sumner. 1999. "Brief Report of Steel Moment Connection Test" 02: 1-14.
- Najjar, S. R., and I. W. Burgess. 1996. "A Nonlinear Analysis for Three-Dimensional Steel Frames in Fire Conditions." *Engineering Structures* 18 (1): 77-89.
- Newman, Gerald M., Jef T. Robinson, and Colin G. Bailey. Fire safe design: A new approach to multi-story steel-framed buildings. Steel Construction Institute, 2000.
- National Institute of Standards and Technology (NIST), (2004), "June 2004 Progress Report on the Federal Building and Fire Safety Investigation of the World Trade Center Disaster, Appendix L- Interim Report on WTC 7," NIST Special Publication 1000-5.

- NIST NCSTAR 1A: Final Report on the Collapse of World Trade Center Building 7, Federal Building and Fire Safety Investigation of the World Trade Center Disaster. (2008). National Institute of Standards and Technology, Gaithersburg, MD.
- NIST NCSTAR 1- 1I: Post-Construction Modifications to Fire Protection, Life Safety, and Structural Systems of World Trade Center 7. (2005). National Institute of Standards and Technology, Gaithersburg, MD.
- NIST NCSTAR 1-3D: Mechanical Properties of Structural Steel, Federal Building and Fire Safety Investigation of the of the Work Trade Center Disaster. (2005). National Institute of Standards and Technology, Gaithersburg, MD.
- NIWA, HIRONORI. "Investigation of Windsor Building Fire in Spain." Report of Obayashi Corporation Technical Research Institute (CD-ROM) 70 (2006): 11-2.
- Quiel, Spencer E., and Maria E. M. Garlock. 2008. "Modeling High-Rise Steel Framed Buildings under Fire." *Structures Congress 2008*, no. 1: 1–10.
- Roeder, Charles W., Douglas A. Foutch, and Subhash C. Goel. 1988. "Seismic Testing Of Full-Scale Steel Building-Part I." *Journal of Structural Engineering* 113 (11): 2130–45.
- Rubert, Achim, and Peter Schaumann. 1986. "Structural Steel and Plane Frame Assemblies under Fire Action." *Fire Safety Journal* 10 (3): 173–84.
- Saab, H.a., and D.a. Nethercot. 1991. "Modelling Steel Frame Behaviour under Fire Conditions." *Engineering Structures* 13 (4): 371–82.
- Sarraj, Marwan. "The behaviour of steel fin plate connections in fire." (2007).
- Selamet, Serdar, and Maria E. Garlock. "Local buckling study of flanges and webs in I-shapes at elevated temperatures." In *ASCE structures congress. Orlando, FL*, pp. 1592-603. 2010.
- STC Technical Report, Swinden Technology Centre, Rotherham, South Yorkshire, UK.
- Sun, Ruirui, Zhaohui Huang, and Ian W. Burgess. 2012. "The Collapse Behaviour of Braced Steel Frames Exposed to Fire." *Journal of Constructional Steel Research* 72: 130–42.
- Yang, Kuo Chen, Sheng Jin Chen, and Ming Chin Ho. 2009. "Behavior of Beam-to-Column Moment Connections under Fire Load." *Journal of Constructional Steel Research* 65 (7). Elsevier Ltd: 1520–27.

Yu, Hongxia, I. W. Burgess, J. B. Davison, and R. J. Plank. 2009. "Experimental Investigation of the Behaviour of Fin Plate Connections in Fire." *Journal of Constructional Steel Research* 65 (3). Elsevier Ltd: 723–36.

Yura, Joseph A., Michael D. Engelhardt, and Eric B. Becker. "Behavior of bolted connections during and after a fire." PhD diss., Austin, The University of Texas at Austin, 2006.